UCRL-ID-133144

Mandrel Development Update - 1/98 to 12/98

Bob Cook
Masaru Takagi
Steve Buckley
Evelyn Fearon
April Hassel

February 1, 1999

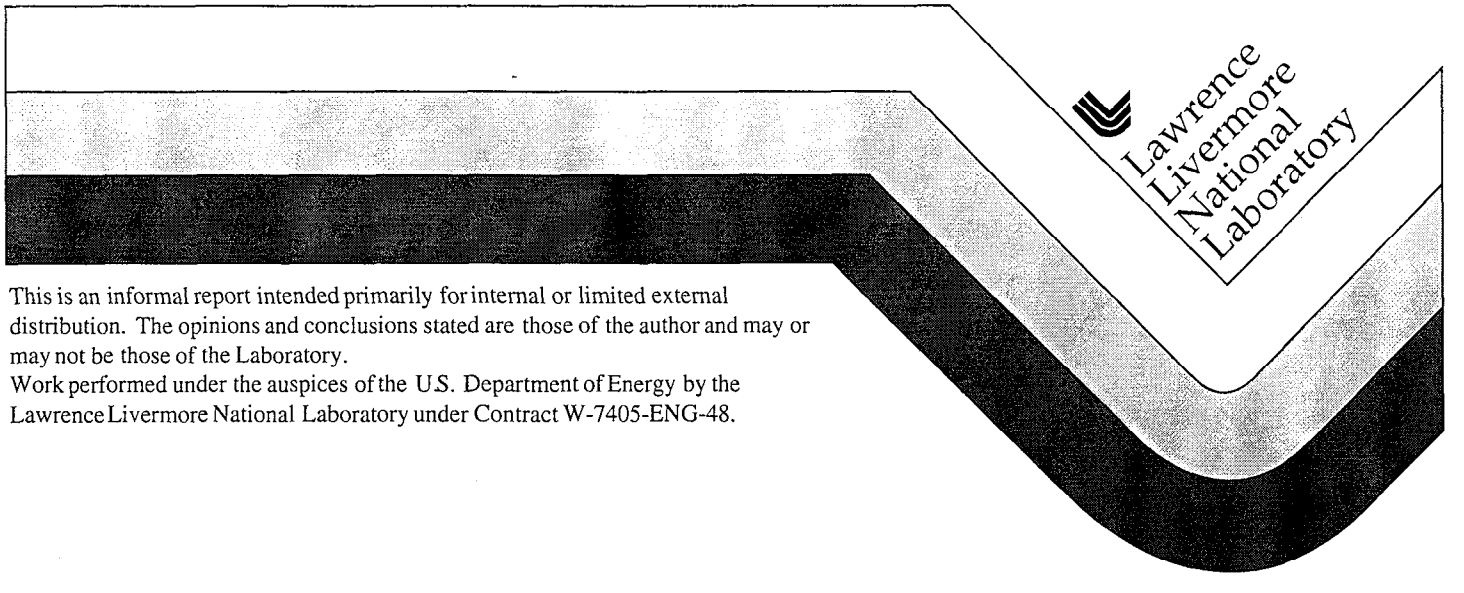

Mandrel Development Update - 1/98 to 12/98

Bob Cook, Masaru Takagi, Steve Buckley, Evelyn Fearon, and April Hassel

February 1, 1999

Overview We report on the progress since January, 1998, in preparing polymer mandrels by microencapsulation for NIF scale ICF capsules that meet the required symmetry and surface finish requirements. During that time we successfully completed our FY98 DOE TDF4.1 milestone of improving the mandrel low mode to meet NIF requirements. A number of batches of 2 mm microencapsulated poly(α-methylstyrene) shells have been produced with mode 2 out-of-rounds of less than 2 μm. Detailed characterization for these and other batches is presented. We have found that the key to reducing mode 2 out-of-round is the density matching of the composite oil/inner core water microencapsulated shell preform to the supporting bath. Density matching of the inner core water to the oil phase seems to be less important, perhaps because core centering is accomplished by other physical means. Shell roughness over the very important mode 10 to 100 region is still too high by at least a decade in power, and work aimed at improving this is the task for FY99.

In addition to basic sphericity results we also report on a number of experiments designed to elucidate the fundamental scientific issues. In most cases the experiments reported are but starting points that will be followed up during FY99.

Lastly we note that no effort has been placed on optimizing the overcoating and thermal decomposition steps, which must follow the successful microencapsulation step. Based upon GA's experience with smaller scale shells we are hopeful that these steps will not degrade capsule symmetry and surface finish. This question should be answered at least in part during FY99 as GA begins to supply finished 2 mm CH mandrels for the polyimide and Be ablator development work.

Background

All NIF Capsule options except machined Be require a mandrel upon which the ablator is deposited. This mandrel sets the base line sphericity of the final capsule, especially over the low modes. Subsequent coating operations may degrade the capsule surface finish but are unlikely to improve it.

History

For Nova capsules the mandrels were historically ~0.5-mm-diam polystyrene thin-walled microshells produced by solution droptower methods.[1] However these methods are limited to shell sizes of less than 1-mm-diam due to heat and mass transfer limitations. An alternative high temperature droptower approach developed in collaboration with scientists from the Lebedev Physical Institute in Moscow avoids some of these problems by using solid polymer granules containing only a few percent of volatile solvent. Using these techniques they have been able to produce high quality shells up to 1.8 mm in diameter, and are hopeful that the techniques can be extended to 2.0 mm.[2] In FY96 we explored using interfacial polymerization techniques developed in Japan[3] to produce plastic shells. In this technique a droplet of the desired size containing one reactant is suspended in an immiscible fluid containing a second reactant, resulting in reaction at the interface to produce a shell. Size control is simple and it was hoped that the interfacial surface tension would provide sphericity. Results were mixed,[4] and it was decided that we would focus our efforts on the more straightforward microencapsulation technique discussed below.

In 1995, the "decomposable mandrel" approach to forming plastic mandrels was developed.[5] This approach, which is now used for the production of mandrels for both Omega and Nova-scale capsules, involves initially producing a spherical mandrel from poly(α-methylstyrene) (PαMS), overcoating it with 5 to 10 μm of plasma polymer, and then finally heating to 300 °C which causes the PαMS mandrel to depolymerize to

---

[1] R. Cook, "Production of Hollow Microspheres for Inertial Confinement Fusion Experiments," in *Mat. Res. Soc. Symp. Proc.* **372**, 101 (1995).

[2] A. I. Nikitenko, S. M. Tolokonnikov, and R. Cook, "Large Shell Fabrication Results Using the Ballistic Furnace," *J. Moscow Phys. Soc.*, **8**, 63 (1998); A. I. Nikitenko, S. M. Tolokonnikov, and R. Cook, "The Design of the Ballistic Furnace and Initial Microshells Formation Experiments," *Fusion Technol.* **31**, 385 (1997).

[3] M. Takagi, M. Ishihara, T. Norimatsu, T. Yamanaka, Y. Izawa, and S. Nakai, "Development of Foam Shell with Plastic Ablator for Cryogenic Laser Fusion Target," *J. Vac. Sci. Technol. A*, **11**, 2837 (1993).

[4] K. E. Hamilton, S. A. Letts, S. R. Buckley, E. M. Fearon, D. Schroen-Carey, G. Wilemski, and R. Cook, "The Role of Reactant Transport in Determining the Properties of NIF Shells Made by Interfacial Polycondensation," *Fusion Technol.* **31**, 391 (1997).

[5] S. A. Letts, E. M. Fearon, S. R. Buckley, M. D. Saculla, L. M. Allison, and R. Cook, "Preparation of Hollow Shell ICF Targets using a Depolymerizing Mandrel," *Mat. Res. Soc. Symp. Proc.* **372**, 125 (1995); S. A. Letts, E. M. Fearon, S. R. Buckley, M. D. Saculla, L. M. Allison, and R. Cook, "Fabrication of Polymer Shells Using a Decomposable Mandrel," *Fusion Technol.* **28**, 1797 (1995).

gaseous products leaving a spherical plasma polymer shell. Under the proper processing conditions the sphericity of the final shell reproduces the sphericity of the PαMS mandrel. One significant advantage of this approach is that the resulting mandrel has extremely uniform wall thickness, key to eliminating P_1 defects in final capsules.

The initial PαMS mandrel for this process can be either a solid PαMS bead or microencapsulated PαMS shell. The key feature is that the outer surface be extremely spherical. The decomposable mandrel approach was originally developed using solid PαMS beads, however we switched to PαMS shells due to the ease of preparing large numbers of tightly size controlled high quality shells using microencapsulation techniques, especially at Nova and Omega-scale. The microencapsulation method was pioneered for ICF capsule fabrication by workers at Osaka,[6] and was used at LLE for many years for the production of small (~0.3-mm-diam) capsules. In this method a water droplet is encapsulated by an immiscible organic phase containing dissolved polymer, and this encapsulated droplet is suspended in an aqueous bath. The organic solvent slowly dissipates into the aqueous bath leaving a solid polymer shell. The internal water droplet can be removed by air-drying. Extension of the microencapsulation approach to 2 mm shells of high quality is the topic of this report, though we note that during FY98 we reexamined techniques for forming spherical beads, including a novel hot density gradient approach. The results of these studies have been reported separately. [7]

At LLNL work on the microencapsulation of NIF-scale PαMS mandrels began in FY97 with partial support from a C&MS LDRD. The principal experimental investigator was Ken Hamilton, a C&MS post-doc. A lengthy report on the experimental investigations conducted by Hamilton has been produced.[8] The focus of most of this experimental work was on understanding the key scientific issues and their relationship to the various processing parameters. Related theoretical work that will be discussed briefly below attempted to interpret experimental observations. Important results from this work included a) a partial climb up a steep learning curve b) the recognition of the sensitivity of shell sphericity to various density matching conditions and processing bath agitation conditions, c) the recognition of significant differences between polystyrene, which had for many years been used in microencapsulation methods of sub-1-mm-diam ICF shells, and PαMS, and d) the extreme sensitivity of shell quality to shell size. Success in producing NIF-scale PαMS shells was limited, size control at 2 mm was easily achieved but shell out-of-round generally exceeded 15 to 20 μm. This characterizes the extent of our experimental progress up to January, 1998, when Dr. Masaru Takagi joined our effort. This report will detail our work since that time.

---

[6] M. Takagi, T. Norimatsu, T. Yamanaka, and S. Nakai, "Development of Deuterated Polystyrene Shells for Laser Fusion by means of a Density Matched Emulsion Method," *J. Vac. Sci. Technol. A*, **9**, 2145 (1991).

[7] R. Cook, S. R. Buckley, E. Fearon, and S. A. Letts, "New Approaches to the Preparation of PαMS Beads as Mandrels for NIF-Scale Target Capsules," *Fusion Technol.*, (1999), in press. In addition a report on the summer work of Brian Parrish, a student from California Polytechnic University, has been distributed. Contact R. Cook for a copy.

[8] K. E. Hamilton, S. R. Buckley, and R. Cook, "The Science of NIF Scale Capsule Development," November, 1997, UCRL-ID-129331.

Modeling.

Before proceeding let us briefly review some of the relevant modeling results that have formed the framework for our experimental work. Given the poor shell sphericity results during 1997, two aspects of the process were examined. The model used was initially a simple homogeneous fluid droplet suspended in a second immiscible fluid,[9] though more detailed consideration of the compound droplet has also been undertaken, both here[10] and elsewhere.[11] For this situation the only force promoting sphericity is the interfacial tension, γ. The distorting forces examined included both a) deformation due to a density mismatch between the droplet and the supporting bath and b) deformation due to hydrodynamic interaction between the bath fluid and the droplet. For the first case one can show that maximum-out-of-round (MOOR), equal to the difference between the maximum and minimum droplet diameters, is given by

$$\mathrm{MOOR} \cong \frac{5gr^3\Delta\rho}{4\gamma} \quad , \tag{1}$$

where g is the acceleration of gravity, r the droplet radius, and $\Delta\rho$ is the density difference between the droplet and supporting fluid. This calculation, which assumes an ellipsoidal deformation, was done for a droplet sitting on a surface, but is also probably accurate for situations where the droplet deformation is more rapid than translational droplet motion. As an example of the effects of hydrodynamic interactions, the case of a fluid droplet in a linear shear gives

$$\mathrm{MOOR} \cong \frac{8\mu G r^2}{\gamma} \quad , \tag{2}$$

where μ is the bath viscosity and G is the linear shear field in the bath. In both examples note the greater than linear dependence on the droplet size. It is clear from these simple models that both good density matching and attention to bath agitation are critical.

As noted above, this report focuses on the progress made since January, 1998, producing high quality 2-mm-diam PαMS shells by microencapsulation. In what follows we will first detail our current methodology and shell quality. Focus has been on reducing the basic mode 2 shell out of round (MOOR) to a level acceptable for NIF, approximately 1 – 2 μm. As will be shown, this goal has been accomplished. A more detailed low mode capsule specification has been recently developed based on

---

[9] R. C. Cook, P. M. Gresho, and K. E. Hamilton, "Examination of Some Droplet Deformation Forces Related to NIF Capsule Sphericity," *J. Moscow Phys. Soc.* (1998), in press.

[10] P. M. Gresho, "Some Aspects of the Hydrodynamics of the Microencapsulation Route to NIF Mandrels," *Fusion Technol.*, (1999), in press.

[11] T. Norimatsu, Y. Izawa, K. Mima, and P. Gresho, "Modeling of the Centering Force in a Compound Emulsion to Make Uniform Plastic Shells for Laser Fusion Targets," *Fusion Technol.*, (1999), in press.

X Division design calculations performed in the summer of 1998,[12] and future shell progress will be measured against this metric. Following this section we will detail a number of our specific scientific studies that have led to this improvement, particularly in the area of density matching, as well as other studies that are preliminary to future improvements. We will conclude with an outline of our planned work for FY99.

Basic Methodologies and Sphericity Results.

Microencapsulation details.

Microencapsulated PαMS shells are produced using a triple orifice droplet generator similar to that shown in Figure 1. The generator has been modified since the last report by Hamilton[13] and because of these modifications it has become more reliable. The generator body is now stainless steel. This eliminates swelling of the previous acrylic body, which led to decreased flows. The coupling, holding the inner and mid orifices, is a solid block of Teflon which is more durable than the septum coupling used previously.

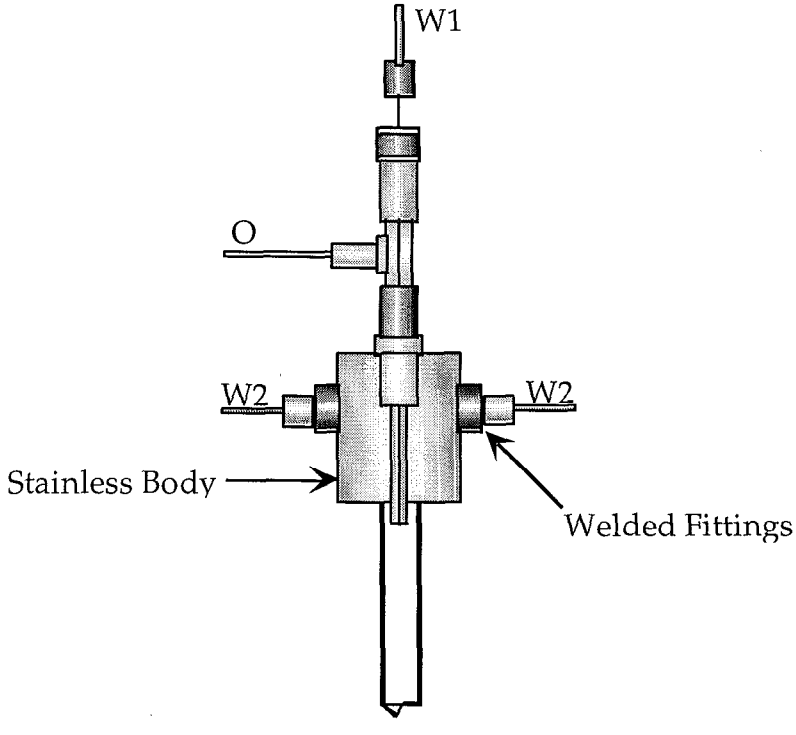

Figure 1. Sketch of droplet generator assembly.

We typically use distilled water as our core (W_1) fluid. The oil phase (O) is a 13 to 18% (wt/vol) solution of PαMS in fluorobenzene (FB) or a roughly 1:1 benzene:dichloroethane (B:DCE). We distill the fluorobenzene two times prior to use to remove impurities. The B and DCE are each distilled once before being mixed for the

[12] S. Haan, private communication.
[13] K. E. Hamilton, S. R. Buckley, and R. Cook, "The Science of NIF Scale Capsule Development," November, 1997, UCRL-ID-129331.

two solvent system. The PαMS (395K M_w, from Scientific Polymer Products, Inc.) is purified by methods developed at General Atomics.[14] This is accomplished by adding 30 g of PαMS to 500 mL of distilled toluene. The polymer solution stands in a covered beaker overnight before filtering with 0.65 and then 0.2 μm filters to remove impurities. The dissolved polymer is then dripped into 1–1.5 L of pre-filtered ethanol to obtain a stringy white polymer precipitate. The solution is allowed to stand in a covered beaker overnight to promote complete reprecipitation of the polymer. The PαMS polymer is washed with filtered ethanol. The washing process is repeated three times, holding the precipitate 2–3 h between decantations. A fiber free paper is placed over the PαMS container and it is placed into a vacuum oven at 60 °C for 3–5 days.

Our stripping fluid (W_2) is generally a 2% (wt/vol) solution of PVA (25K M_w, 88% hydrolyzed, Polysciences) which is filtered through a 0.2 μm filter. On some earlier occasions the PVA solution was saturated with fluorobenzene, however, this practice has been omitted in later experiments. An ammonium nitrate solution is added to the PVA, which we place in the receiving vessel prior to every run. The NH_4NO_3 solution is filtered with a 0.2 μm filter and 100 g of a 10 wt% stock solution is placed into the 1000 mL receiving beaker containing 500 mL of the 2 wt% PVA solution.

There were primarily two methods used for suspending the emulsion during the organic solvent removal process. A non-contact method using a rotary evaporator was tried for several runs but resulted in less than adequate sphericity. A second method utilizing a pair of external mixing blades as shown in Figure 2 is now used almost exclusively for keeping the emulsion suspended.

Operating the droplet generator requires that the PαMS solution be made up at least one day in advance in order to ensure complete dissolution of the PαMS. 500 mL of 2 wt% PVA solution is added to the 1 L collection flask and heated in a microwave for 3 min to a temperature of about 50 °C. We then add 110 mL of 10% NH_4NO_3 dissolved in 2 wt% PVA solution to the beaker. The droplet generator is started by turning on the pump controlling the 2 wt% PVA stripping solution. Flow rates are generally 20–25 mL per min depending on the viscosity of the organic phase; higher polymer concentrations require a greater stripping velocity than low concentrations to produce 2 mm capsules. The organic phase is then started, generally using a gastight syringe, however we have also used a 25 mL glass syringe on occasion. Then the internal water phase (W_1) pump is started and the composite flow is delivered into an empty beaker. It is important to note the initial water droplet formation at the end of the needle, if the water droplet forms on one side and drops off then it is a good possibility that it is not wetting and the needle must be cleaned or replaced.

Internal water (W_1), oil phase (O), and stripping fluid (W_2) flow rates are generally variables of a given experiment, but are usually in the ranges: W_1 rate of 0.8–1.6 mL/min, O rate from 0.6–0.9 mL/min, and W_2 rate from 20–25 mL/min. Normally we run two experiments together, each using half of the volume of the polymer solution in the 25 mL syringe. Typically anywhere from 1 to 5 mL of polymer solution is consumed during the initial start up of the encapsulation process.

[14] B. McQuillan, General Atomics, private communication

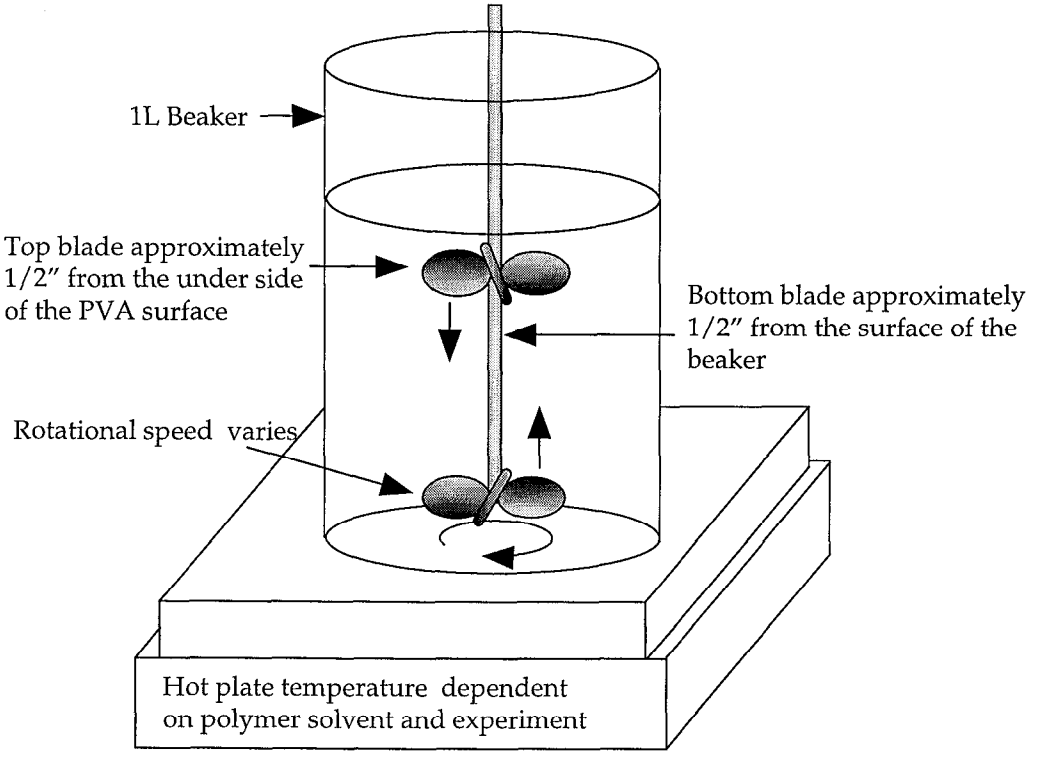

Figure 2. Droplet suspension.

Each beaker of encapsulated droplets is topped off with 2 wt% PVA to bring the total volume to 1100 mL, placed on a hot plate and the stirrer inserted. The stir motor is set to approximately 25–50 rpm initially to obtain a homogeneous dispersion of shells throughout the PVA. The stir rate is then ramped to 150 rpm. The hot plate is set to control the solution temperature at 45 °C. The timer is set to turn off the hot plate after 23 h of heating.

The hardened PαMS shells and stripping solution are removed from the heat and stirring devices and are decanted into a filter funnel with no paper installed in the filter holder to facilitate fluid draining. In order to remove residual PVA from the shell surface they are rinsed thoroughly with copious amounts of tap water followed by rinsing with one liter of distilled water heated in a microwave oven to a temperature of about 80 °C. After all residual PVA is removed, the shells are rinsed with 150 mL of 0.2 μm-filtered ethanol.

The encapsulated water droplet in the hardened PαMS shell is removed using vacuum oven drying. The entire batch of shells is placed in a 50 mL beaker, covered with a fiber-free cloth, and put into a vacuum oven at about 20–30 mtorr and 60 °C. Water removal is completed in five days.

Batch characterization

Batch characterization begins with the encapsulation step. Shell diameter is controlled by the stripping (W_2) flow rate and shell wall thickness is a function of polymer concentration and ratio of the W_1 and O flow rates. The W_1 and O solutions are injected from glass syringes using a precision pump to control flow rates. Optical

measurements with a stereo microscope are used to assess the initial wall thickness and diameter of the emulsion as it is produced.

A normal experimental run can produce nearly 1800 encapsulated droplets. Typically about 90% are processed through to dry shells. Losses are primarily due to loss of the inner water droplet before curing, generally because of collisions with the stir blade or beaker walls. Within a given batch of dry shells, 5 to 10 which appear to be of good quality when viewed with a stereo microscope are selected for sphericity measurements on our shadowgram measuring apparatus (called Rapid Asphericity Characterization Instrument or RACI). These measurements involve analyzing three roughly orthogonal shadowgrams, fitting each image to an ellipse to determine the major and minor diameters. Table I summarizes the results for six of our better batches. The detailed data sheets are presented in Appendix A. Given in Table I are the batch average diameter as well as the batch average single view out-of-round (OOR), the difference between the major and minor axes of a single view, and the 3 view OOR, which is the difference between the largest major axis and smallest minor axis for the three views of a shell. This latter measurement gives a better picture of capsule symmetry for more highly distorted capsules, though some uncertainty is introduced in the comparison of independent images. Examination of the data sheets in Appendix A shows that for most individual shadowgrams where the one view OOR is less than about 2 μm, the column labeled "Angle" has a 0.0 entry. This indicates that the shell sphericity is better than an instrument-inherent distortion in the x-direction of about 1.4 to 1.7 μm (an optical distortion present in the microscope used in the system). Thus for shells with OOR's of less than about 2 μm, AFM spheremap analysis is necessary to compare shells. Shell wall thickness is determined from the shell mass and outer diameter using a PαMS density of 1.075 g/cm^3.

Table I. Batch Diameter and OOR Data

Batch	Average Diam (μm)	Range (μm)	1 view OOR (μm)	Range (μm)	3 view OOR (μm)	Range (μm)	Wall (μm)
1058	1939	1890-2089	1.9	0.8-4.0	1.9	0.8-4.0	15
1059	1980	1945-2017	1.1	0.3-2.7	1.5	0.2-1.8	20
1088	1895	1790-2168	1.1	0.4-2.5	1.7	1.0-2.5	20
1089	1964	1779-2115	1.1	0.1-2.6	1.8	1.1-2.7	20
1104	2325	2297-2356	2.0	0.2-5.3	2.7	1.4-5.3	38
1105	2256	2211-2344	1.4	0.2-2.6	2.2	1.6-2.8	43

As can be seen in Table I, diameter control within a batch is frequently not precise, presumably because the size of the internal water droplet varies somewhat from encapsulated droplet to droplet, and to a lesser extent due to variations in the amount of oil phase delivered to each droplet. This is in some contrast to what is seen for Omega scale capsules, and is probably due to the much slower droplet generation rate necessary for the larger shell size.

Individual shell spheremap results.

As noted above the RACI data can at best be used as a screening tool. Based on these results individual shells are selected for spheremapping. Appendix A provides both the trace and power spectrum data for a number of the shells that were spheremapped from the batches in Table I. For the purposes of the discussion that follows, Figure 3 below shows representative traces from a shell and Figure 4 shows the power spectra of a few of the best shells produced at LLNL. It should be emphasized that we have actually spheremapped relatively few shells; our focus has been more on developing an understanding of and control over the basic mode 2 out-of-round.

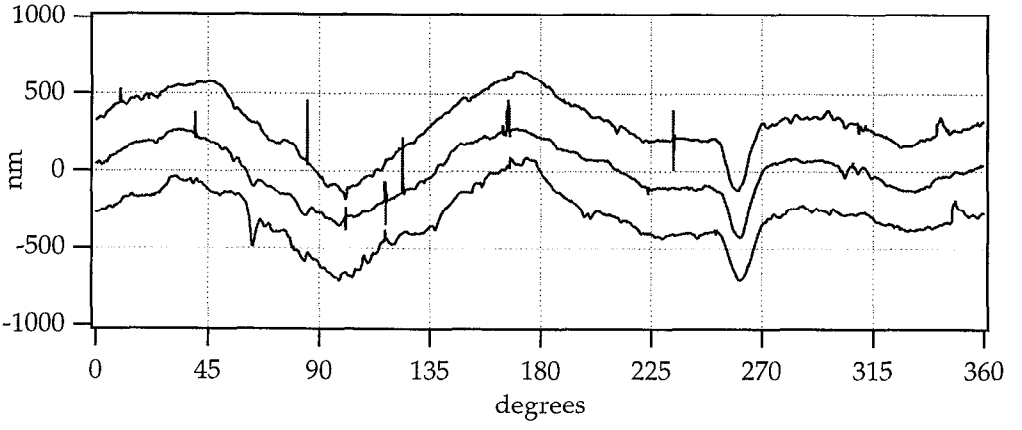

Figure 3. An example of traces from a shell showing some of the mid and high frequency defects as described in the text.

There are several features of Figure 3 that should be noted. First, in addition to a general mode 2 wave to the traces there are also smaller squiggles, as much as 100's of microns wide with relative amplitudes of a few 100 nm or less. We believe these features may be due to collisions of the viscous shell with either another shell, a wall, or the stir blade at a time after full relaxation is possible. The details of this will be discussed later in the section on shell drying; at this point it is only necessary to note these features. Second, there are a number of relatively sharp spikes on the traces. Because of the difference in horizontal and vertical scales, these spikes are in fact much wider than they are high. We believe that many of these features are debris of some sort on the shell surface, possibly acquired during post process characterization handling. These spikes give rise to most of the high frequency power in the spectra in Figure 4.

We have also found that the PαMS shells are more difficult to scan on the sphere mapper than shells of other materials. We believe there is increased AFM tip interaction with PαMS in the form of static charge build-up. The AFM tip suddenly hops up as much as 1 to 2 μm for part of the scan and then drops back down to the original surface. The hopping is an artifact of the tip interaction, not the real shell surface. We use a static control device—a fan which blows a stream of ionized particles across the AFM head and sample—to somewhat alleviate the hopping problem, but it adds high frequency noise to the traces. Shown in Figure 5a are traces from a bare PαMS shell taken with the ion fan on. Notice on the left side of the first and third traces small hops in the trace still present even with the ion fan on. There is also a region of increased noise on the right side of the traces. This feature typically appears in the same location, between

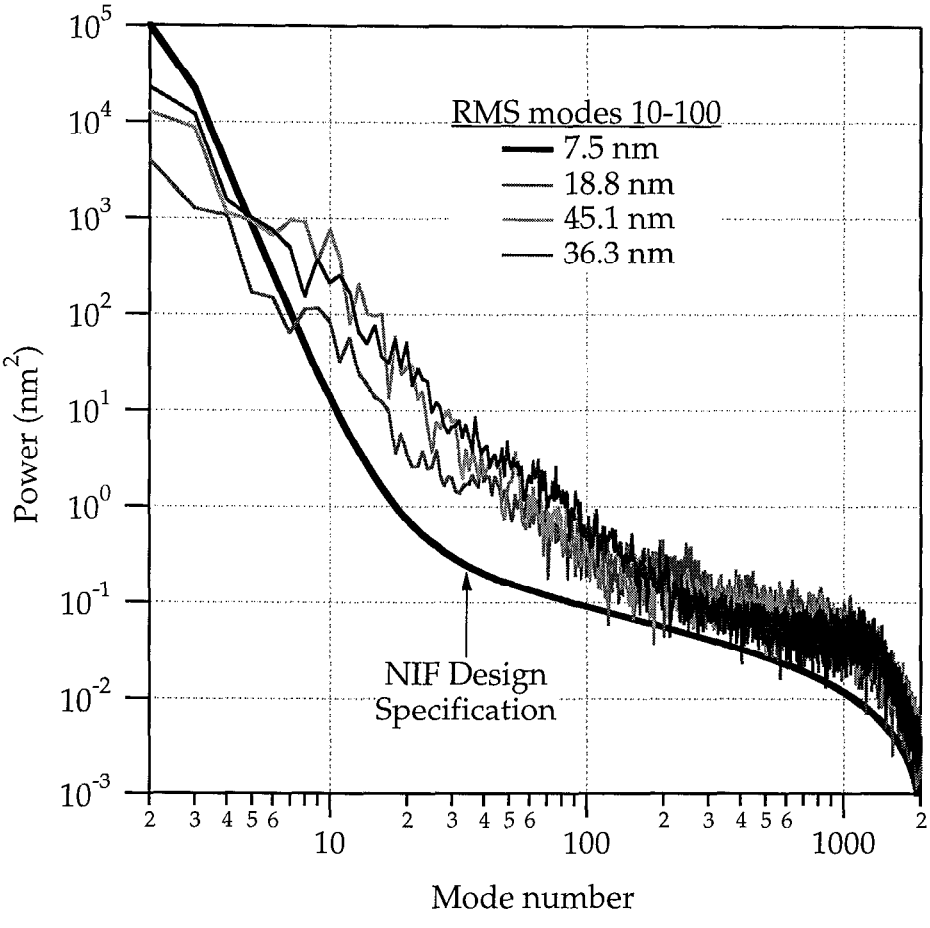

Figure 4. Power spectra of a few of the better 2 mm shells produced at LLNL. Also shown is the NIF model power spectrum.

about 270 and 360 deg, suggesting a mechanical problem. However it appears only when the ion fan is on for PαMS. In Figure 5b traces from the same shell (though a different orientation) are presented after the shell had been coated with a sub-micron layer of plasma polymer. The shell was easily scanned without hops in the traces and without the need to run the ion fan. In a high frequency sense the shell is clearly smoother, but especially compared to the uncoated shell in the 270 to 360 deg region.

In Figure 6 we present the three power spectra for this shell. Shown are the spectrum for the original uncoated shell (two of the nine sets of trace data were excluded because of especially strong tip/shell interaction), the spectrum of the as coated shell, and the modified spectrum after a few isolated debris spikes were mathematically removed from the traces. This last step is necessary in order to examine the intrinsic surface finish of the capsule, and is especially justified because of the heavy handling the shell underwent during multiple characterizations. The full sets of traces for this shell are shown in Appendix C. The primary point to be made is that the coated shell shows better intrinsic power spectra, consistent with the differences in the trace profiles.

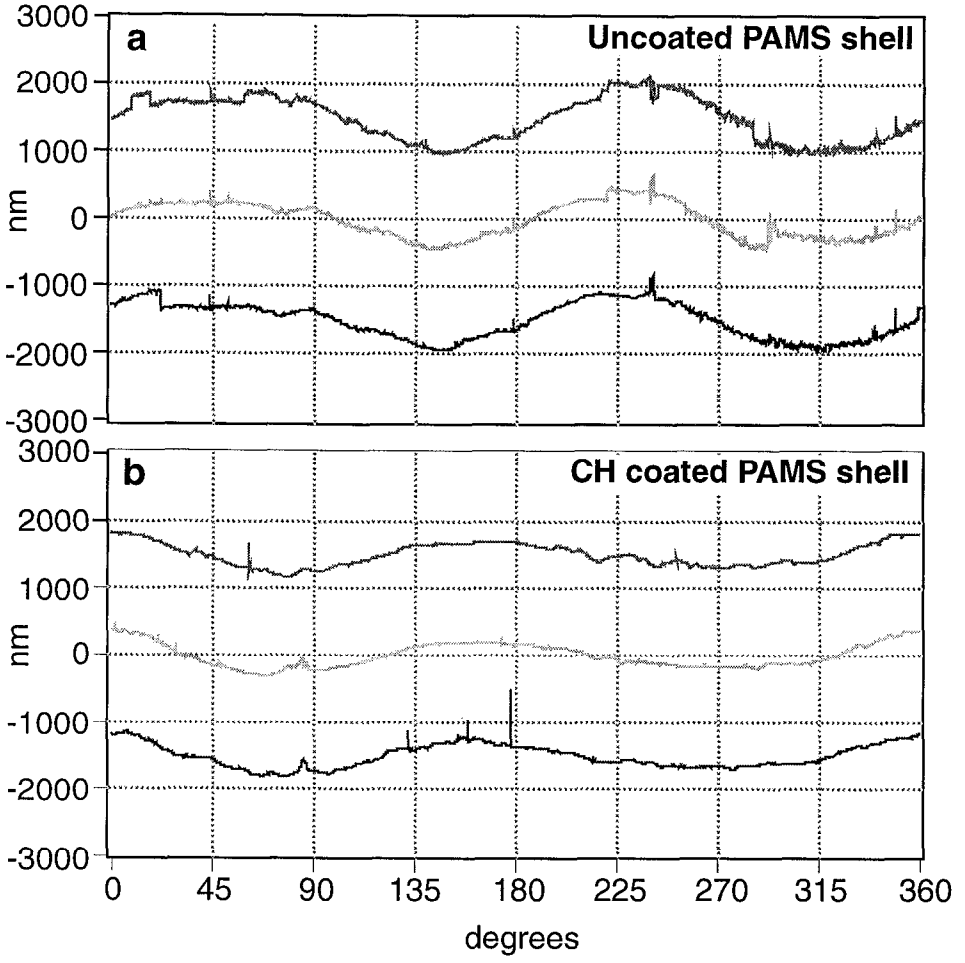

Figure 5. a) A set of 3 traces from a bare PαMS shell. b) Another set of traces from the same shell after coating with a sub-micron layer of plasma polymer.

Topical Investigations and Discussion

Density Matching - General Considerations

Detailed fluid density measurements of the relevant materials have been made with an Anton Paar DMA 5000 Density Meter. This meter uses vibrational frequency changes of a solution-filled quartz "U" tube to measure densities at temperatures from 0 to 90 °C. Appendix B is a compilation of the density data we have taken on the solutions used in our process. The typical temperature range of interest was from 20 to 65 °C.

There are two aspects of density matching to consider, the match of the inner water (W_1) to oil (O) and the match of the compound drop (W_1/O) to the bath (W_2). The former can in principal be matched at the initial time by control of temperature and PαMS concentration. However our typical initial conditions of 45 °C and 13 or 18 wt % PαMS in FB represent a density mismatch of about 0.02 to 0.025 g/cm^3 (oil phase

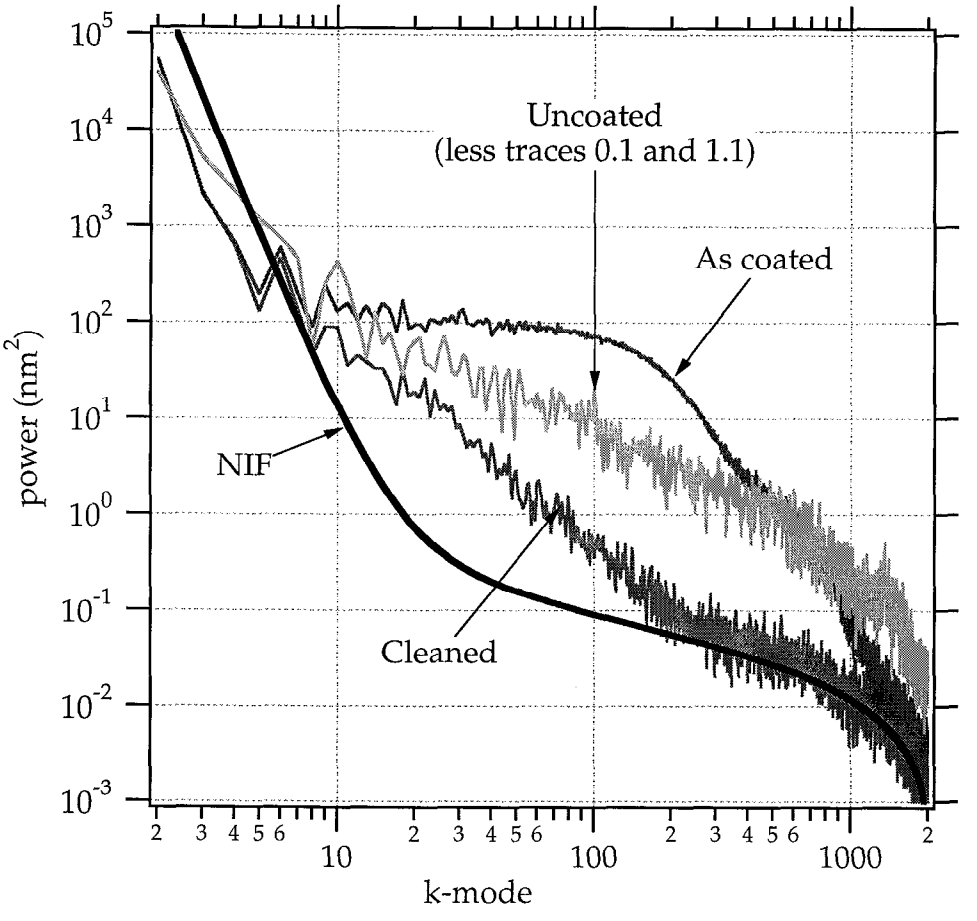

Figure 6. Power spectra of shell PαMS -1113 before overcoating, as coated, and after a few debris spikes have been mathematically removed from traces (See Appendix C).

heavier) as can be seen from the data in Appendix B. As time proceeds and the oil phase becomes more concentrated the density difference increases. However this difference may not play a significant role. Although McQuillan has shown a clear correlation between a wall thickness P_1 and out of round,[15] it is not clear that a P_1 is produced by a small density difference. Even in the case of perfect density matching, one might still expect an unperturbed water core to execute a random walk through the oil phase, leading to a P_1 defect. However Norimatsu[16] has proposed that there are core centering mechanisms associated with the shell agitation, and these mechanisms may overcome small density differences. Clearly the experimental results are that for good quality shells the P_1 shell wall thickness defect is very small.

We have found the matching of the composite (W_1/O) droplet density to the bath to be much more critical for reducing the P_2 out of round of the final shell. The

[15] B. McQuillan, presented at the April, 1998, Target Fabrication Specialists' Meeting in Jackson Hole, WY.

[16] T. Norimatsu, "Modeling of the Centering Force in a Compound Emulsion to Make Uniform Plastic Shells for Laser Fusion Targets," presented at the April, 1998, Target Fabrication Specialists' Meeting in Jackson Hole, WY, and accepted for publication by *Fusion Technology*.

likely deformation mechanism is gravitational sag, and has been briefly discussed earlier in connection with eq 1. Because the oil phase density is changing during the drying, a density match at all times is not feasible, though it could be improved by a careful manipulation of the bath temperature. However it is useful to examine the time dependent density of the compound droplet, and this can be done as follows.

For the purposes of the calculations below, we will assume that once formed the volume of water in the core and the amount of polymer in the oil phase do not change. The latter is clearly true, but as will discussed later there is good evidence that the volume of core water does change perhaps in part due to diffusion through the oil phase. We will examine the possible effect of this on density matching later.

For the compound droplet its time dependent composite density, $\rho_{cd}(t)$, is clearly

$$\rho_{cd}(t) = \frac{m_w + m_o(t)}{V_w + V_o(t)} \tag{3}$$

where m is the mass and V is the volume of the inner water (w) and oil (o) phases. Clearly m_0 and V_0 are time dependent due to the drying process. Let r be the radius of the inner water droplet (assumed constant) then

$$V_w = \frac{4}{3}\pi r^3 \quad \text{and} \quad m_w = V_w \rho_w \tag{4}$$

where ρ_w is the temperature dependent density of water. At the time of formation the volume of oil, $V_o(0)$, can be characterized by the initial wall thickness of the oil layer, which we will call $d(0)$. From this clearly

$$V_o(0) = \frac{4}{3}\pi\left[(r + d(0))^3 - r^3\right] \tag{5}$$

and if the initial concentration of polymer is given by $c(0)$, where c is given in units of g polymer per cm^3 solution (i.e. a 13 wt/vol % solution has c = 0.13) then the mass of polymer, m_p, is given by $m_p = c(0)V_o(0)$. Since m_p doesn't change with time, we can express $V_o(t)$ as

$$V_o(t) = m_p \,/\, c(t) \tag{6}$$

and $m_o(t)$ as

$$m_o(t) = \rho_o(t)V_o(t) = m_p \frac{\rho_o(t)}{c(t)} \tag{7}$$

Using these expressions we can rewrite eq 3 as

$$\rho_{cd}(t) = \frac{m_w + m_o(t)}{V_w + V_o(t)} = \frac{m_w + m_p \dfrac{\rho_o(t)}{c(t)}}{V_w + \dfrac{m_p}{c(t)}} \tag{8}$$

The required input to use this expression, in addition to the well-defined quantities at time zero, is the relationship between the $c(t)$ and $\rho_o(t)$. Let us first point out that $c(t)$ changes from its initial concentration, $c(0)$, typically 0.13 or 0.18 g/cm^3, to a final "concentration" equal to the density of pure polymer; for PαMS this is 1.075 cm^3 at 20 °C. Thus, though we don't know the actual time evolution, we can plot the compound droplet density as a function of PαMS concentration, over the range from the initial concentration to dry polymer. What is needed then is the density of these PαMS solutions.

Data exist (Appendix B) for pure FB as well as 0.13 and 0.18 g PαMS /cm^3 solution at various temperatures, but obtaining ρ_o at higher concentrations is problematic because solutions of known concentration cannot be easily prepared. However, a set of measurements (Appendix B) were made on samples with concentrations between 0.32 and 0.41 g PαMS /cm^3 as follows. A solution of approximately 0.30 g PαMS /cm^3 in FB was prepared, and then allowed to slowly evaporate. After some time, a ~3 mL sample of was removed from the bulk solution, now at a higher concentration than the original solution. The current concentration was determined by mass: approximately 1 mL of the solution was placed on a piece of aluminum foil, and immediately weighed, while the rest of the sample was injected into the densitometer for analysis. The sample on the foil was then dried to constant mass in a 60 °C oven over several days. The measured density of the solution at 20 °C was used to calculate the original volume of the solution on the foil, and thus the wt/vol concentration was calculated from this volume and the mass of the dried PαMS. We were unable to exceed concentrations of about 0.40 g PαMS /cm^3 in FB because these more viscous solutions are prohibitively difficult to inject into the densitometer.

We have fit the density as a function of concentration data along with the density of pure solvent and pure polymer as shown in Figure 7. The density (and concentration) of pure PαMS at 45 °C was taken as 1.07 g/cm^3 consistent with a 1.075 g/cm^3 density at 20 °C and the literature value of 2 x 10^{-4} K^{-1} for the volume expansion factor for polystyrene.[17] In the absence of the pure polymer data there is no reason to trust the quadratic fit any more than the upper (brown) linear one, but to use eq 8 through dryness requires that we have the correct value for the density of the dry polymer, thus we will use both the quadratic fit and the lower linear "fit" in the discussion that follows. Use of the lower (green) linear fit gives qualitatively the same results as the quadratic fit under typical experimental conditions as shown in Figure 8.

[17] Brandup and Immergut, eds, *Polymer Handbook*, 2nd ed.

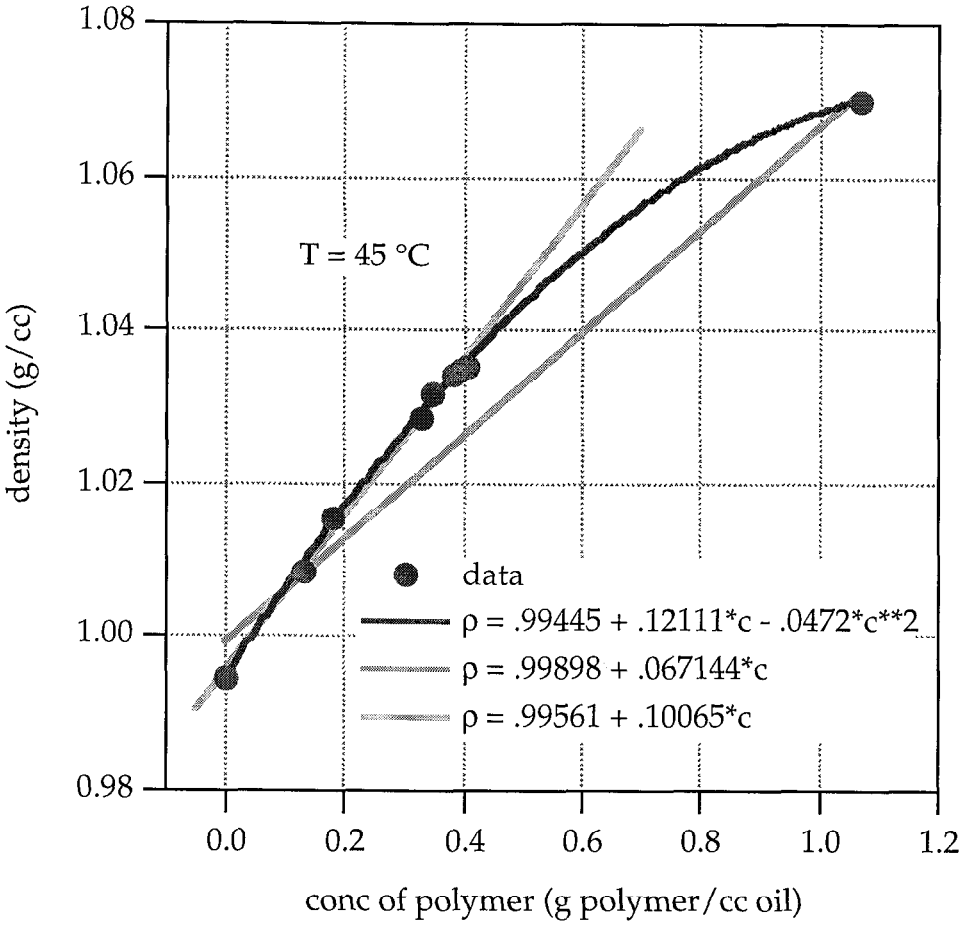

Figure 7. Shown are two fits to the density of PαMS in FB solutions as a function of concentration at 45 °C.

In the data shown in Figure 8a we have taken the inner core radius, *r*, to be 0.1 cm, the initial PαMS concentration, *c*(0), to be 0.13 g PαMS /cm^3, and the temperature to be 45 °C. Shown are curves for different initial wall thickness of the oil phase from 50 to 500 μm, which at the stated initial PαMS concentration correspond to final dry wall thickness (at 20 °C) of 6.3 to 87.8 μm, respectively. There are some differences between the linear and quadratic fits at thicker initial layers. But most important is to note that a) initial layer thickness has a significant effect on the composite density and b) that the change in density as a function of polymer concentration also depends upon the initial layer thickness. For the data presented here an initial layer thickness in the vicinity of 200 to 300 μm gives a roughly flat profile (especially for the linear approximation), due primarily to the fact that the initial and final densities are about equal. For much thicker initial layers the initial and final densities are significantly different, thus requiring a slope in the density curve. Noted in the left margin are the densities of a 2% PVA and 2% PVA plus 1% NH_4NO_3 bath at 45 °C. The latter is very close to the 250 μm initial layer thickness density and thus would represent a reasonable density match. Thinner walled shells would tend to float in this bath, which is catastrophic if they reach the surface.

In Figure 8b we show the effect of capsule size on the composite W_1/O density. In this case we have fixed the initial oil wall thickness at 250 μm, and varied the inner

core water droplet diameter from 1 to 5 mm. The 250 μm initial oil phase wall thickness with a polymer concentration, *c*, of 0.13 would produce a dry polymer wall of 44 μm on the 1 mm droplet and 33 μm on the 5 mm droplet. Note that the composite density becomes less sensitive as the droplet size increases, a result due to the increasing dominance of the water droplet on the composite density.

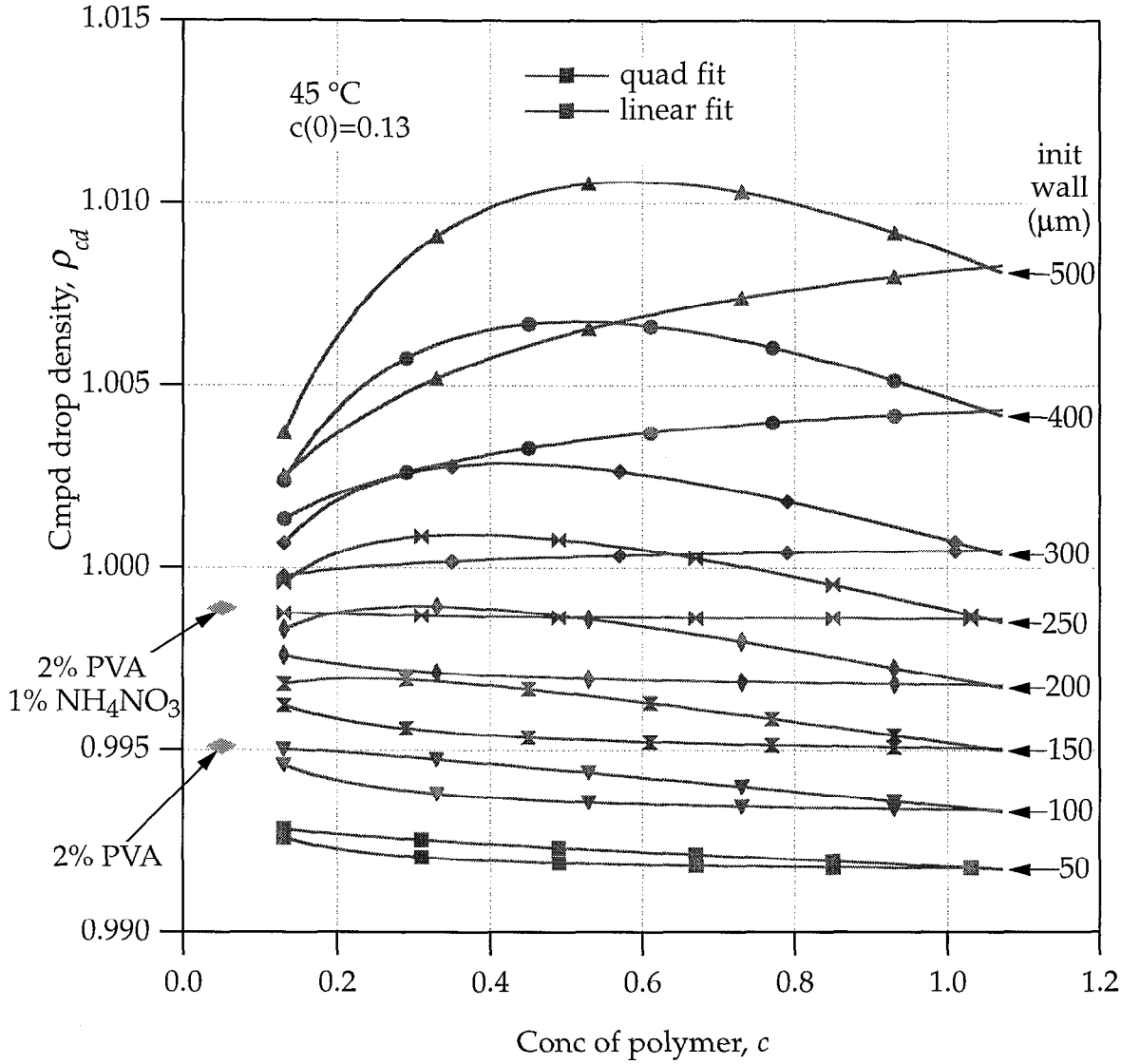

Figure 8a. Shown is the density of the compound droplet as a function of polymer concentration for different initial wall thickness (indicated at right), using both the linear and quadratic approximation for oil density as a function of concentration.

It is important to point out that these calculations are at best illustrative of the effects that one will see experimentally. As noted initially, the loss of water from the core is not taken into consideration. The effect is relatively small, as shown in Figure 9. In this example we have taken the linear fit data for the 250 μm initial wall from Figure 8a and recalculated the compound droplet density with the condition that 15 or 30 % of the core water is lost during the period up to a polymer concentration of 0.7

g/cm^3. The 30% loss is consistent with the wall thickening data which will be presented later. Figure 9 (scale same as in Figure 8) shows that the effect on the compound drop density is relatively small. It can also be noted here that decreasing the size of the inner water droplet increases the compound drop density, while increasing it decreases the density.

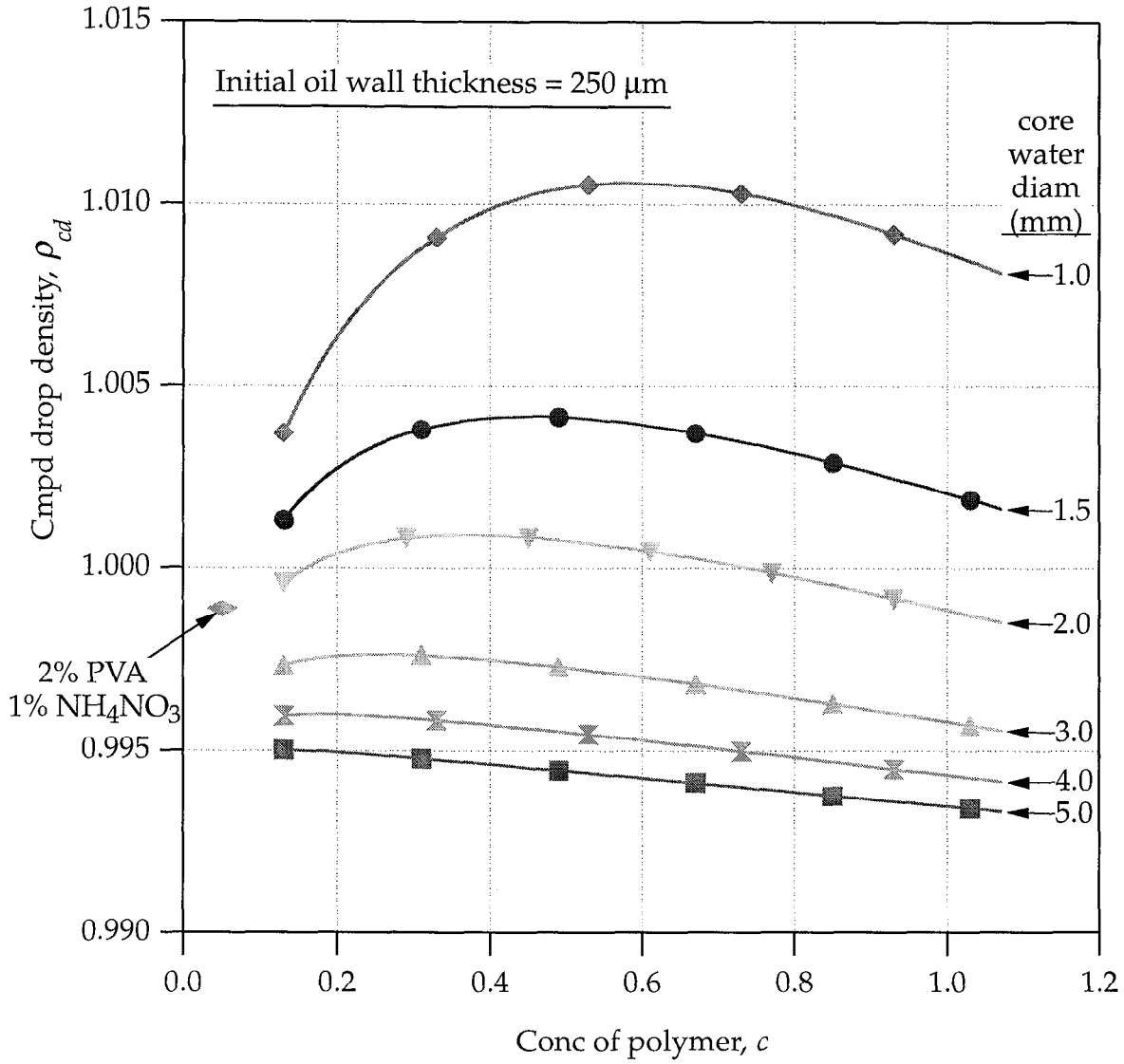

Figure 8b. Shown is the density of the compound droplet as a function of polymer concentration for different core water diameters (indicated at right). In each case the initial oil wall thickness was taken as 250 μm, and we have used the quadratic approximation for oil density as a function of concentration.

The calculations we have presented were done at 45 °C and are representative. At higher temperatures the densities of all components decrease. However the density of the oil phase decreases more rapidly, thus relative to the aqueous bath the compound droplet becomes lighter and the best density matching condition would occur for a thicker initial wall.

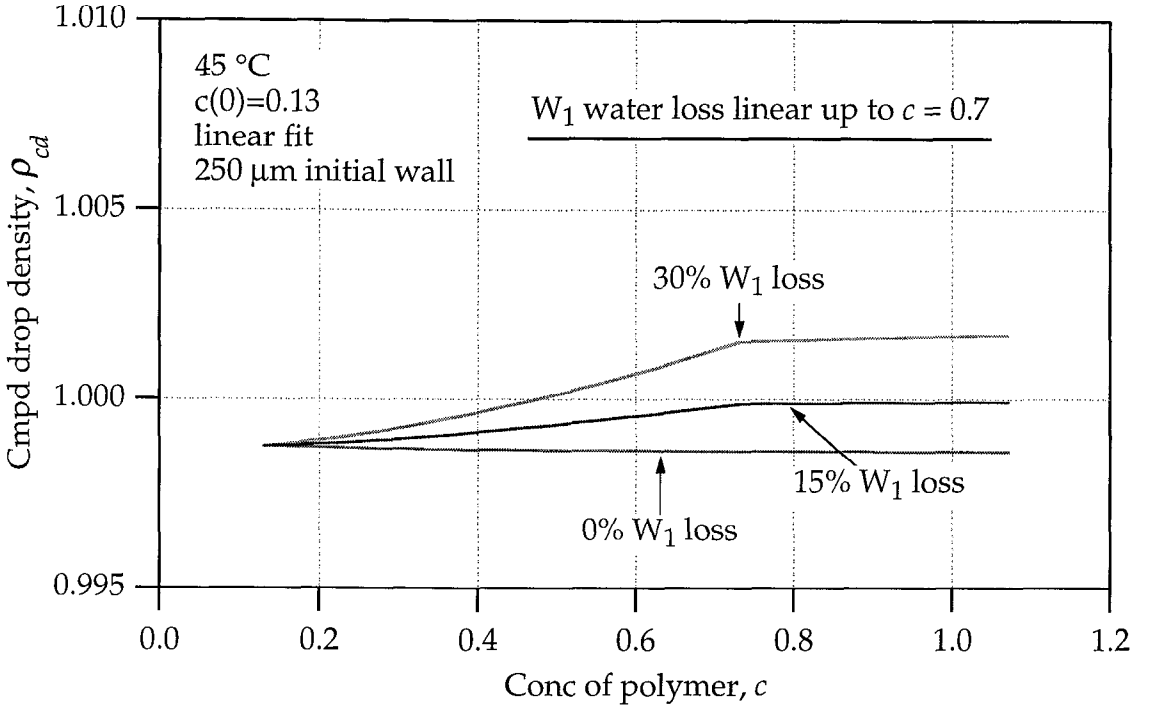

Figure 9. Effect of inner core water loss on the compound drop density.

In summary these somewhat idealized calculations represent useful guides for designing real experiments and interpreting experimental results.

Density Matching - Experiments

A number of individual studies with a focus on density matching concerns have been performed, and their results are discussed here. In most cases they represent only a starting point or a small piece of a bigger puzzle.

As mentioned at the beginning of the Density Matching - General Considerations section above, there is a density mismatch of the core fluid and oil phase of about 0.025 g/cm^3. One obvious remedy is to add a little D_2O to the core fluid to increase its density to match the oil phase. This was attempted by Ken Hamilton several years ago and again earlier this year when we had better control over the process. However these experiments were uniformly unsuccessful, stable encapsulated droplets could not be maintained through the cure. We believe the reason may be that there is relatively rapid water transport through the oil phase, and that the heavier D_2O moves slower than the H_2O leading to a flux of water into the core causing rupture. We have no experimental evidence for this hypothesis other than the observed shell instability, and believe that a better understanding of water transport through the oil phase is a valuable objective. This topic will be discussed more fully below in the section entitled Shell Wall Thickness and Core Water Transport.

We have examined the issue of density matching of the composite W_1/O droplet with the bath in a number of ways. Shown in Figure 10 is a scatter plot of the average batch MOOR as a function of the density of the initial W_1/O composite droplet. This latter quantity was back-calculated from the dimensions of the final dry shells, assuming no water loss from the core during cure. Though scatter is clearly the

operative word, there seems to be some weak correlation. However the density of the bath under these conditions is about 0.999, and one might expect the minimum OOR to occur for a composite droplet density equal to the bath density. Several factors must be considered, however. First, as discussed in a later section, there is core water loss during cure. This has the effect of increasing the density and would thus shift the displayed data to higher densities. Second, the desired density match condition is when the shell is beginning to harden. At this point its density has increased, again a move of the displayed data in the correct direction. Lastly, shells that were formed significantly *less* dense than the bath will float and thus not survive. In this sense the data shown can only be for shells that were more dense than the bath, the best match thus occurring for the lowest calculated density for surviving shells.

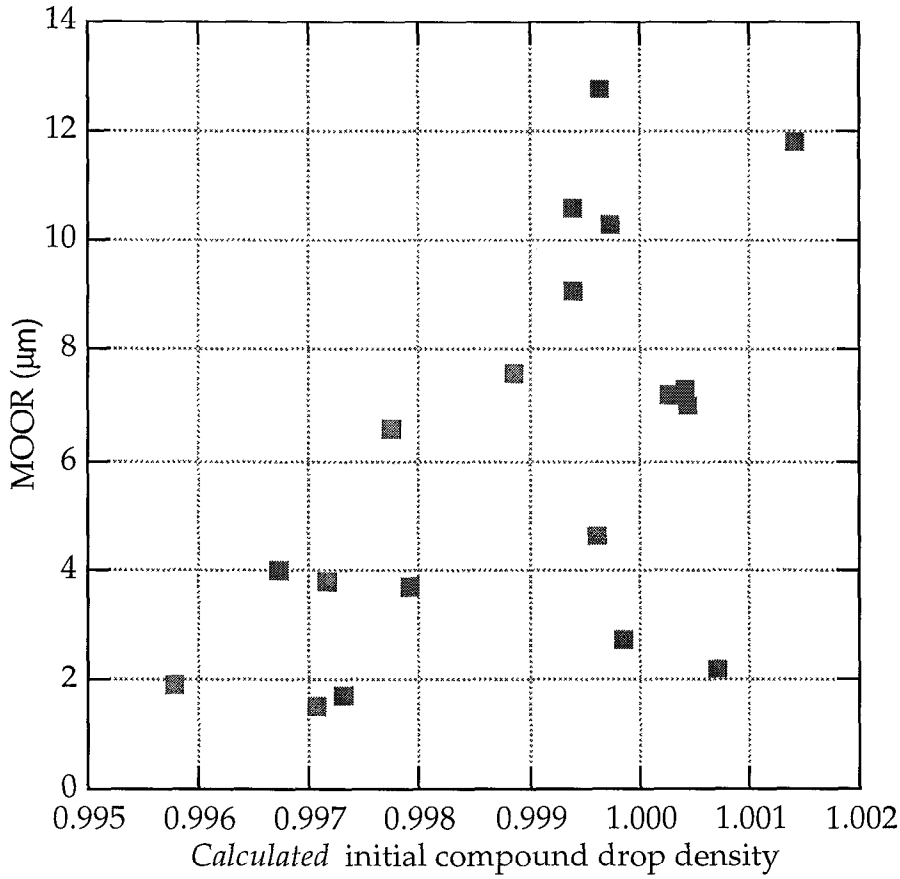

Figure 10. Batch average MOOR as a function of the density at 45 °C of the initial W_1/O composite droplet.

Organic Solvent Choice.

The solvent system originally used in the development of the microencapsulation process at Osaka was a mixture of two solvents, typically benzene (B, ρ = 0.879 g/cm^3, BP = 80 °C) and 1,2-dichloroethane (DCE, ρ = 1.2521 g/cm^3, BP = 83.5 °C). One of the motivations for using this solvent system instead of fluorobenzene was improved control over the initial density of the solvent phase, allowing for better density matching between the microencapsulated shell and the surrounding water. The two-

solvent system was also believed to have higher interfacial tension with water than fluorobenzene. Because interfacial tension is the primary force than promotes sphericity, it would be advantageous to produce the highest interfacial tension possible through our choice of solvents.

However, the solubilities of B and DCE in water are quite different, 0.1791 wt% and 0.81 wt%, respectively, and the density of the two-solvent oil phase might be expected to change significantly during the drying process. Thus, although the composition of the oil phase can be carefully chosen to density-match with the inner water phase, or to match the overall shell density (W_1/O) with the surrounding water (W_2), this composition may change due to the unequal solubilities of the two solvents. This will be particularly true for encapsulated droplets delivered into an aqueous bath containing no dissolved organics.

Once the aqueous bath becomes saturated with the oil phase, in a ratio of approximately 1:4 (B:DCE) based on the solubility of each component, the composition in the oil phase will have changed slightly, becoming enriched in benzene because DCE is more soluble in water. From this point on, further losses from the oil droplets will be controlled by the rate of evaporation from the bath surface. This rate of evaporation of each component of the oil phase is determined by Raoult's Law $p_A = X_A p_A^\circ$, where p_A° is the vapor pressure of the component, and X_A is the mole fraction of the pure component in the oil droplet. The reason why the mole fraction of each component in the oil phase is used instead of the mole fraction of each organic in the aqueous phase can best be understood by considering the equilibrium state of the system, where the organic vapor is in equilibrium with the organics dissolved in the aqueous phase, which are also in equilibrium with the organic phase in the oil droplet. Thus, the chemical potentials of the organic components in all three "phases" are the same, and one can argue that the organic phase in the droplet is in a direct equilibrium with the organic vapor. When more organics are evaporated from the surface of the aqueous bath, this vapor will have a composition determined by the composition of the oil droplet, and the vapor pressures of the two components, which in the case of B and DCE are very similar. Once the aqueous phase is saturated, one expects the composition of the organic phase in the droplet to remain nearly unchanged, also because of the similar pure component vapor pressures.

Because the overall magnitude and effect of this solubility difference was not completely understood, a study was conducted to determine the change in composition (and therefore density) of the oil phase due to differential solubilities into water. The density of the oil phase in a microencapsulated shell is almost impossible to measure directly, so extractions of an aliquot of oil into water were performed in a separatory funnel, using a ratio of oil to surrounding water approximately modeling the microencapsulation process. The two phases were shaken thoroughly, then allowed to separate while submerged in a temperature bath, after which the oil phase was removed and the density was measured. Several parameters of the experiment were varied, including the temperature, saturation of the aqueous phase with the oil mixture, and addition of salt to the aqueous phase. Based on the solubility of each solvent in water, a theoretical density change of -0.039 g/cm^3 can be calculated. An average density change of -0.026 g/cm^3 was determined for the experimental runs, which is

approximately 66% of the theoretical change.[18] Thus, there is a significant change expected in the density of the oil phase of the two-solvent system during the drying process, most likely caused by the organic components saturating the aqueous phase, but the effect of this change on producing spherical shells is yet to be determined. It should be emphasized that in these experiments the aqueous phase was initially unsaturated; presaturation of the aqueous phase will essentially eliminate this density fluctuation.

PαMS versus PS

During this past year we have used both PαMS and PS in shell fabrication. The PS used was brought from Japan and is a polydisperse sample, M_W = 100-140K, while the PαMS is a M_W = 395K monodisperse sample. The use of PαMS is of course necessary for the "decomposable mandrel" route, however the differences and similarities between PαMS and PS may be of interest in trying to determine what the relevant process variables are. In general we have shown that good quality shells can be prepared from PS using either the traditional Japanese B:DCE solvent system or FB, as shown by batches 1084 and 1101 in Appendix A. AFM trace data for two shells from PS batch 1101 are shown in the Appendix, they show mode 2 sphericity of less than 0.5 μm, better in general than we obtain for PαMS shells. The traces do show significant middle mode roughness. The power spectra for these two shells as well as two PαMS shells from batch 1059 are shown in Figure 11 below.

Critical for good PS shell quality has been appropriate density matching conditions, which are different for PS, since it has a slightly lower density than PαMS. We also note that the T_g for PS is about 100 °C in contrast to about 170 °C for PαMS. This is likely to affect at what degree of "dryness" the shell hardens as the plasticizing solvent is removed. The roles of the molecular weight and polydispersity (for PS or PαMS) are unknown, and have largely been unexplored.

Droplet Deformation

We conducted a number of video capture experiments to examine droplet deformations of individual fluid homogeneous and microencapsulated droplets. In these experiments a special cell is used to film a single droplet suspended in a temperature controlled aqueous bath. Captured images of the droplets are then analyzed for their dimensions.

In Figure 12 we show a series of homogeneous droplets of 18 wt/vol % PαMS in FB suspended in a 70 °C aqueous bath containing 1 wt/vol % NH_4NO_3 and 2 wt/vol % PVA. This is close to the density matching condition and the droplet is actually suspended. In each case the droplet is slightly deformed so that the vertical axis, d_v, is larger than the horizontal axis, d_h, due either to a small density mismatch and/or possible slow motion of the droplet. Using eq 1 and assuming an interfacial tension, γ, of 10 dyne/cm would indicate values of $\Delta\rho$ from 0.012 to 0.004 g/cm^3 for the pictured

[18] For a complete description and discussion of this extraction experiment, please see A. Hassel, M. Takagi and B. Cook, "Exploration of composition and density changes due to the solubility of solvents and water in the dual-solvent system", TAT 98-049.2, October 13, 1998.

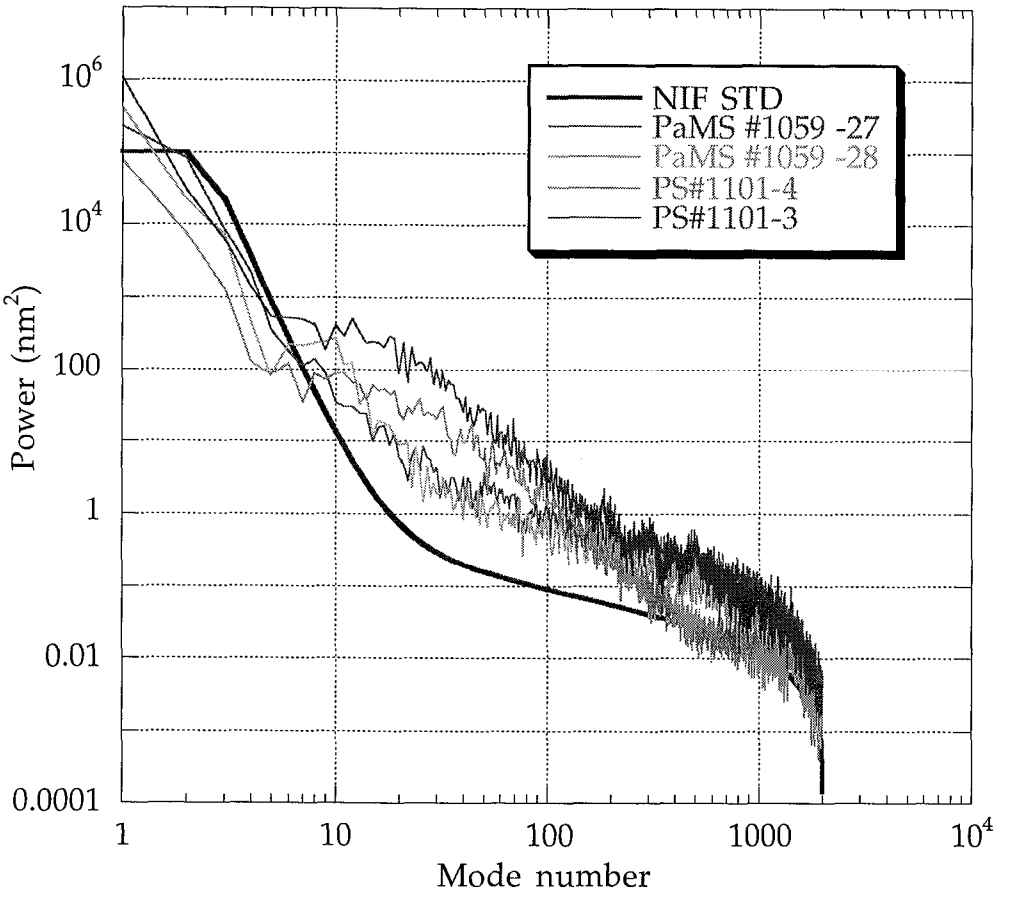

Figure 11. Power spectra of PS and PαMS shells

droplets as the size increases. Smaller γ(which is likely) would mean smaller $\Delta\rho$'s. Note that the magnitude of the deformation increases with droplet size.

Similar experiments were performed for microencapsulated droplets, and a similar size dependence was observed but the magnitude of the deformation was considerably greater. In these experiments the composite density of the O/W_1 droplet was matched to the bath (allowing it to be suspended) but under these conditions the inner water phase (W_1) is lighter than the oil (O) phase and it rises to the top, perhaps distorting the compound droplet shape giving rise to the greater deformation.

To probe this issue further we made a series of measurements on suspended droplets in which the temperature was varied to achieve near density matching between the W_1 and O phases as shown in Figure 13. The temperature range of the three photos is less than 1 °C, demonstrating the sensitivity of density matching to temperature. In this experiment we have measured the horizontal and vertical outer diameters of both the oil phase and the inner water phase. We find that when the inner droplet is well centered the overall droplet deformation is at a minimum. One can also see that in this experiment that most of the distortion of the outer oil phase is seen also in the inner water phase.

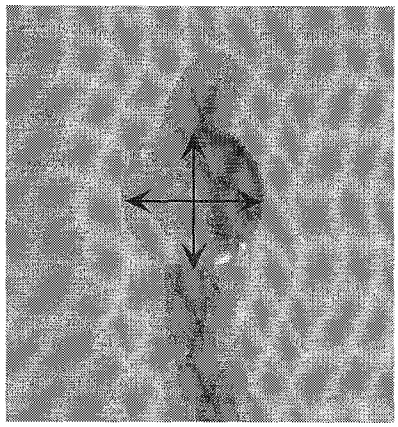

d_h = 1572 μm
d_v = 1579 μm
Δd = 7 μm

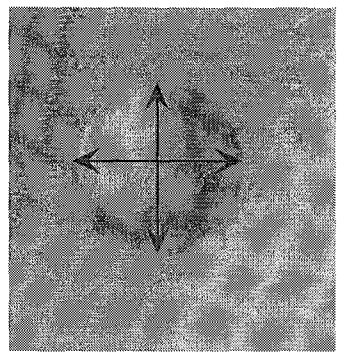

d_h = 1861 μm
d_v = 1870 μm
Δd = 9 μm

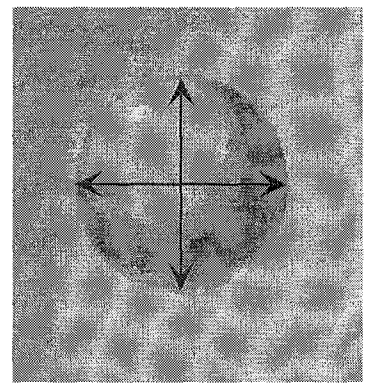

d_h = 2314 μm
d_v = 2333 μm
Δd = 19 μm

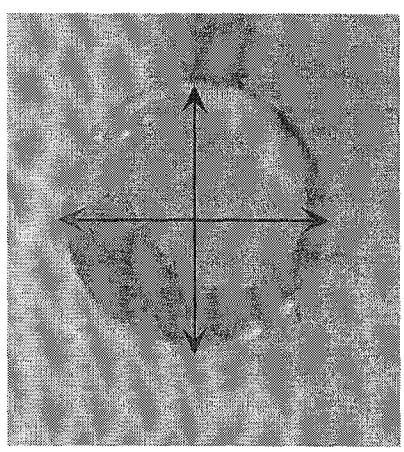

d_h = 2893 μm; d_v = 2913 μm
Δd = 20 μm

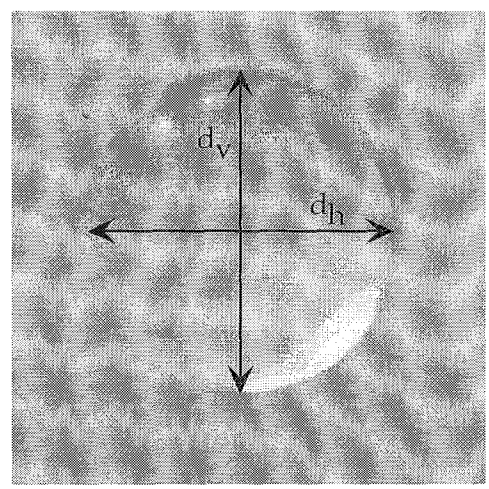

d_h = 3502 μm; d_v = 3531 μm
Δd = 29 μm

Droplet: 18 wt/vol % PαMS in FB
Bath: 1 wt/vol % NH_4NO_3 in 2wt/vol % PVA
T = 70 °C

Figure 12. MOOR of oil drop is dependent on droplet size.

Interfacial Tension

The primary force resisting deformations (at any mode number) from sphericity for the fluid droplet is the interfacial tension between the oil phase and the aqueous bath, thus any changes that can be made to increase the interfacial tension should lead to higher sphericity at all modes. The interfacial tension is controlled by the nature of the aqueous bath and oil phase. The addition of PVA to the bath probably decreases the interfacial tension somewhat, while the addition of salt may increase it. In the case of the oil phase the only parameter is the solvent choice, and, as will be described below,

O: 18 wt/vol % PαMS in FB
W_1: 6 wt/vol % NH4NO3
W_2: 7 wt/vol % NH4NO3, 2 wt/vol % PVA

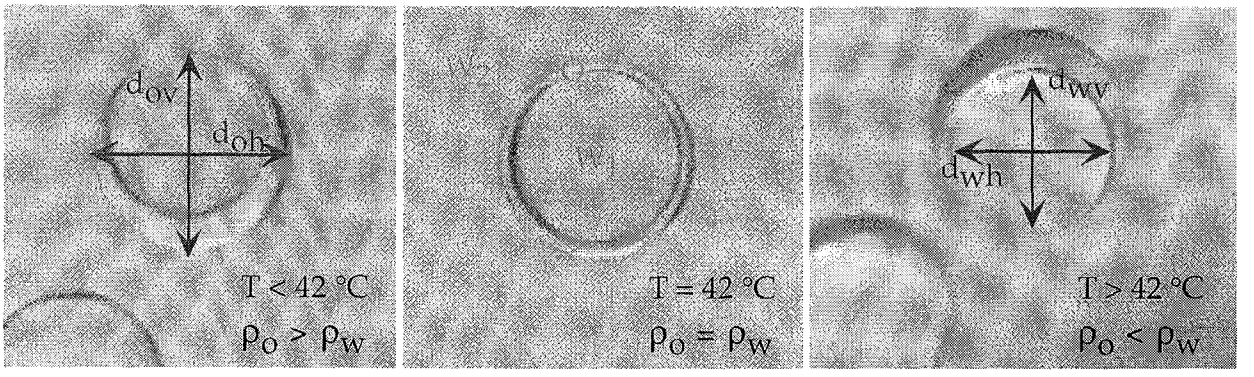

d_{oh} = 2092 μm	d_{oh} = 2092 μm	d_{oh} = 2116 μm
d_{ov} = 2139 μm	d_{ov} = 2098 μm	d_{ov} = 2166 μm
Δd_o = 47 μm	Δd_o = 6 μm	Δd_o = 50 μm
d_{wh} = 1662 μm	d_{wh} = 1809 μm	d_{wh} = 1691 μm
d_{wv} = 1704 μm	d_{wv} = 1813 μm	d_{wv} = 1738 μm
Δd_w = 42 μm	Δd_w = 4 μm	Δd_w = 47 μm

Figure 13. When the inner core water is well centered the droplet deformation is a minimum.

an early indication that a change to the B/DCE solvent system may increase the interfacial tension relative to FB motivated much of our work. Thus we have undertaken a number of experiments to determine the interfacial tension between various phases, and the results are outlined below. It is fair to say that the data is at best inconsistent, but this is an area that needs continued attention.

The increase in interfacial tension associated with the B/DCE system was indicated by initial measurements made by the Kruss company in 1997, which showed B/DCE-water to have an interfacial tension of 42 dynes/cm, compared to 10 dynes/cm for FB-water. However, the solutions used for this analysis were not distilled, and may have contained impurities, which could greatly affect the interfacial tension. A second set of measurements have recently been made by ThetaDyne (formerly Kruss) using clean solvents which show that the first analysis was most likely incorrect. This will be discussed below.

As a qualitative measure of interfacial tension we measured phase separation velocities (see Figure 14) as follows. Equal quantities of oil and aqueous (W_2) phases are added to a 100 mL graduated cylinder and vigorously shaken to form an emulsion, causing a huge increase in the interfacial area. The cylinder is then set up right and allowed to separate. The volume of the separated aqueous phase is recorded as a function of time. From this a separation velocity (mL/min) can be calculated.

Studies were conducted with both FB and 1:1 B/DCE solvents at a variety of PVA concentrations. The results are shown in Figure 15. Also shown on the plot is the aqueous PVA/air surface tension. The lowest concentration of PVA shown is

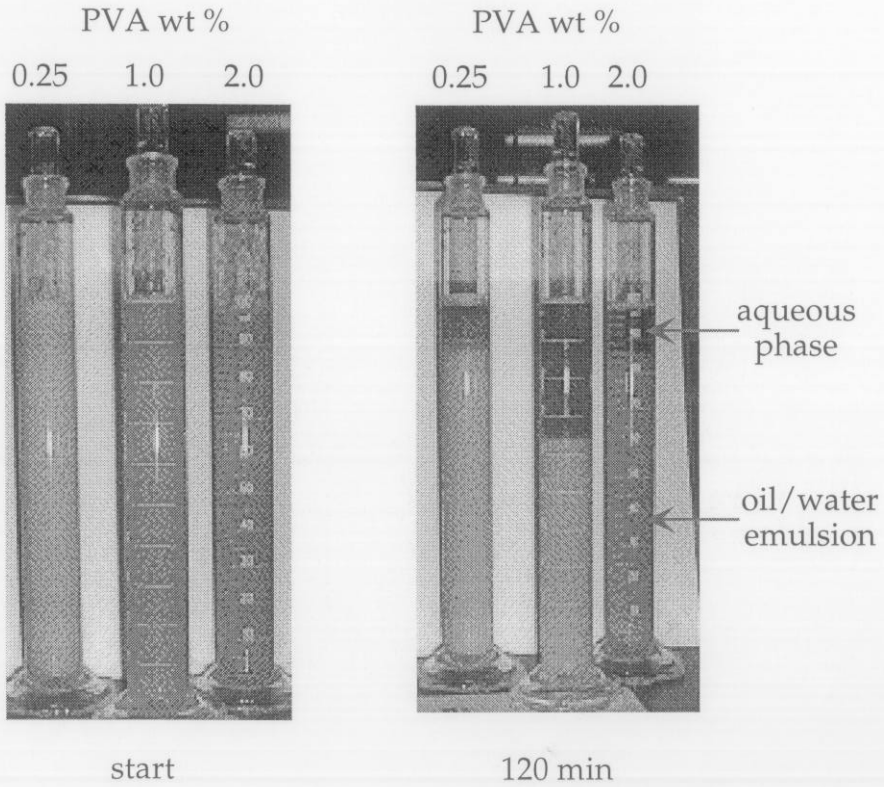

Figure 14. Method of measuring separation velocity. Green dye has been added to help in visualization.

0.1 wt/vol %; without any PVA the phases separate essentially instantaneously. There are several features worth noting. First, for both organic solvents there seems to be an initial dip and then a maximum at about 1 wt/vol %. Second, the apparent higher separation velocity of the 1:1 B/DCE at lower PVA concentrations was initially thought to be an indication of higher interfacial tension. However this conclusion is unwarranted since the density difference between the aqueous phase and 1:1 B/DCE is greater than for FB, and this will certainly increase the separation velocity.

In our laboratory, we have attempted to use the sessile drop method for measurement of interfacial tension. For this type of measurement, a drop of the more dense component is dispensed from a gas-tight syringe into the less dense component and settles on either a wire mesh lining the bottom of a quartz cuvette, or the bottom of the cuvette itself, where it deforms from spherical due to gravity. The amount of deformation is determined by the interfacial tension between the two phases. Once the drop reaches equilibrium, the horizontal diameter at its largest point and the vertical radius from the diameter to the top of the drop are measured, and used with the density difference between the two phases to calculate the interfacial tension, using, for example, eq 1. The dimensions of the deformed drop are determined from a video-captured image of the drop, see Figure 16.

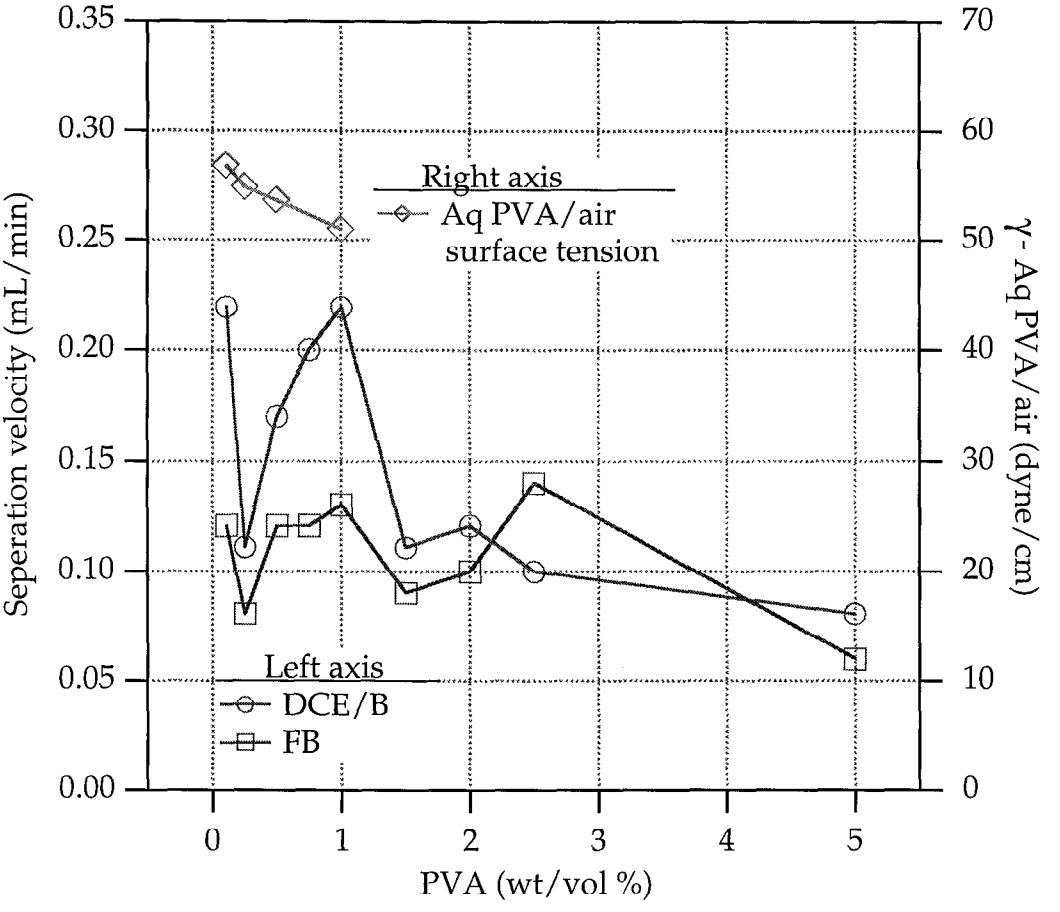

Figure 15. Separation velocity of aqueous phase as a function of PVA concentration.

The results of the interfacial tension measurements made by the sessile drop method have been confusing and inconsistent. The full details have been released separately and will not be repeated here.[19] For some measurements, the drop was allowed to rest on a fine wire mesh, which is useful for temperature-buoyancy studies, but introduces the unknown wire-drop interaction into the system. These results initially appeared to support the preference of B/DCE indicated by the first Kruss analysis, but the results were not conclusive. In addition, the interfacial tension appeared to change with the size of the solvent drop. Interfacial tension should be an intensive property, dependent only on the components of the system and independent of the size of the droplet. Thus, these results were questionable, and did not completely support the preference of B/DCE. Further problems were encountered in finding a mathematical expression to calculate the interfacial tension from the deformed drop dimensions, for two different expressions, both derived for the sessile drop method, gave results differing by more than an order of magnitude.

[19] A. Hassel, "A Summary of Interfacial Tension Measurements Made for the Microencapsulation Process," TAT 99-057.2M, January 6, 1999.

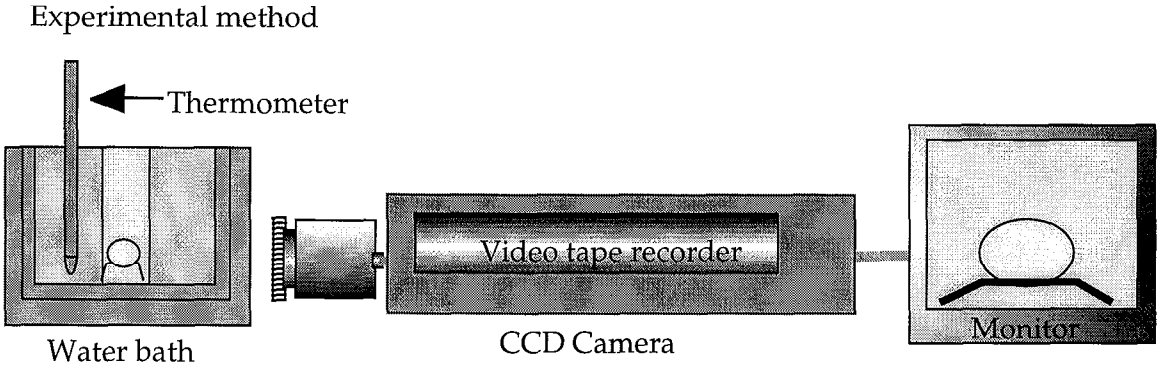

Figure 16. A direct measurement of interfacial tension uses gravitationally induced droplet deformation

The recent analysis by ThetaDyne measured FB-water to have an interfacial tension of 44 dynes/cm, compared to 30 dynes/cm for B/DCE-water. This is opposite of their first analysis, but due to the clean condition of the solvents analyzed (distilled and filtered), this result is believed to be more trustworthy. For the most part, no measurements of interfacial tension made in our laboratory have agreed with these values. One series of measurements, made in a quartz cuvette without a wire mesh, gave values of 21.5 and 8.3 dynes/cm for FB-water and B/DCE water, respectively. While these do not agree completely with the ThetaDyne values, they do show the same general trend, that B/DCE does not appear to create a higher interfacial tension with water than FB, and most likely would not be more useful than FB in creating spherical shells.

We continue to consider interfacial tension to be a key factor in promoting shell sphericity, and plan to make a more careful study in FY99, with focus on modifications to the aqueous phase that lead to increased interfacial tension. First, however, reliable techniques for interfacial tension measurements must be adopted.

Time Dependant Shell Hardening

When initially formed, the fluid microencapsulated shell should be extremely elastic, and have a fast relaxation in response to an externally imposed deformation. However as the shell loses solvent it becomes increasingly viscous, and relaxation times must increase. At this point in the cure it is clear we must be more careful about imposed deformations from the bath hydrodynamics including the action of the stirring device. In order to begin to scope out experiments that will allow us to determine when this time occurs, we conducted a series of preliminary experiments to examine the time dependence of shell drying in the water bath using a crude optical technique as follows.

Shells were produced in the normal fashion, and then after 2 h a selection was removed from the bath into a small dish with a considerably higher surface to volume ratio than in the bath, resulting in an accelerated drying. At a series of subsequent times individual shells were then "squeezed" with a pair of tweezers and the response of the shell after release was recorded on video. Figure 17a shows the results after 20 minutes in the smaller bath. Within 20 s of the release of the tweezers the shell had recovered its original spherical shape, showing no obvious defect due to the imposed deformation. In contrast, Figure 17b shows the results after 40 minutes in the smaller bath. In this case

evidence of the imposed deformation fades much more slowly and is still visible after 2 minutes.

These preliminary experiments demonstrate that deformation relaxation times are clearly cure time dependent. A more thorough and careful study needs to be conducted to determine the relaxation time/cure time relationship. Such studies are being planned for FY99.

Sampling time is 120 min after solvent extraction began.

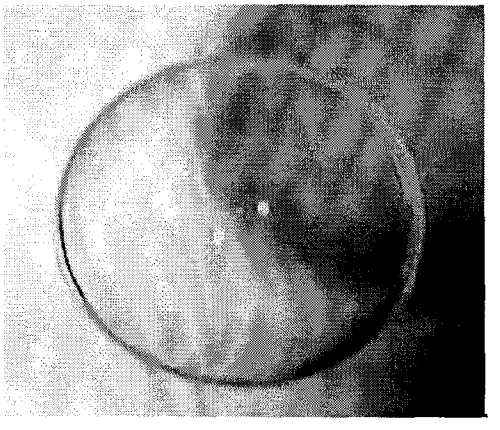

Original W_1/O

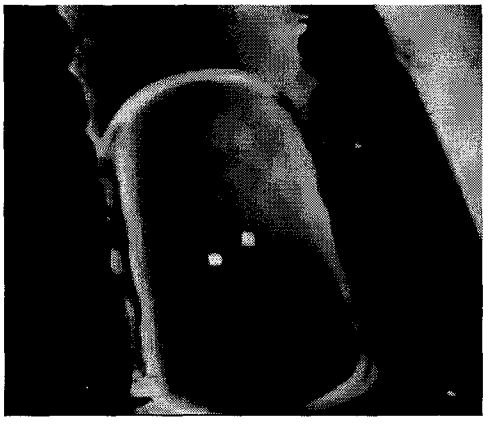

Pick up W_1/O by tweezers
20 min after sampling

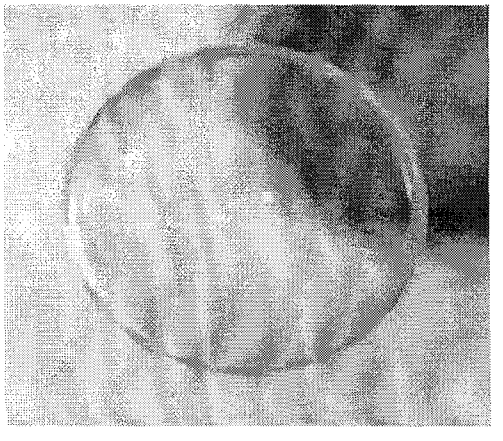

W_1/O after 5 sec

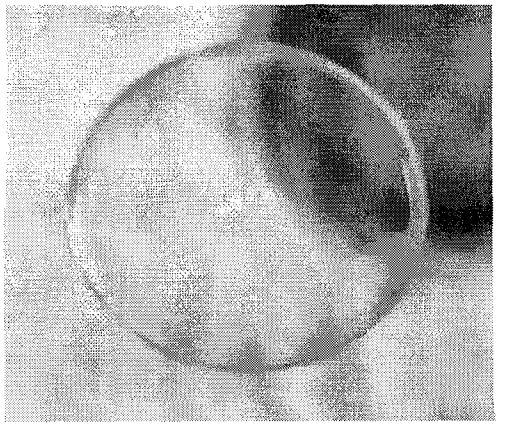

W_1/O after 20 sec

Figure 17a. Shown are photos of a fluid shell that has been in the smaller bath for 20 minutes. After an imposed deformation it recovers in a few seconds.

Sampling time is 160 min after solvent removal step began.

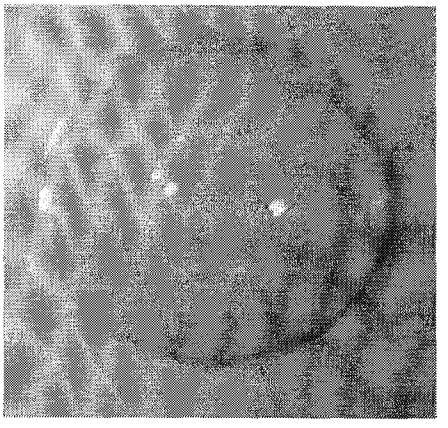

Original W_1/O

Pick up W_1/O by tweezers
40 min after sampling

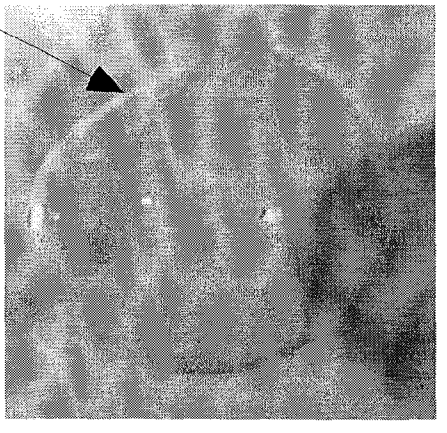

W_1/O after 20 sec

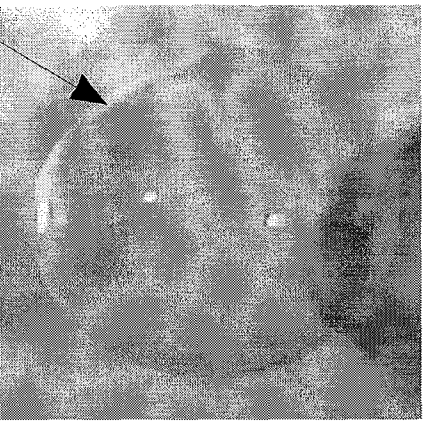

W_1/O after 40 sec

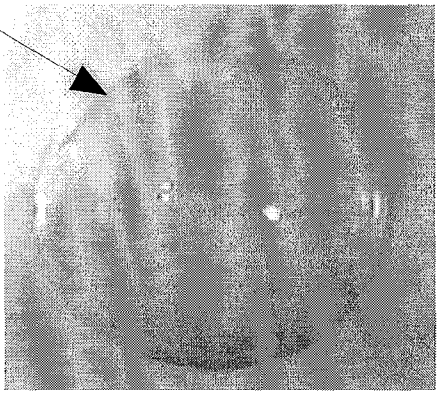

W_1/O after 60 sec

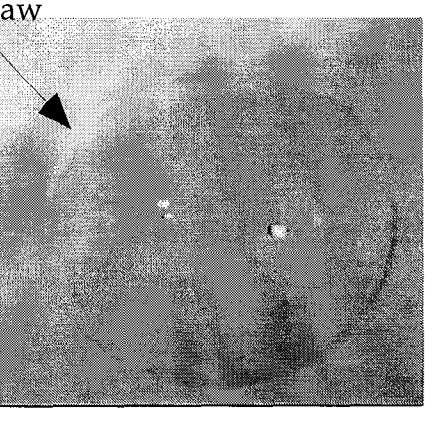

W_1/O after 120 sec

Figure 17b. Shown are photos of a fluid shell that has been in the smaller bath for 40 minutes. After an imposed deformation it has not completely recovered after 120 s.

Shell wall thickness and core water transport.

Shell wall thickness is determined experimentally from the shell mass and outer diameter using a PαMS density of 1.075 g/cm^3. From a knowledge of the relative flow rates of the oil and inner water phases along with the concentration of polymer in the oil phase one can calculate the expected wall thickness. Let

R be the outer dry shell radius (diameter/2)
w be the shell wall thickness
r_r be the ratio of the flow rate of W_1 to the flow rate of O
c_p be the concentration (w/v) of polymer in the oil phase expressed as decimal (i.e. c_p = 0.18 g polymer/cm^3 solution)

Clearly the volume of W_1 delivered to make a shell is

$$V_{w_1} = \frac{4}{3}\pi(R-w)^3 \tag{9}$$

and the volume of *dry* polymer in the shell is

$$V_p = \frac{4}{3}\pi\left[R^3 - (R-w)^3\right] . \tag{10}$$

The volume of oil, V_o, needed to supply this much dry polymer can be calculated from the concentration as

$$c_p = \frac{\text{mass of p}}{V_o} = \frac{V_p\rho_p}{V_o} \quad \text{or} \quad V_o = \frac{V_p\rho_p}{c_p} , \tag{11}$$

where ρ_p is the density of dry polymer. Assuming no losses of W_1 or O during the microencapsulation process it must be true that

$$\frac{\text{w}_1 \text{ flow rate}}{\text{o flow rate}} = r_r = \frac{V_{w_1}}{V_o} \tag{12}$$

and using eq 9-11 one can show that

$$w = R\left(1 - \left[\frac{1}{\left(1 + c_p / r_r\rho_p\right)}\right]^{1/3}\right) . \tag{13}$$

Thus the ratio of the dry wall thickness to the shell radius is a constant that depends only on the polymer concentration, dry polymer density, and ratio of flow rates. For a given batch where these quantities do not change, w/R should be both constant *and* calculable.

However, if we look at some data from runs 1104 and 1105 we find an apparent contradiction. These were runs with very good mode 2 sphericity. For each run several of the characterized shells were also weighed to determine the wall thickness. The relevant data is reproduced in Table II below.

Table II. Shell diameter and wall thickness values

Run 1104

$c_p = 0.18$ $r_r = 1.6/0.8$ $\rho_p = 1.075$ theor (eq 13) $w/R = .0283$

shell	MOOR	R	w(exp)	w(calc from eq 13)	w(exp)/R
1	2.0	2297.7	38.9	32.5	.0339
3	2.4	2319.9	36.9	32.8	.0318
5	2.3	2301.2	38.8	32.6	.0337
7	1.4	2309.3	37.9	32.7	.0328

Run 1105

$c_p = 0.18$ $r_r = 1.6/0.9$ $\rho_p = 1.075$ theor (eq 13) $w/R = .0316$

shell	MOOR	R	w(exp)	w(calc from eq 13)	w(exp)/R
1	1.6	2239.1	42.8	35.4	.0382
3	1.6	2244.0	35.5	35.5	.0316
4	2.1	2211.7	41.8	35.0	.0378
5	2.2	2246.4	47.2	35.5	.0420

Note that for Run 1104 the observed experimental wall thickness and those calculated based on the flow rates are individually consistent, but the experimental walls are 4 to 6 μm *thicker* than the predicted values. One might explain these data by asserting that the flow rate was incorrect, that in fact there was more oil relative to water than thought. Flow rates have been checked carefully, but this is still an area for concern under experimental conditions. The inconsistency in the Run 1105 data, with experimental walls from 35 to 47 μm, all values equal to or significantly greater than the calculated value of about 35 μm, suggests a droplet to droplet consistency problem in addition to whatever is causing the wall thickening seen in Run 1104. Data on flow rates and wall thickness from Barry McQuillan's Omega scale runs show the same trends, thicker walls than one would predict.[20]

A possible explanation for these results is loss of water from the core during drying in the bath due to water transport through the oil phase. We have evidence from our D_2O work (discussed briefly above in the section on density matching) that water transport is probably pretty rapid. In the case of these runs, the bath contains salt, NH_4NO_3, at 1%, as well as PVA. Thus there is a chemical potential (osmotic) driving

[20] B. McQuillan, General Atomics, private communication.

force to have a net flux of water out of the core, thus slightly thickening the wall. Clearly the rate will be dependent on the oil wall thickness. In principle, the magnitude of the flux could be calculated if we had knowledge of the diffusion rate of water through the oil phase (presumably needed as a function of polymer concentration).

We initially tested the idea with a simple experiment, namely putting more salt in the W_1 phase than in the W_2 phase. Assuming the chemical potential effects of the PVA are small, this should lead to a net flux of water into the shell during drying, leading to a wall thinning and perhaps wall smoothing as well. The current possible net flux out may be in part responsible for some of the intermediate mode roughness which is perhaps caused by the shell trying to shrink slightly at a point when the polymer wall has gotten very viscous. We hoped the reversed salt experiment might shed some light on this.

Several batches were prepared, the results from three of them are reported here, full characterization data for these batches are in Appendix A. Table III contains the results for a few of the best shells in terms of sphericity. In general the MOOR of the shells in these batches was poor because the addition of salts upset the density matching conditions, and no effort to reoptimize was made in these preliminary experiments. What is clear, however, is that no shell thinning was observed, and in some case the shells are relatively thicker than those reported above. Again there is also no consistency. The observed continued shell thickening certainly requires us to rethink the water transport model explanation given above. It would appear if these experimental results are to be trusted that there is a different route for shell wall thickening. Our only suggestions at this point are that 1) the relative flow rates have been incorrectly determined and/or are varying during the shell production process and 2) that there is water loss from the core either at the time of encapsulation or due to interaction of the still fluid shell with the stir blades. We believe that these experiments need to be repeated under more controlled circumstances. Specifically the flow rates need to be recalibrated and carefully monitored, and evidence for shell breakup and partial core water loss due to physical interaction needs to be examined. One symptom of this might be a very wide distribution of shell sizes, certainly a tight distribution of shell sizes is inconsistent with random loss of the core water.

Table III. Results of the reversed salt experiment. Selected shells from runs 1138, 1140, 1141 (complete data in Appendix A). In each case the core aqueous phase was 2% NH_4NO_3. The bath for runs 1138 and 1140 contained 1% NH_4NO_3, for run 1141 was salt free.

shell	MOOR	R	w(exp)	w(calc from eq 13)
1138/4	8.1	2086	39	28
1140/2	2.5	2182	51	25
1140/4	2.0	2193	55	26
1141/3	6.3	2256	37	26

FY99 Plans

At the end of December, 1998, work on mandrel development in LLNL laboratories ceased, and the task was transferred to General Atomics where Dr. Masaru Takagi, supported by LLNL, will work with other scientists at GA to improve microencapsulated shell sphericity. A detailed experimental plan will be developed in January. It is clear, however, that the key area to address is middle mode roughness. The source of this roughness (which in fact is very small by any conventional standards) is not completely understood. From the work to date two possible independent sources have emerged. First, there is some evidence that shell interaction with the stir blade, beaker walls, or other shells followed by incomplete relaxation in the hardening shell may leave residual long wavelength defects. Secondly, there may be some shell "crumpling" as it hardens due either to water egress from the core or simply due to some differential hardening from the outside to the inside. Throughout this document we have highlighted certain activities for future experiments. Central to some of these is the accurate determination of the time dependent solidification of the shell, and careful experiments will be planned to elucidate this. Given this information we can then attempt to modify the agitation mode at the time the shell hardens. In addition, as noted earlier, we need to more thoroughly understand the nature of water transport through the oil phase, since this may be both part of the cause of the middle mode roughness as well as a route to its amelioration. Lastly, we need to get a better handle on the nature of the interfacial tension, both in its measurement as a practical matter, and a better understanding of how it can be increased, perhaps by control of the additives added to the aqueous phase as well as possible modification of the organic phase.

Appendix A - Selected Batch and Shell Characterization Data.

On the pages that follow are the Batch Characterization sheets for a selection of batches produced. Included are the better PαMS batches, two polystyrene batches, and three batches discussed in the section on water transport from the center core during solvent extraction. At the head of each page is a summary of the experimental conditions that produced this particular batch of shells. The following is a description of the information provided in each line:

1. The batch number
2. The number of shells characterized from this batch
3. The concentration of the polymer solution in weight %, the type of polymer (PαMS or PS), and the approximate molecular weight of the polymer
4. The solvent used to make the polymer solution, with the volume ratio of two solvents, if applicable, and the volume of polymer solution dispensed.
5. The concentration of the PVA-water solution in weight %, with the type of PVA used(amount hydrolyzed, molecular weight)
6. The type of stir mechanism, the speed of stirring and length of time for each speed (in hours, a total of 23 hours)
7. The salt added to the solution during drying, concentration in weight %
8. The temperature of the drying bath, the drying time and the method of heating
9. For some batches, the flow rates of the oil and the inner water phases

After this experimental information, the data from the shell characterization is presented. For each shell, three measurements are made looking down on the shell, where the shell is rotated 90° between each measurement. Thus, the three measurements are orthogonal to each other. For batch 1058, two measurements are made per shell, perpendicular to each other. The Major Axis value is the largest diameter of the shell in μm, the Minor Axis is the diameter orthogonal to the Major Axis, and the Angle is the angle of the Major Axis with respect to the positive x-axis. diameter is the difference between the two diameters, and MOOR is the Maximum Out of Round for the shell, defined as the smallest diameter of the 6 measurements subtracted from the largest diameter. Average values for the batch are found along the bottom. For selected shells from the batch, the shell was weighed, and an average wall thickness was calculated using the average diameter of the shell, the density of solid PαMS, and the mass of the shell.

In the instance where shells from the batch were run on the Sphere Mapper, the trace data and power spectra appear after the Batch Characterization sheet.

PAMS1058 µ-encapsulated PAMS shells RACI results							
10 randomly chosen shells from a larger batch							
13% PaMS 395K							
Fluorobenzene							
2 wt% polysciences PVA 88% hydrolyzed 25K Mw							
Propellar @ 150rpm							
1 wt% NH4NO3 salt added to flask during solvent extraction							
Bath temp @ 45°C for 23h							
	Ellipse fit results						
	Diameter (µm)						
Sample	major	minor	angle	dia (µm)	Ave diameter	mass (mg)	Wall (µm)
#1	1891.0	1890.0	0	**1.0**	1891.2	0.142	12
#1b	1893.1	1890.5	58	**2.6**			
#2	2088.6	2084.8	78	**3.8**	2086.7		
#3	1932.4	1930.8	0	**1.6**	1932.2	0.1962	16
#3b	1933.7	1931.8	76	**1.9**			
#4	1962.0	1960.9	0	**1.1**	1961.3	0.2233	17
#4b	1961.5	1960.7	0	**0.8**			
#5	2008.9	2006.5	-73	**2.4**	2007.7		
#6	1922.0	1918.0	77	**4.0**	1920.0		
#7	1909.9	1908.4	0	**1.5**	1909.5	0.1712	14
#7b	1910.5	1909.3	0	**1.2**			
#8	1925.6	1923.4	-88	**2.2**	1924.5		
#9	1940.7	1939.3	0	**1.4**	1939.8		
#9b	1940.9	1938.4	20	**2.6**			
#10	1910.1	1908.9	0	**1.2**	1909.4	0.2011	17
#10b	1909.8	1908.6	0	**1.2**			
						<wall>=	**15**
			Ave dia	**1.9**			

PAMS1059 µ-encapsulated PAMS shells RACI results
10 randomly chosen shells from a larger batch
13wt% 395K PaMS
Fluorobenzene
2 wt% polysciences PVA 88% hydrolyzed 25K Mw
Propellar @ 150rpm
1 wt% NH4NO3 salt added to flask during solvent extraction
Bath temp @ 45°C for 23h

Meas. #	Major Axis	Minor Axis	Major Angle	dia	M.O.O.R.
#21-x	2017.0	2016.2	0	0.8	**1.7**
#21-y	2016.9	2015.4	0	1.6	
#21-z	2016.5	2015.5	0	0.9	
#22-x	1982.7	1981.3	0	1.4	**1.7**
#22-y	1982.6	1981.0	0	1.6	
#22-z	1981.9	1981.7	0	0.2	
#23-x	1983.5	1982.4	0	1.1	**1.4**
#23-y	1983.7	1982.3	0	1.3	
#23-z	1983.5	1982.2	0	1.2	
#24-x	1950.2	1949.9	0	0.3	**1.7**
#24-y	1950.4	1948.7	0	1.7	
#24-z	1950.4	1948.6	0	1.7	
#25-x	1963.5	1963.2	0	0.3	**2.4**
#25-y	1965.3	1963.6	0	1.8	
#25-z	1964.7	1963.0	0	1.7	
#26-x	2000.3	1999.1	0	1.2	**1.6**
#26-y	2000.0	1999.4	0	0.6	
#26-z	2000.0	1998.7	0	1.3	
#27-x	2007.0	2006.6	0	0.5	**0.9**
#27-y	2007.0	2006.6	0	0.5	
#27-z	2007.0	2006.1	0	0.8	
#28-x	1946.1	1945.3	0	0.8	**1.1**
#28-y	1945.7	1945.5	0	0.3	
#28-z	1946.0	1945.0	0	1.1	
#29-x	2007.4	2005.9	0	1.5	**1.7**
#29-y	2006.7	2005.7	0	0.9	
#29-z	2006.8	2006.0	0	0.8	
#30-x	1988.8	1988.5	0	0.3	**1.3**
#30-y	1989.0	1987.9	0	1.1	
#30-z	1989.2	1988.6	0	0.6	
Ave dia	**1984.2**		Average dia	**1.0**	
				Ave MOOR	**1.5**

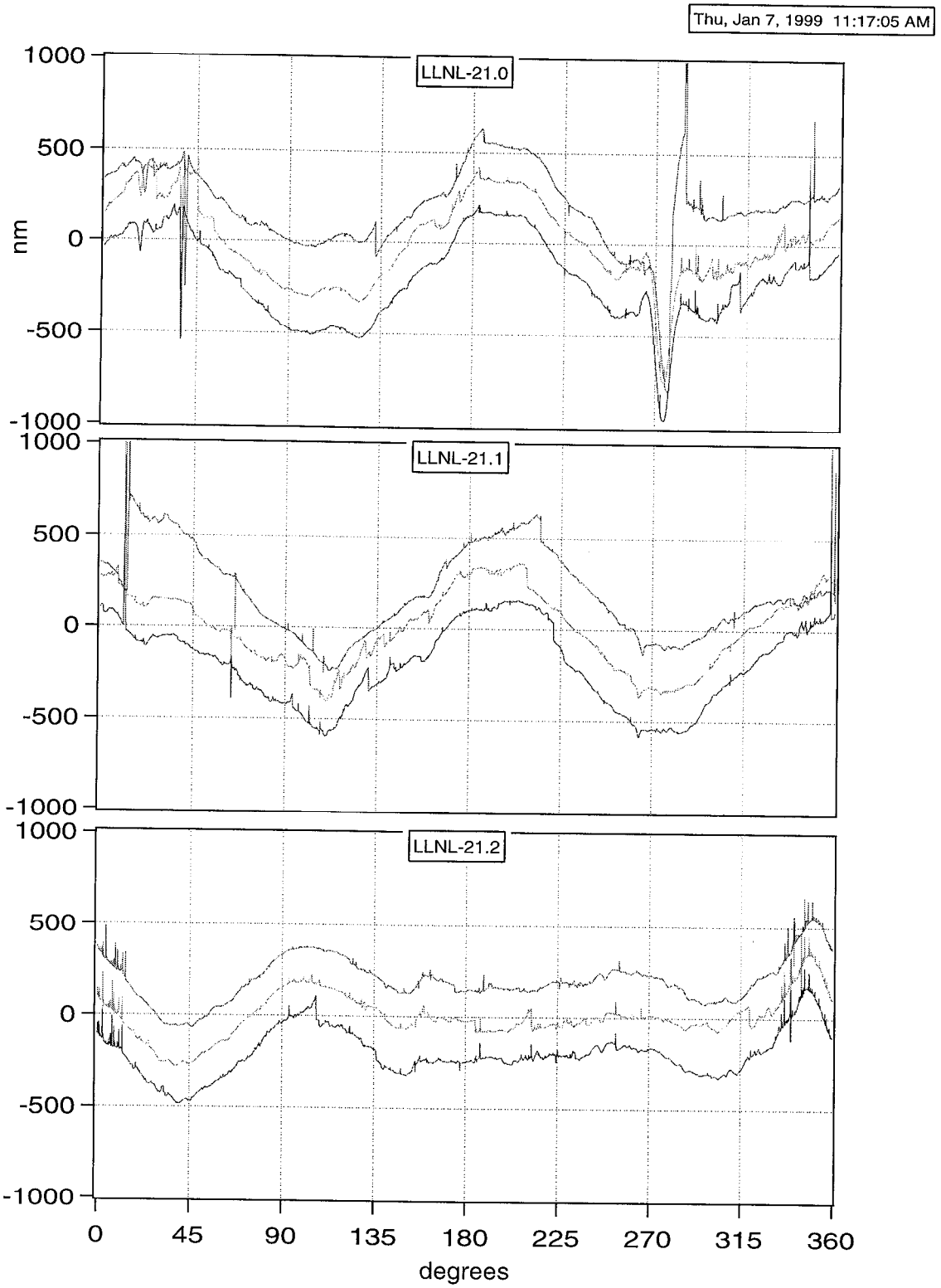

Traces labeled LLNL are shells from batch 1059, Sphere Mapper data scanned at General Atomics for us. LLNL-21 is our shell PaMS 1059 #21.

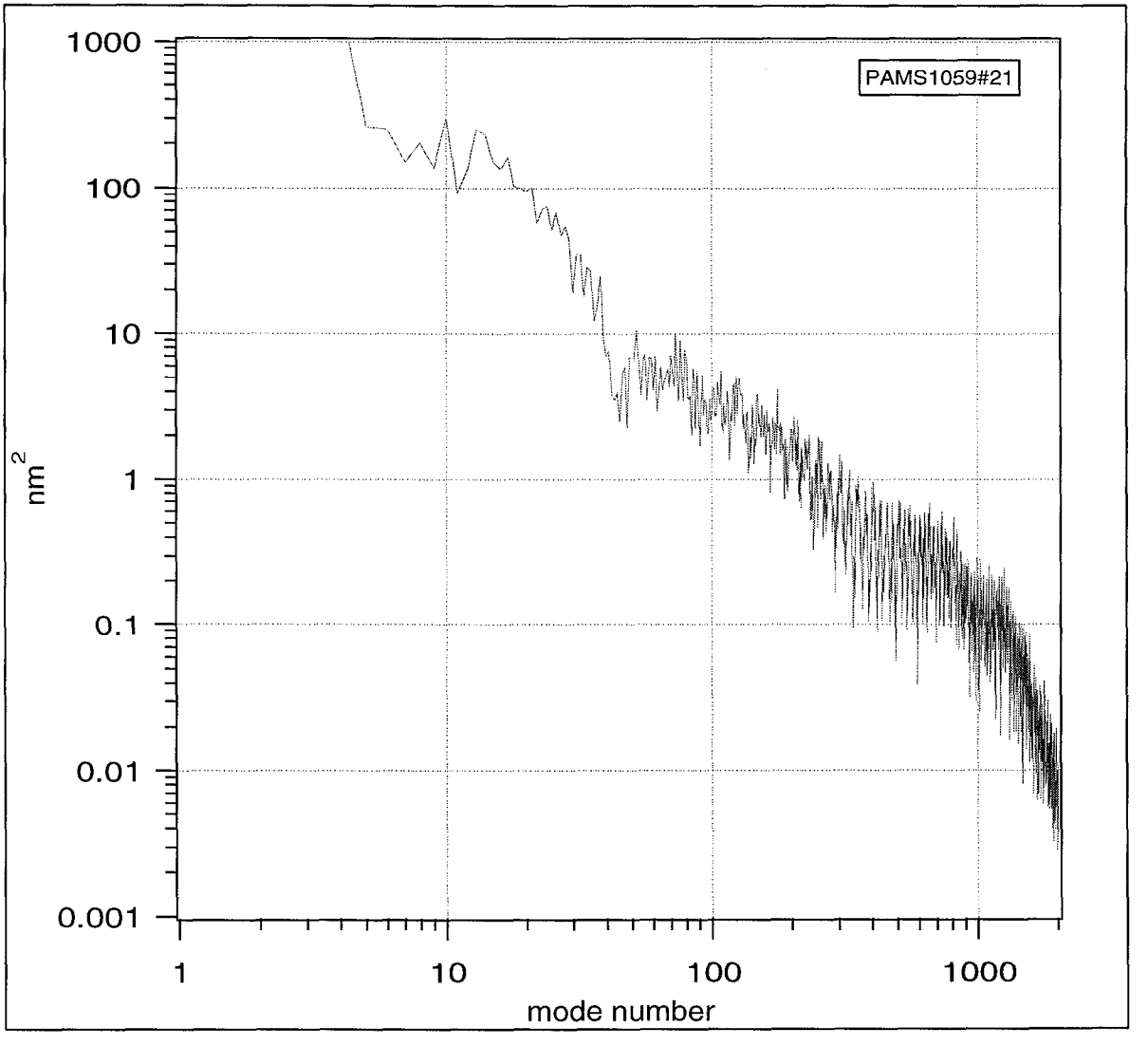
Thu, Jan 7, 1999 11:18:40 AM
PAMS1059#21
1000
100
10
1
0.1
0.01
0.001
nm2
1
10
100
1000
mode number

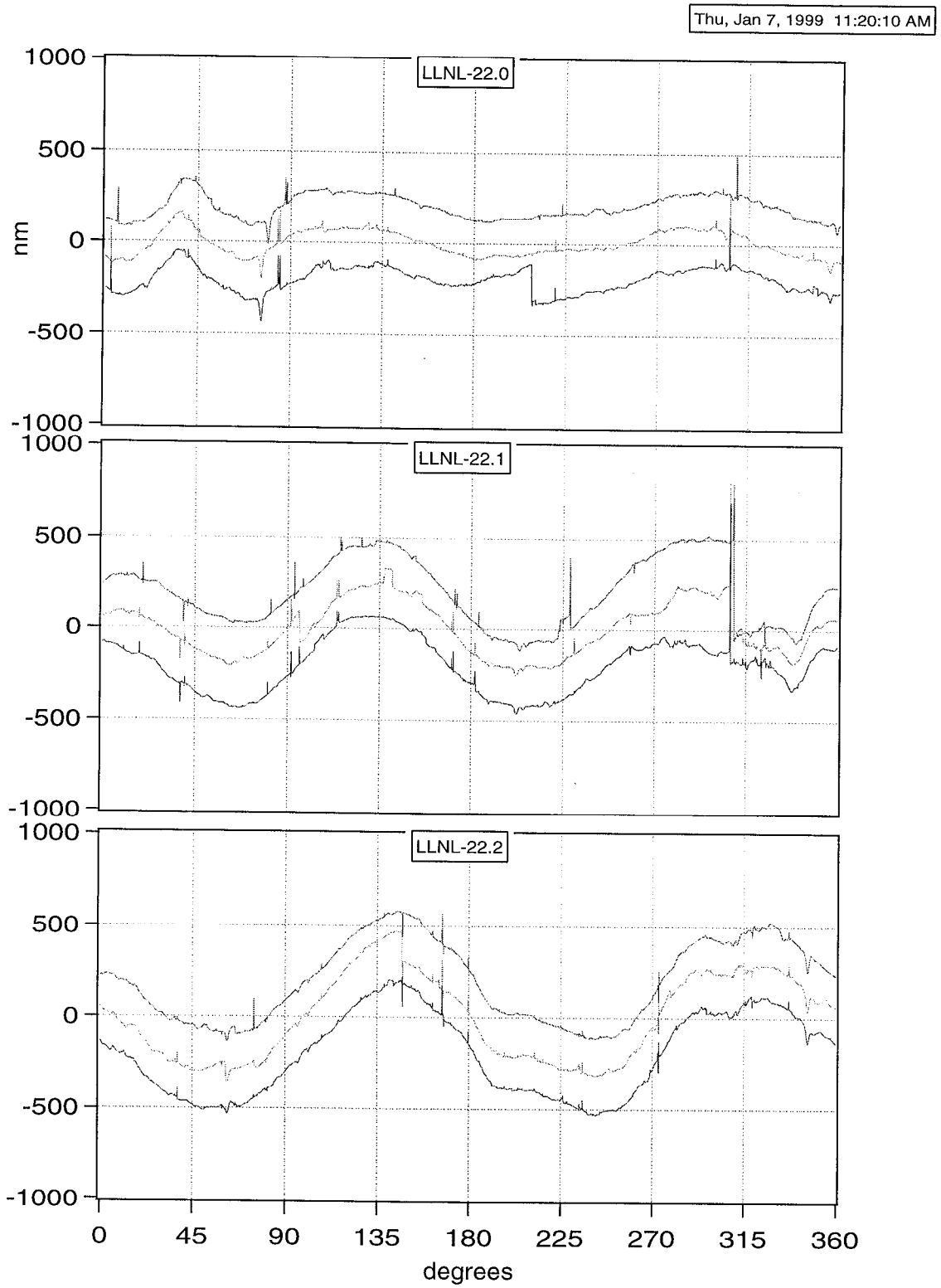

Traces labeled LLNL are shells from batch 1059, Sphere Mapper data scanned at General Atomics for us. LLNL-22 is our shell PaMS 1059 #22.

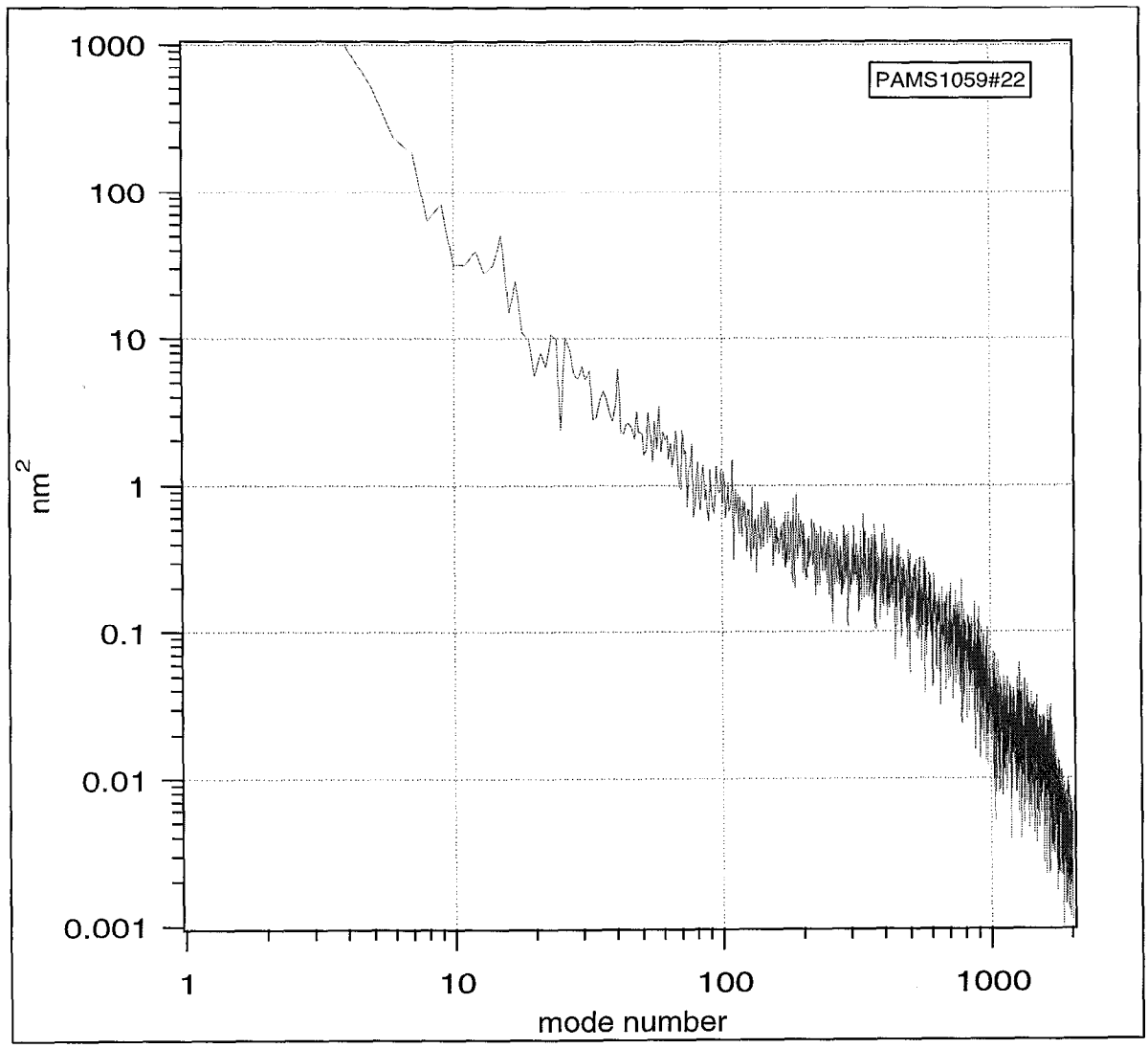
Thu, Jan 7, 1999 11:21:25 AM
PAMS1059#22
1000
100
10
1
0.1
0.01
0.001
nm2
1
10
100
1000
mode number

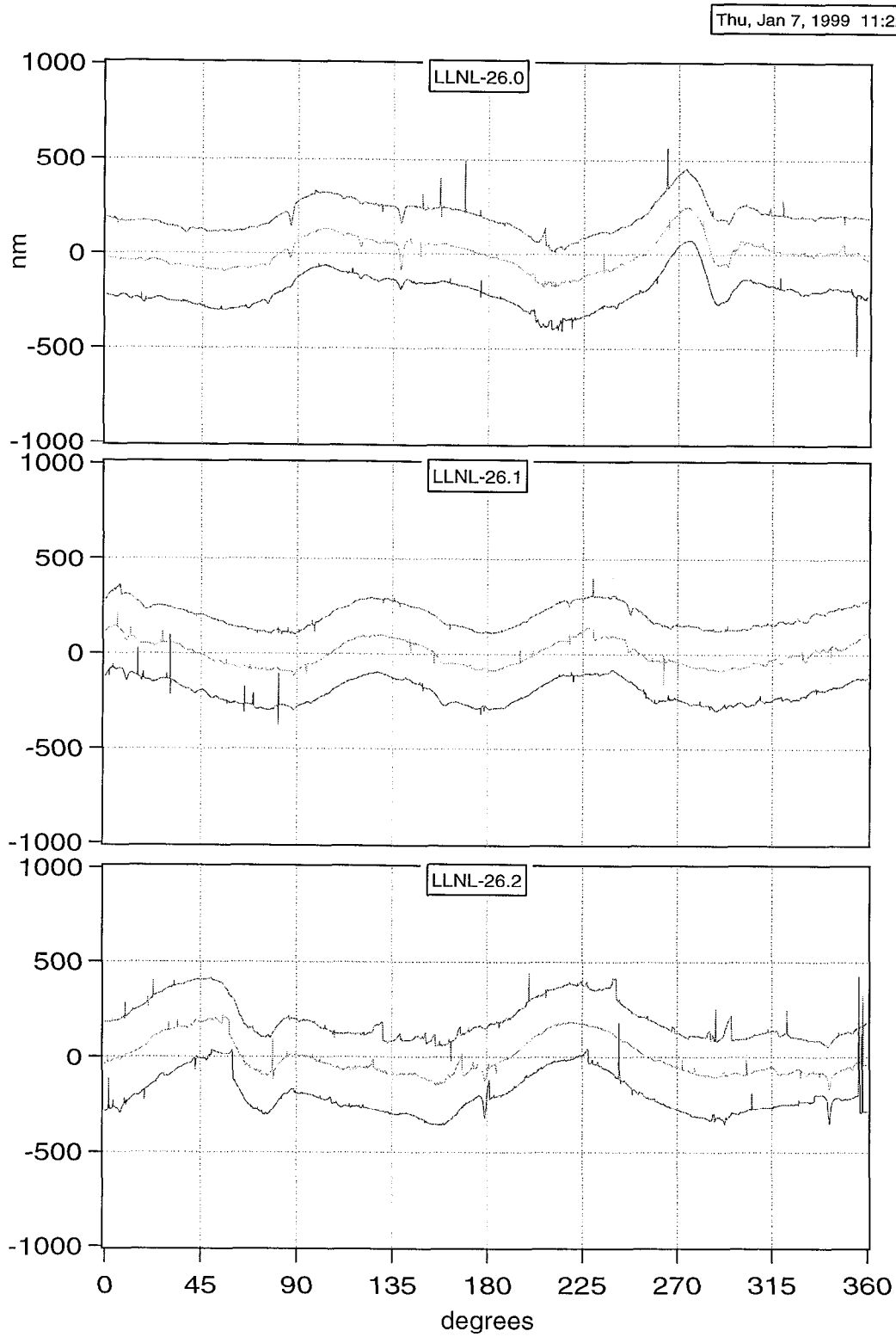

Traces labeled LLNL are shells from batch 1059, Sphere Mapper data scanned at General Atomics for us. LLNL-26 is our shell PaMS 1059 #26.

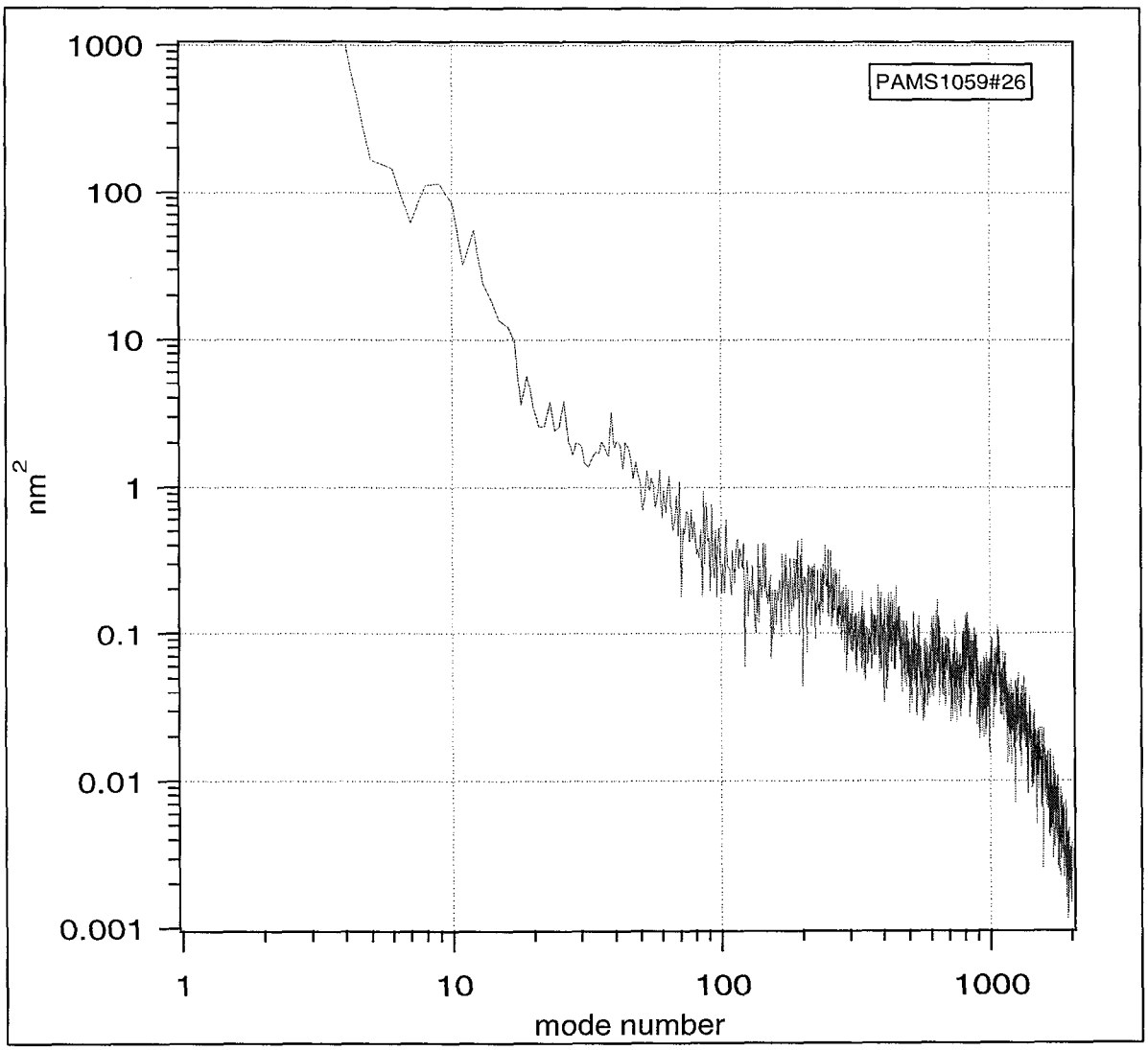
Thu, Jan 7, 1999 11:24:22 AM
PAMS1059#26
1000
100
10
1
0.1
0.01
0.001
nm2
1
10
100
1000
mode number

Polystyrene 1084 µ-encapsulated polystyrene shells RACI results

10 randomly chosen shells from a larger batch
15wt% 100-140k polystyrene
1,2 DCE/Benzene 15 ml (1:1)? old
2 wt% polysciences PVA 88% hydrolyzed 25K Mw
Propellar @ 120rpm / 23h
1 wt% NH4NO3 salt added to flask during solvent extraction
Bath temp @ 45°C for 23h Hot plate

One view — lots of tiny imperfections looks like they're inside

Sample	Ellipse fit results Diameter (µm) Major Axis	Minor Axis	Angle	dia	MOOR
#1	2272.7	2271.8	0.0	**0.9**	1.9
	2272.4	2271.4	0.0	**1.0**	
	2271.7	2270.8	0.0	**0.9**	
#2	2258.7	2257.9	0.0	**0.8**	1.4
	2259.3	2258.2	0.0	**1.1**	
	2259.1	2258.4	0.0	**0.7**	
#3	2278.5	2277.7	0.0	**0.8**	1.6
	2278.3	2277.3	0.0	**1.0**	
	2278.9	2278.1	0.0	**0.8**	
#4	2198.1	2197.1	0.0	**1.0**	1.4
	2198.1	2197.0	0.0	**1.1**	
	2198.2	2196.8	0.0	**1.4**	
#5	2315.8	2314.9	0.0	**0.9**	2.1
	2316.2	2315.0	0.0	**1.2**	
	2315.1	2314.1	0.0	**1.0**	
#6	2251.7	2251.0	0.0	**0.7**	1.5
	2252.3	2251.2	0.0	**1.1**	
	2251.7	2250.8	0.0	**0.9**	
#7	2258.4	2257.5	0.0	**0.9**	1.2
	2258.6	2257.7	0.0	**0.9**	
	2258.7	2257.5	0.0	**1.2**	
#8	2299.8	2298.7	0.0	**1.1**	1.4
	2299.5	2298.5	0.0	**1.0**	
	2299.9	2298.8	0.0	**1.1**	
#9	2255.7	2254.7	0.0	**1.0**	1.3
	2255.6	2254.7	0.0	**0.9**	
	2255.5	2254.4	0.0	**1.1**	
#10	2311.3	2310.2	0.0	**1.1**	1.2
	2311.0	2310.1	0.0	**0.9**	
	2311.3	2310.2	0.0	**1.1**	
ave diameter	**2269.6**	Ave dia		**1.0**	
				Ave MOOR	**1.5**

PaMS 1088 µ-encapsulated PaMS shells RACI results					
10 randomly chosen shells from a larger batch					
13wt% 395k(p) polymer					
Fluorobenzene	15 ml				
2 wt% polysciences PVA 88% hydrolyzed 25K Mw					
Propellar @ 120rpm / 4h + 150rpm / 19h					
1 wt% NH4NO3 salt added to flask during solvent extraction					
Bath temp @ 45°C for 23h			Hot plate		
Three views				<wall> =	20 µm
	Ellipse fit results				
	Diameter (µm)				
Sample	Major Axis	Minor Axis	Angle	dia	MOOR
#1	1791.7	1790.2	0.0	**1.5**	1.6
	1790.9	1790.3	0.0	**0.6**	
	1791.8	1790.4	0.0	**1.4**	
#2	1818.1	1817.4	0.0	**0.7**	1.0
	1818.3	1817.3	0.0	**1.0**	
	1818.2	1817.3	0.0	**0.9**	
#3	2167.9	2166.8	0.0	**1.1**	1.1
	2167.8	2166.9	0.0	**0.9**	
	2167.6	2166.8	0.0	**0.8**	
#4	1852.7	1850.9	0.0	**1.8**	2.0
	1851.5	1850.8	0.0	**0.7**	
	1851.3	1850.7	0.0	**0.6**	
#5	1885.1	1883.6	0.0	**1.5**	2.0
	1885.2	1883.2	42.0	**2.0**	
	1884.6	1883.6	0.0	**1.0**	
#6	1824.8	1822.3	34.0	**2.5**	2.5
	1824.2	1822.9	0.0	**1.3**	
	1823.9	1823.1	0.0	**0.8**	
#7	2048.9	2047.6	0.0	**1.3**	2.1
	2049.2	2047.9	0.0	**1.3**	
	2049.7	2047.7	0.0	**2.0**	
#8	1985.7	1985.1	0.0	**0.6**	1.0
	1986.1	1985.4	0.0	**0.7**	
	1985.9	1985.5	0.0	**0.4**	
#9	1699.8	1697.9	62.0	**1.9**	2.0
	1699.9	1698.5	0.0	**1.4**	
	1699.0	1698.5	0.0	**0.5**	
#10	1877.4	1876.0	0.0	**1.4**	1.5
	1877.5	1876.2	0.0	**1.3**	
	1877.1	1876.5	0.0	**0.6**	
			Ave dia	**1.1**	
				ave MOOR	**1.7**

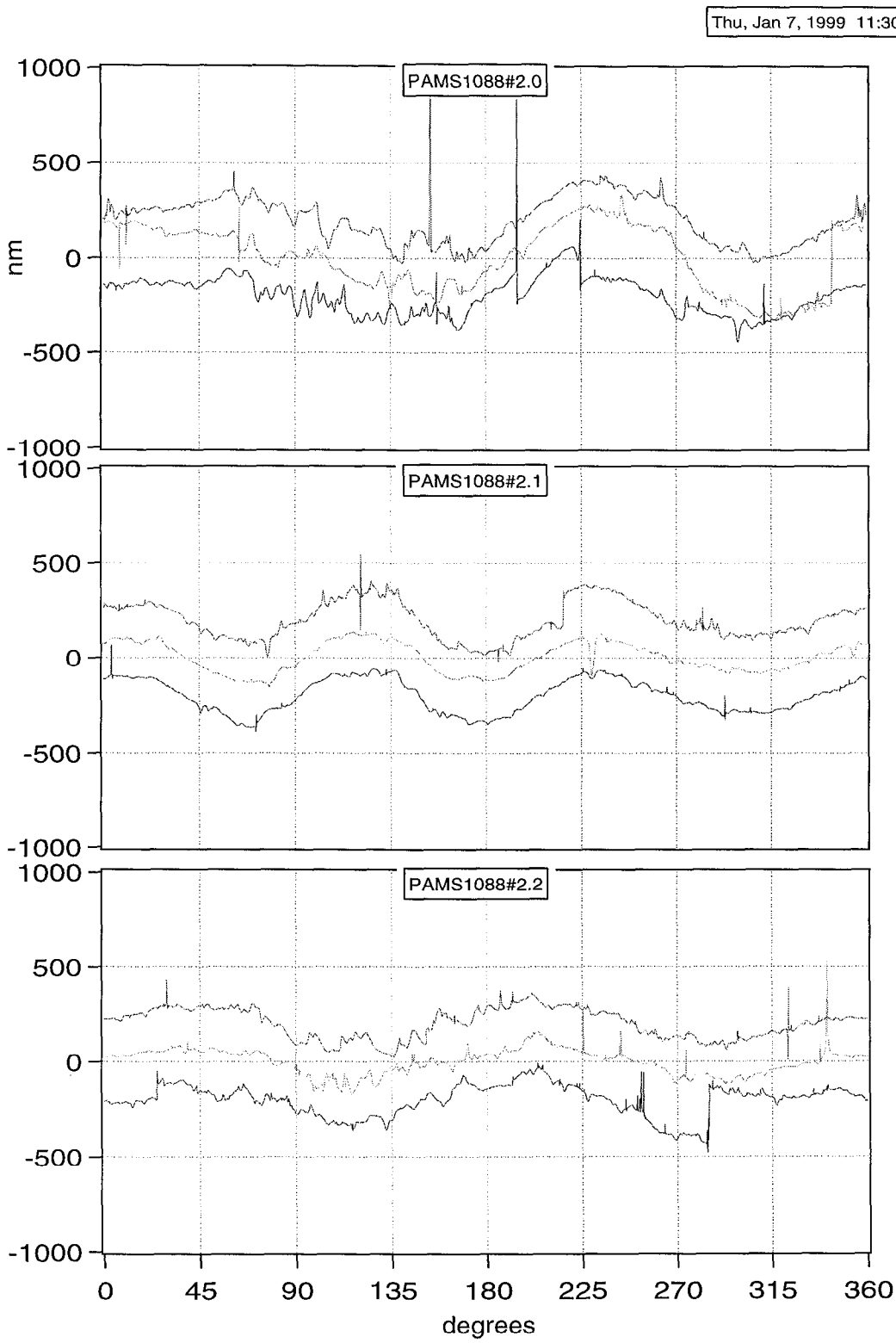
Thu, Jan 7, 1999 11:30:06 AM
PAMS1088#2.0
PAMS1088#2.1
PAMS1088#2.2
nm
1000
500
0
-500
-1000
0
45
90
135
180
225
270
315
360
degrees

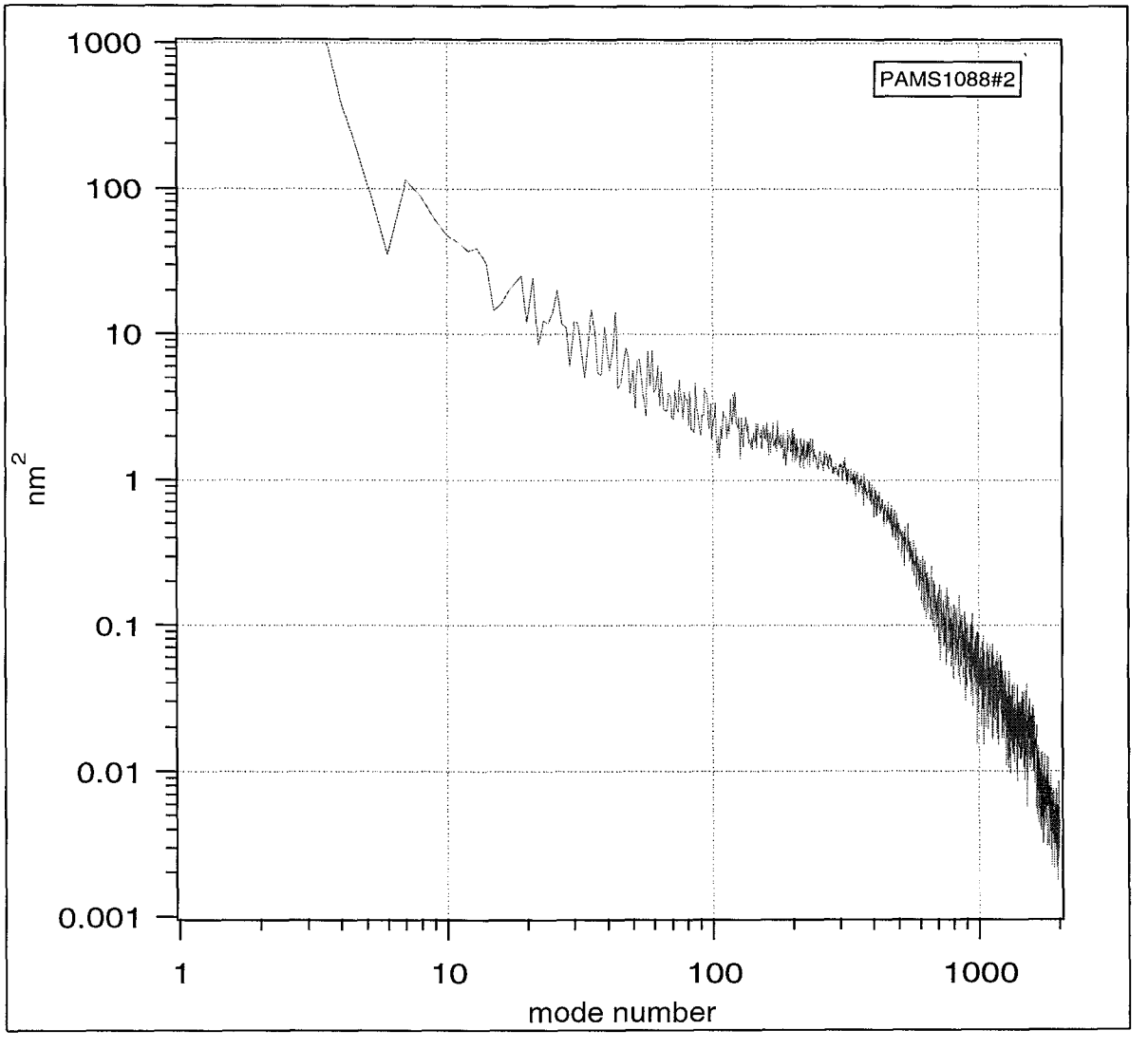
Thu, Jan 7, 1999 12:00:32 PM
PAMS1088#2
1000
100
10
1
0.1
0.01
0.001
nm2
1
10
100
1000
mode number

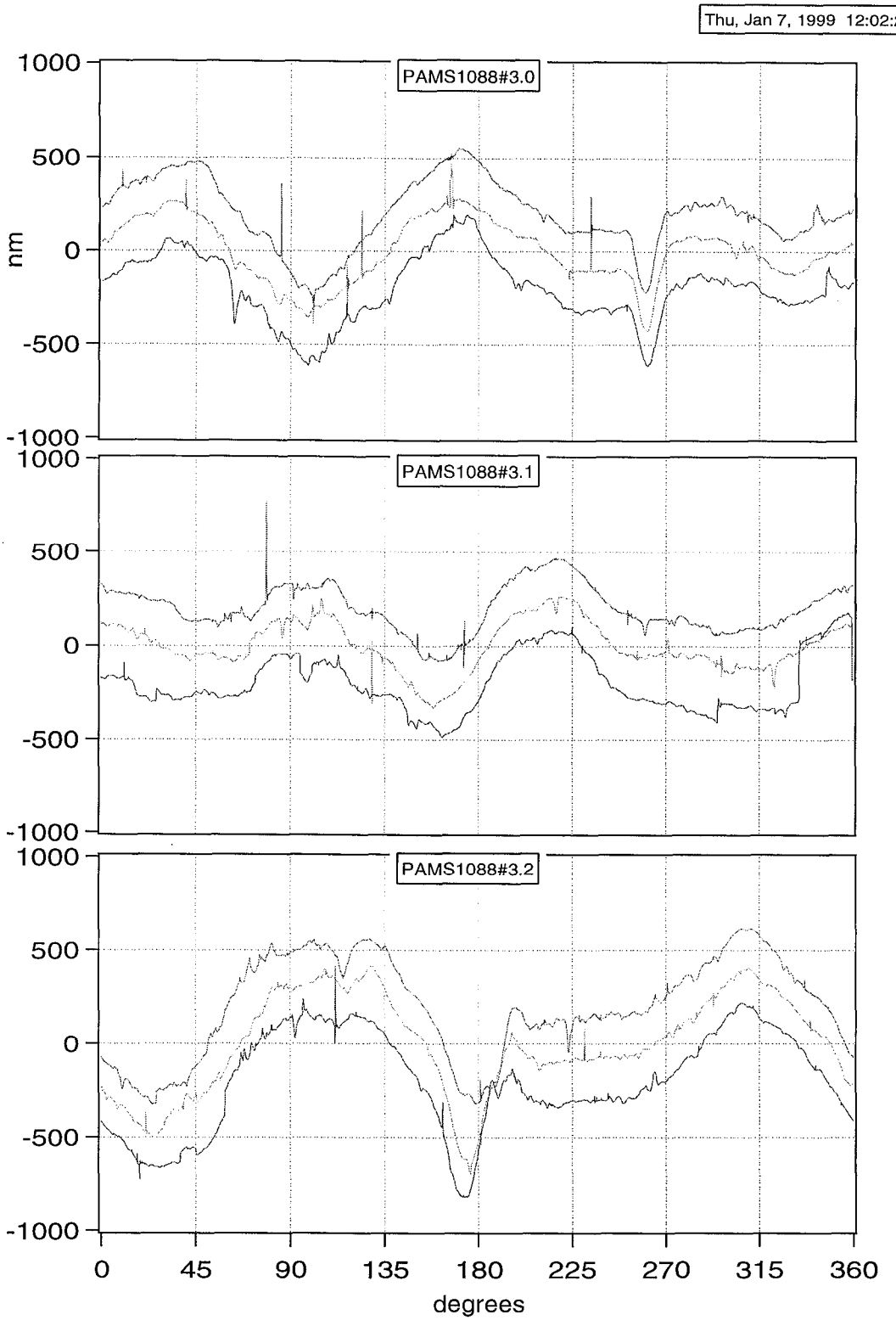
Thu, Jan 7, 1999 12:02:20 PM
PAMS1088#3.0
PAMS1088#3.1
PAMS1088#3.2
nm
1000
500
0
-500
-1000
0
45
90
135
180
225
270
315
360
degrees

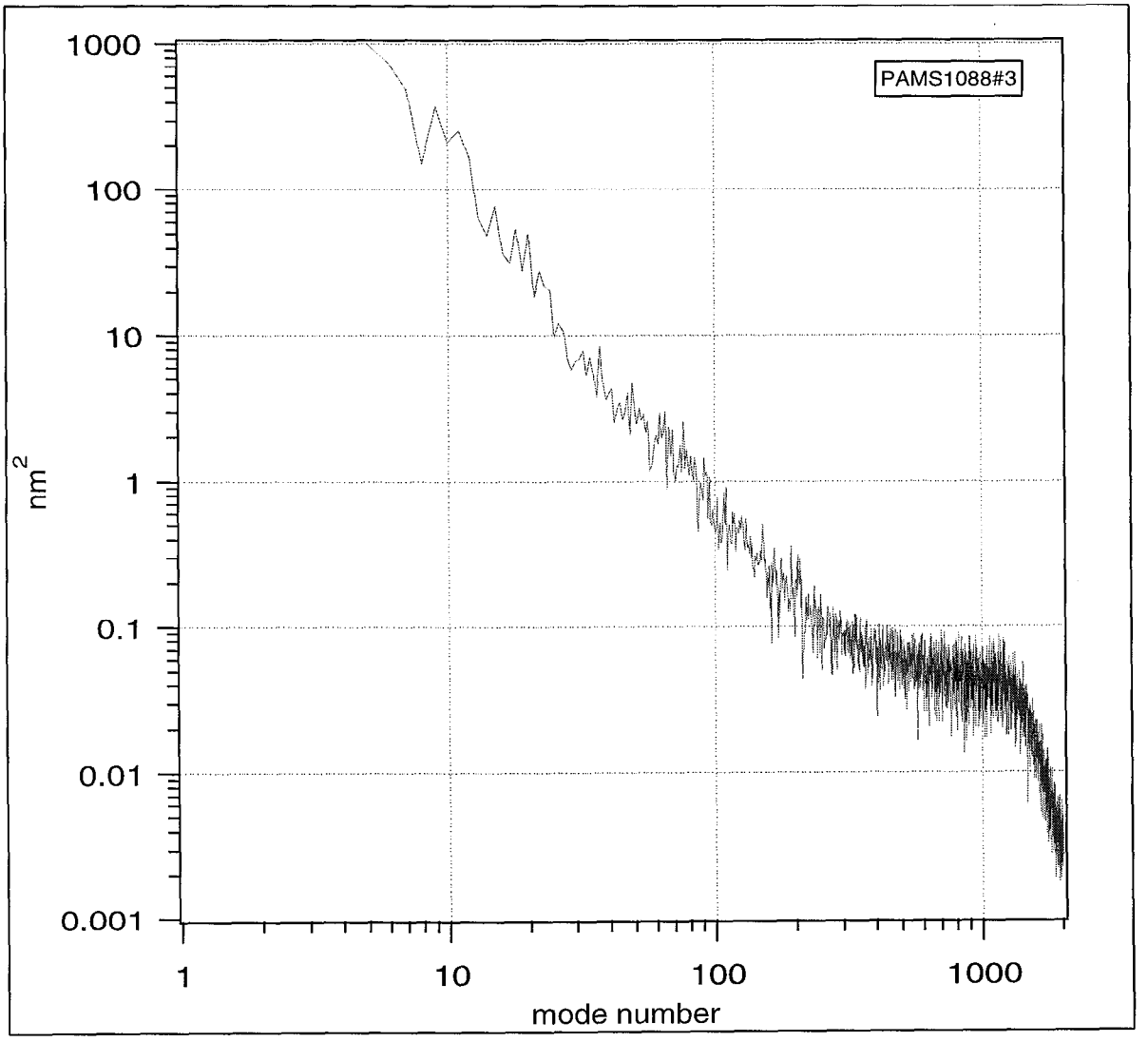
Thu, Jan 7, 1999 12:03:48 PM
PAMS1088#3
1000
100
10
1
0.1
0.01
0.001
nm2
1
10
100
1000
mode number

PaMS 1089 µ-encapsulated PaMS shells RACI results					
10 randomly chosen shells from a larger batch					
13wt% 395k(p) polymer					
Fluorobenzene	15 ml				
2 wt% polysciences PVA 88% hydrolyzed 25K Mw					
Propellar @ 120rpm / 4h + 150rpm / 19h					
1 wt% NH4NO3 salt added to flask during solvent extraction					
Bath temp @ 45°C for 23h			Hot plate		
Three views				<wall> =	20 µm
	Ellipse fit results				
	Diameter (µm)				
Sample	Major Axis	Minor Axis	Angle	dia	MOOR
#1	1980.0	1979.6	0.0	**0.4**	1.1
	1979.9	1978.9	0.0	**1.0**	
	1979.7	1979.6	0.0	**0.1**	
#2	2014.6	2013.9	0.0	**0.7**	1.7
	2014.5	2013.7	0.0	**0.8**	
	2014.9	2013.2	0.0	**1.7**	
#3	1780.3	1779.4	0.0	**0.9**	1.5
	1779.8	1779.0	0.0	**0.8**	
	1780.5	1779.4	0.0	**1.1**	
#4	1905.1	1904.0	0.0	**1.1**	1.9
	1905.4	1904.5	0.0	**0.9**	
	1905.9	1905.1	0.0	**0.8**	
#5	2065.8	2064.7	0.0	**1.1**	1.6
	2066.3	2065.2	0.0	**1.1**	
	2065.6	2065.1	0.0	**0.5**	
#6	2115.0	2114.1	0.0	**0.9**	1.3
	2114.8	2113.7	0.0	**1.1**	
	2114.9	2113.7	0.0	**1.2**	
#7	1928.9	1927.2	0.0	**1.7**	2.7
	1929.9	1927.3	75.0	**2.6**	
	1928.5	1927.3	0.0	**1.2**	
#8	1968.9	1967.9	0.0	**1.0**	1.3
	1969.1	1967.8	0.0	**1.3**	
	1968.8	1968.0	0.0	**0.8**	
#9	2010.6	2009.0	0.0	**1.6**	2.3
	2011.3	2009.0	66.0	**2.3**	
	2010.2	2010.0	0.0	**0.2**	
#10	1875.1	1872.5	57.0	**2.6**	2.6
	1874.6	1873.9	0.0	**0.7**	
	1874.9	1874.4	0.0	**0.5**	
			Ave dia	1.1	
				ave MOOR	1.8

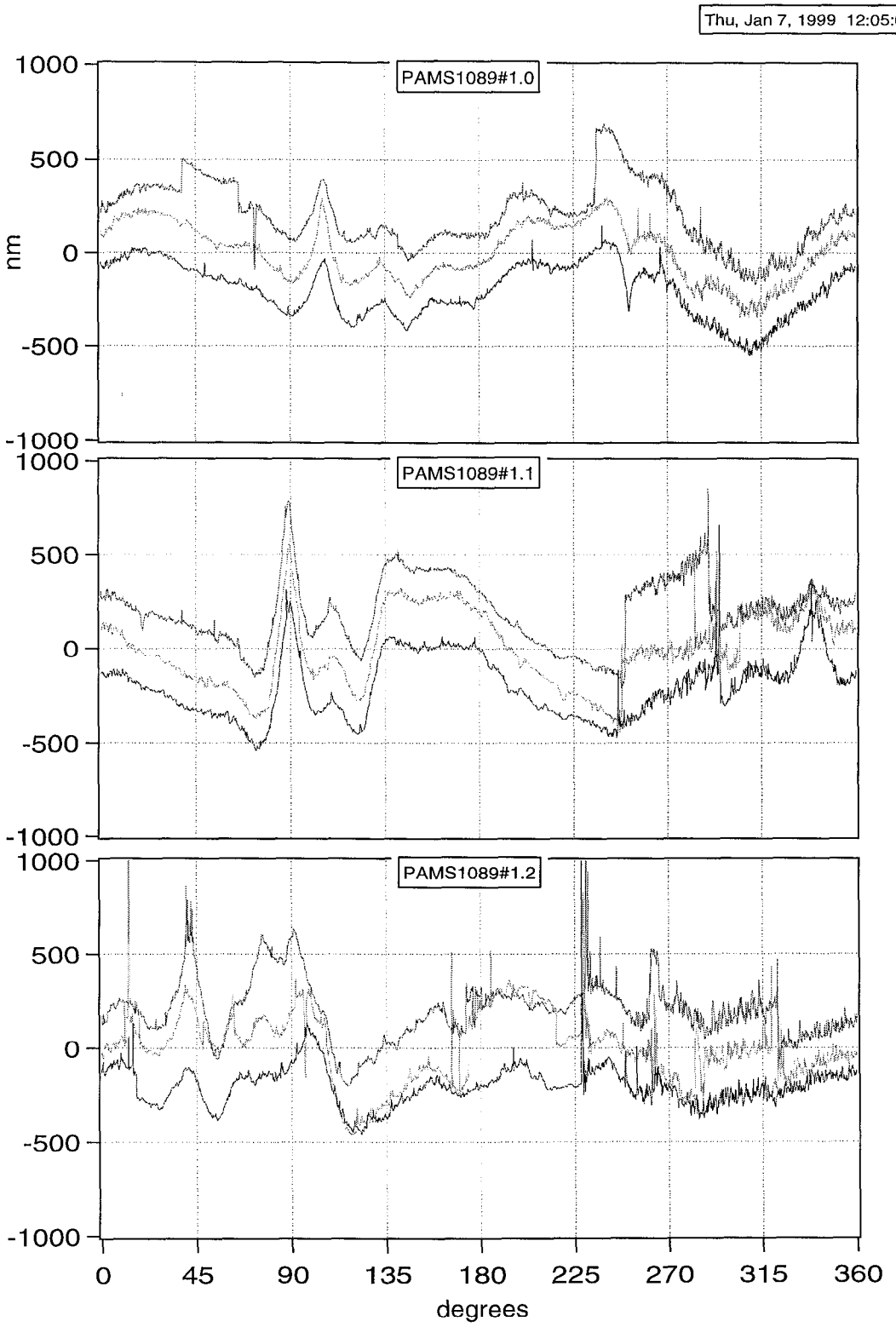
Thu, Jan 7, 1999 12:05:07 PM
PAMS1089#1.0
PAMS1089#1.1
PAMS1089#1.2
nm
1000
500
0
-500
-1000
0
45
90
135
180
225
270
315
360
degrees

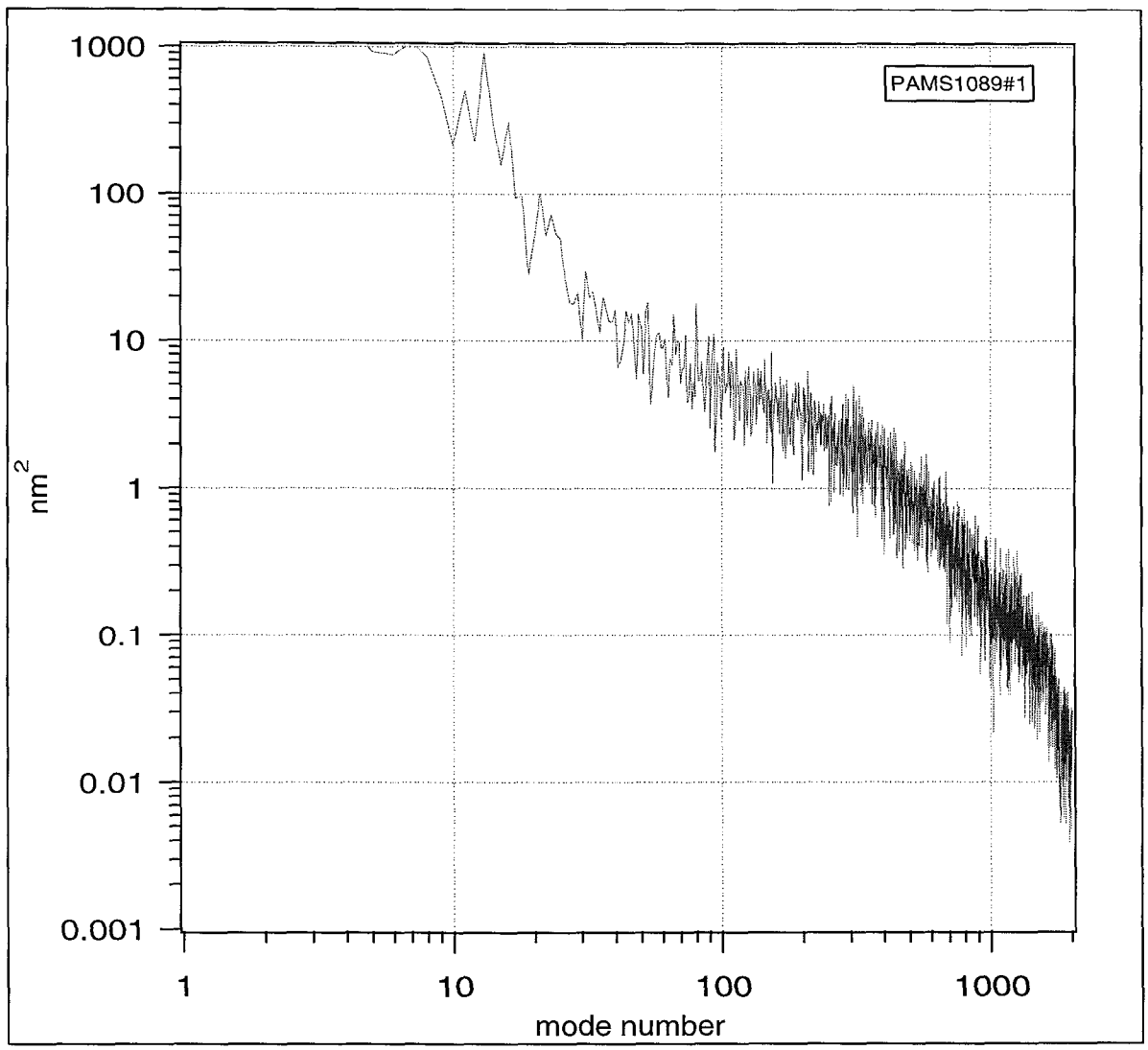
Thu, Jan 7, 1999 12:06:30 PM
PAMS1089#1
1000
100
10
1
0.1
0.01
0.001
nm2
1
10
100
1000
mode number

Polystyrene1101 µ-encapsulated polystyrene shells RACI results

10 randomly chosen shells from a larger batch
20wt% 100-140k polymer
Fluorobenzene 15 ml
2 wt% polysciences PVA 88% hydrolyzed 25K Mw
Propellar @ 150rpm / 23h
1 wt% NH4NO3 salt added to flask during solvent extraction
Bath temp @ 45°C for 23h Hot plate
Rate Oil 0.8 mL/m Rate W1 1.3 mL/m

Three views

	Ellipse fit results Diameter (µm)				
Sample	Major Axis	Minor Axis	Angle	dia	MOOR
#1	2000.2	1999.0	0.0	**1.2**	1.4
	1999.8	1998.8	0.0	**1.0**	
	1999.9	1999.1	0.0	**0.8**	
#2	2105.5	2104.4	0.0	**1.1**	1.4
	2105.8	2104.9	0.0	**0.9**	
	2105.4	2104.5	0.0	**0.9**	
#3	1924.9	1924.0	0.0	**0.9**	0.9
	1924.8	1924.0	0.0	**0.8**	
	1924.8	1924.1	0.0	**0.7**	
#4	2033.7	2032.9	0.0	**0.8**	1.7
	2033.8	2032.9	0.0	**0.9**	
	2034.4	2032.7	0.0	**1.7**	
#5	2260.7	2259.6	0.0	**1.1**	1.9
	2260.8	2258.9	0.0	**1.9**	
	2260.5	2259.0	0.0	**1.5**	
#6	1871.8	1871.2	0.0	**0.6**	1.6
	1872.8	1871.4	0.0	**1.4**	
	1872.7	1871.3	0.0	**1.4**	
#7	1851.3	1849.8	0.0	**1.5**	1.5
	1851.1	1850.0	0.0	**1.1**	
	1850.7	1850.3	0.0	**0.4**	
#8	2098.2	2097.0	0.0	**1.2**	1.5
	2098.0	2096.7	0.0	**1.3**	
	2097.8	2096.9	0.0	**0.9**	
#9	1866.9	1866.0	0.0	**0.9**	2.1
	1866.0	1865.4	0.0	**0.6**	
	1867.5	1865.9	0.0	**1.6**	
#10	2248.3	2247.3	0.0	**1.0**	1.0
	2248.2	2247.4	0.0	**0.8**	
	2248.3	2247.4	0.0	**0.9**	
ave diameter	**2025.6**		Ave dia	**1.1**	
				ave MOOR	**1.5**

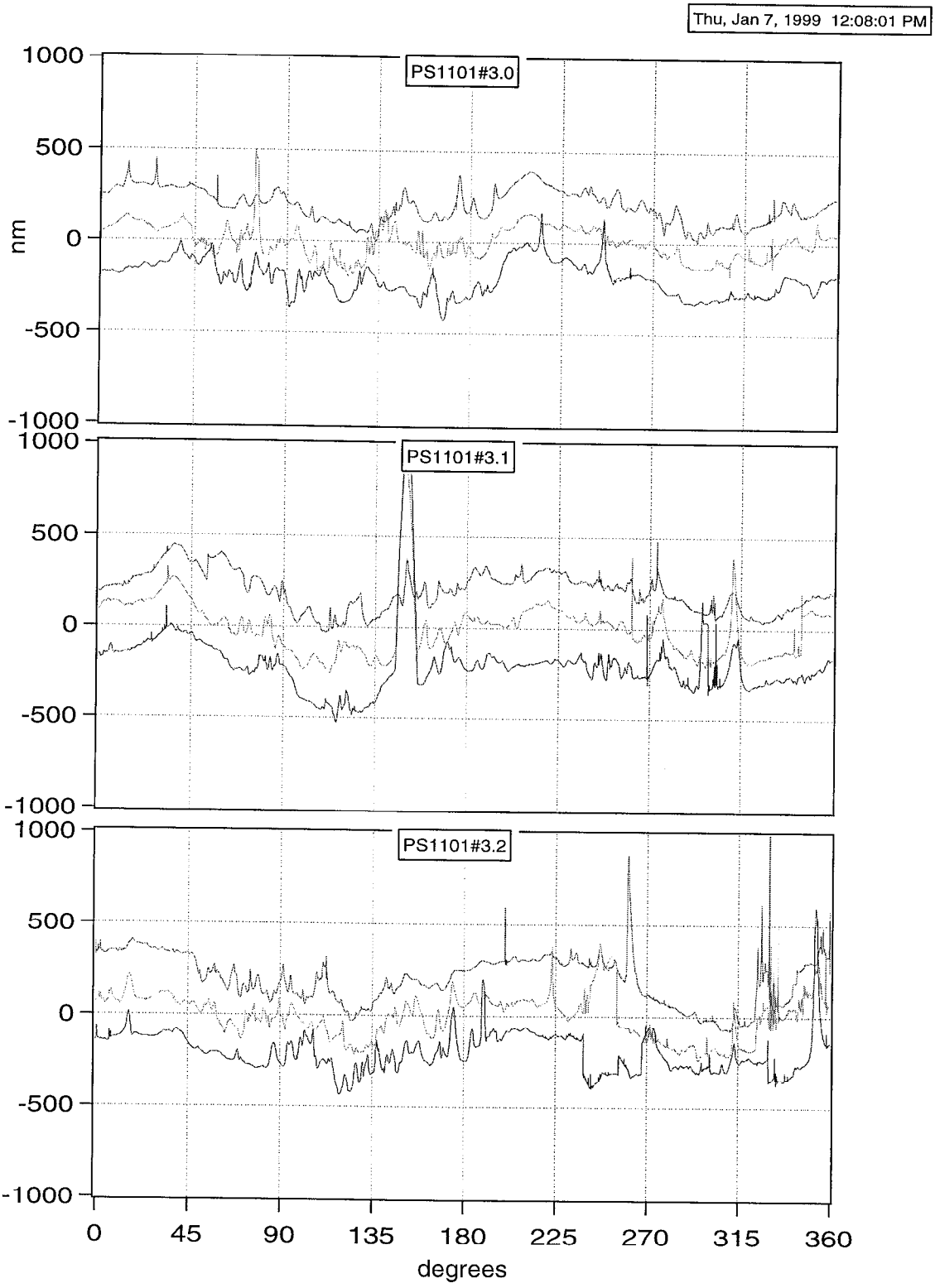
Thu, Jan 7, 1999 12:08:01 PM
PS1101#3.0
PS1101#3.1
PS1101#3.2
nm
1000
500
0
-500
-1000
0
45
90
135
180
225
270
315
360
degrees

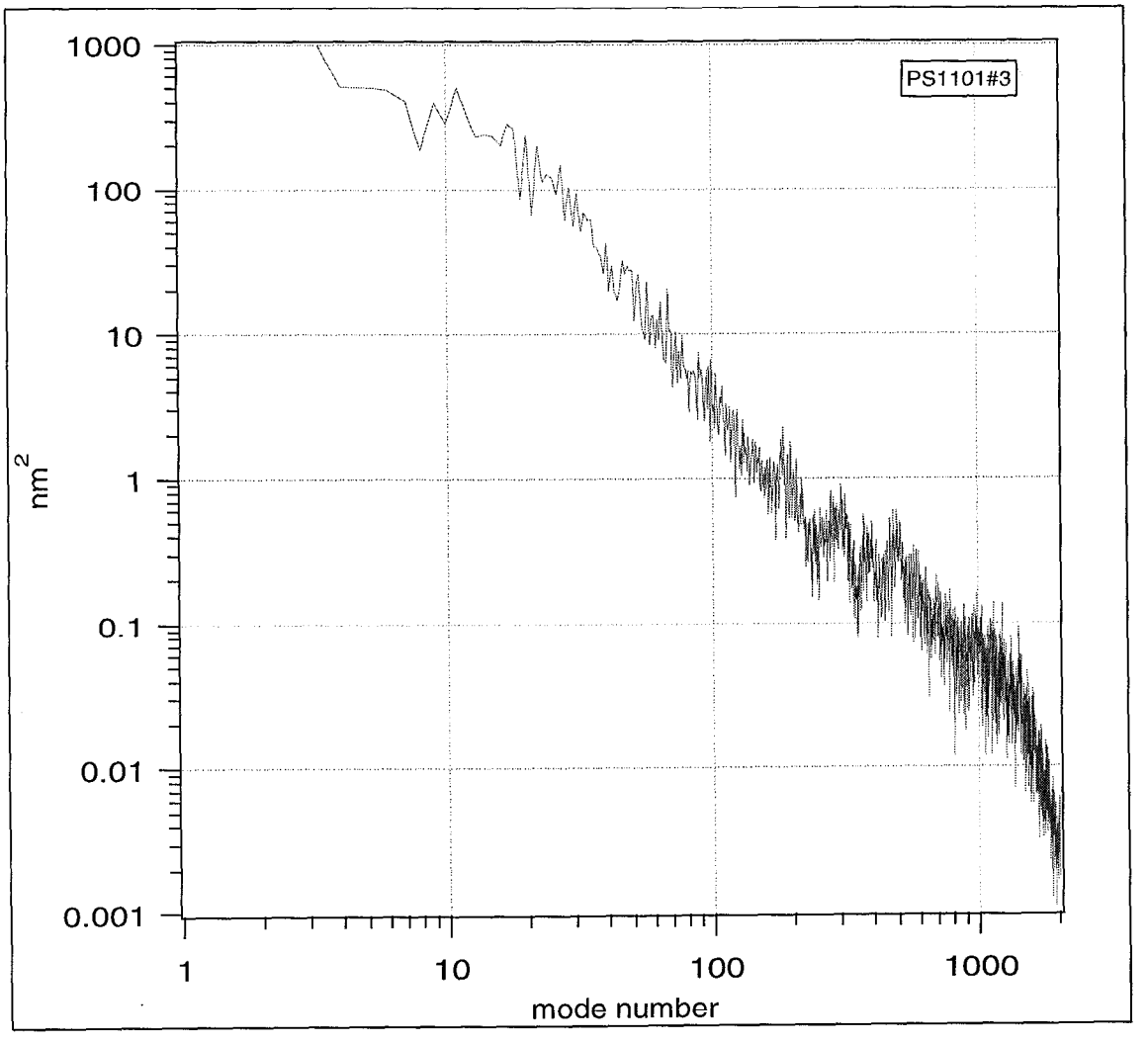
Thu, Jan 7, 1999 12:09:21 PM
PS1101#3
1000
100
10
1
0.1
0.01
0.001
nm2
1
10
100
1000
mode number

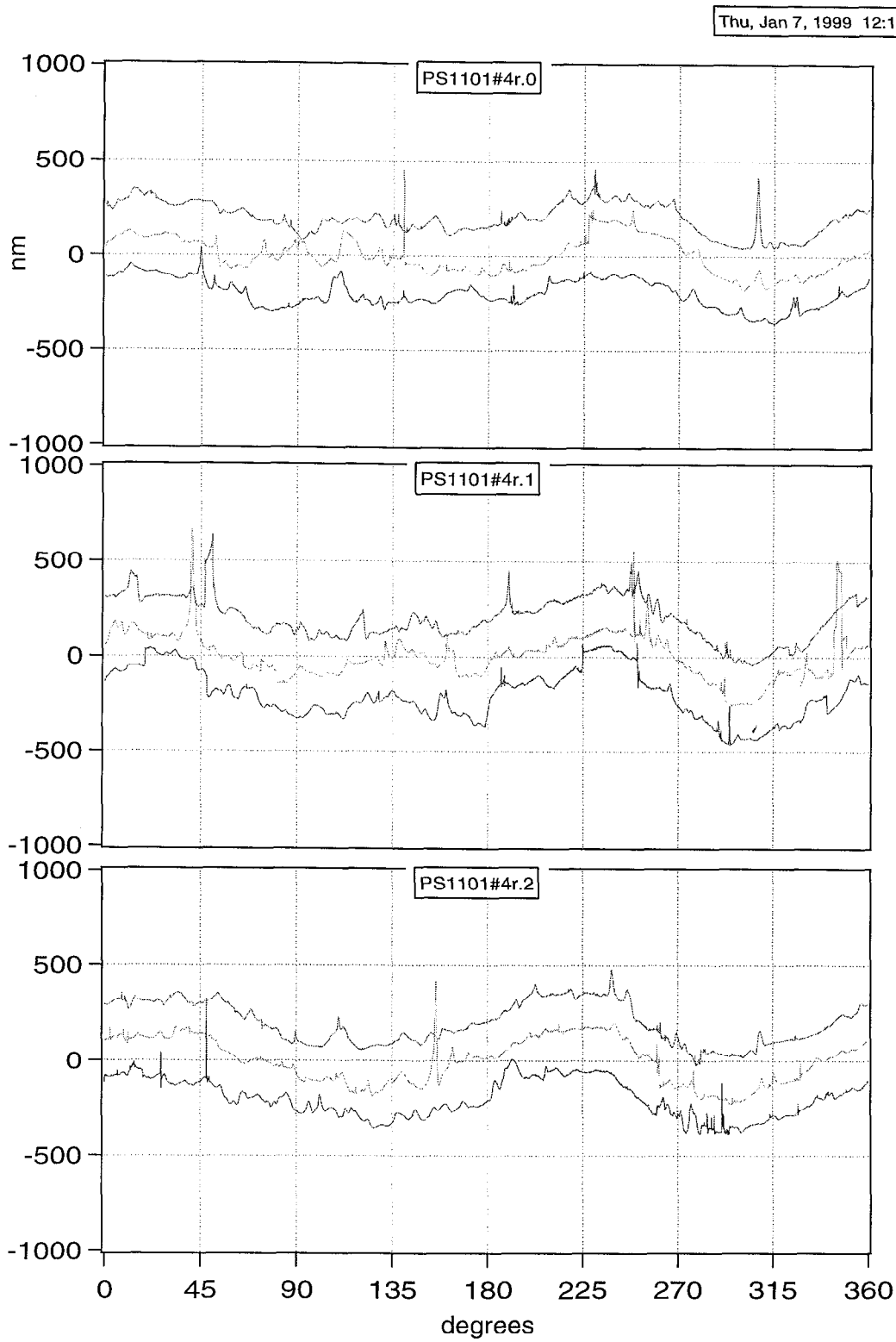
Thu, Jan 7, 1999 12:10:25 PM
PS1101#4r.0
PS1101#4r.1
PS1101#4r.2
nm
1000
500
0
-500
-1000
0
45
90
135
180
225
270
315
360
degrees

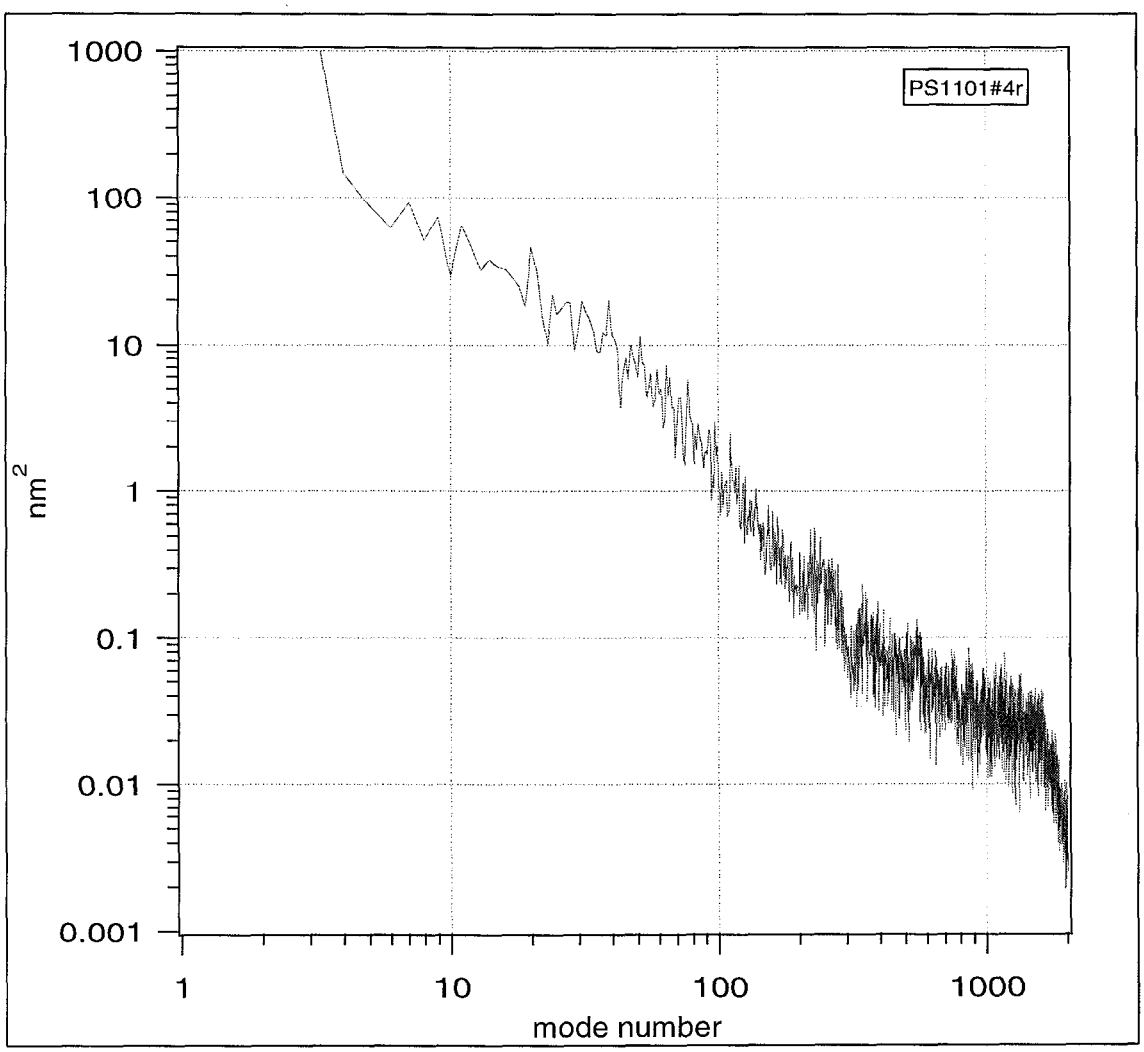
Thu, Jan 7, 1999 12:11:47 PM
PS1101#4r
1000
100
10
1
0.1
0.01
0.001
nm2
1
10
100
1000
mode number

PaMS 1104 µ-encapsulated PaMS shells RACI results							
10 randomly chosen shells from a larger batch							
18 wt% 395k(p) polymer							
Fluorobenzene	15 ml						
2 wt% polysciences PVA 88% hydrolyzed 25K Mw							
Propellar @ 120 rpm / 3h + 150 rpm / 20h							
1 wt% NH4NO3 salt added to flask during solvent extraction							
Bath temp @ 45°C for 23h		Hot plate					
Rate O	0.8 mL/m	Rate W1	1.6 mL/m				
						<wall> =	38 µm
	Ellipse fit results						
	Diameter (µm)						
Sample	Major Axis	Minor Axis	Angle	dia	MOOR (µm)	mass (mg)	wall (µm)
#1	2298.3	2296.6	0.0	**1.7**	2.0	0.6705	39
	2298.3	2297.0	0.0	**1.3**			
	2298.6	2297.6	0.0	**1.0**			
#2	2355.5	2352.6	-1.0	**2.9**	5.3		
	2355.8	2353.7	0.0	**2.1**			
	2356.5	2351.2	60.0	**5.3**			
#3	2320.8	2319.6	0.0	**1.2**	2.4	0.6504	37
	2320.8	2319.4	0.0	**1.4**			
	2320.6	2318.4	0.0	**2.2**			
#4	2345.6	2342.9	46.0	**2.7**	2.7		
	2345.3	2343.1	0.0	**2.2**			
	2345.6	2344.0	0.0	**1.6**			
#5	2302.3	2300.5	0.0	**1.8**	2.3	0.6707	39
	2302.0	2300.0	0.0	**2.0**			
	2301.7	2300.6	0.0	**1.1**			
#6	2336.4	2334.4	0.0	**2.0**	2.6		
	2336.1	2334.6	0.0	**1.5**			
	2336.8	2334.2	54.0	**2.6**			
#7	2310.0	2308.6	0.0	**1.4**	1.4	0.6604	38
	2310.0	2308.7	0.0	**1.3**			
	2309.3	2309.1	0.0	**0.2**			
#8	2348.1	2346.4	0.0	**1.7**	1.8		
	2348.1	2347.1	0.0	**1.0**			
	2347.6	2346.3	0.0	**1.3**			
#9	2312.3	2311.0	0.0	**1.3**	1.9		
	2312.7	2311.2	0.0	**1.5**			
	2312.2	2310.8	0.0	**1.4**			
#10	2330.7	2327.0	23.0	**3.7**	4.6		
	2331.5	2327.2	25.0	**4.3**			
	2329.7	2326.9	-78.0	**2.8**			
			Ave dia	**2.0**			
				ave MOOR	**2.7**		

PaMS 1105 µ-encapsulated PaMS shells RACI results							
10 randomly chosen shells from a larger batch							
18 wt% 395k(p) polymer							
Fluorobenzene	15 ml						
2 wt% polysciences PVA 88% hydrolyzed 25K Mw							
Propellar @ 120 rpm / 3h + 150 rpm / 20h							
1 wt% NH4NO3 salt added to flask during solvent extraction							
Bath temp @ 45°C for 23h			Hot plate				
Rate Oil	0.9 mL/min	Rate W1	1.6 mL/min				
	Ellipse fit results					<wall> =	43 µm
	Diameter (µm)						
Sample	Major Axis	Minor Axis	Angle	dia	M.O.O.R.	mass (mg)	wall (µm)
#1	2239.6	2239.1	0.0	**0.5**	1.6	0.6969	43
	2239.7	2238.9	0.0	**0.8**			
	2239.2	2238.1	0.0	**1.1**			
#2	2290.9	2290.6	0.0	**0.3**	2.6		
	2291.1	2290.7	0.0	**0.4**			
	2292.5	2289.9	73.0	**2.6**			
#3	2244.8	2243.8	0.0	**1.0**	1.6	0.5848	35
	2244.7	2243.5	0.0	**1.2**			
	2244.2	2243.2	0.0	**1.0**			
#4	2212.3	2210.6	0.0	**1.7**	2.1	0.6647	42
	2212.7	2211.1	0.0	**1.6**			
	2212.4	2211.0	0.0	**1.4**			
#5	2246.9	2245.5	0.0	**1.4**	2.2	0.7711	47
	2247.6	2245.6	0.0	**2.0**			
	2247.6	2245.4	0.0	**2.2**			
#6	2219.2	2217.1	0.0	**2.1**	2.5		
	2218.2	2216.7	0.0	**1.5**			
	2218.6	2216.9	0.0	**1.7**			
#7	2264.7	2264.5	0.0	**0.2**	2.0		
	2264.8	2263.5	0.0	**1.3**			
	2265.0	2263.0	0.0	**2.0**			
#8	2342.9	2340.9	0.0	**2.0**	2.6		
	2343.1	2342.5	0.0	**0.6**			
	2343.5	2341.4	0.0	**2.1**			
#9	2224.9	2223.2	0.0	**1.7**	2.2		
	2225.0	2222.8	0.0	**2.2**			
	2224.5	2223.8	0.0	**0.7**			
#10	2275.8	2273.9	0.0	**1.9**	2.8		
	2275.2	2273.0	0.0	**2.2**			
	2275.1	2273.6	0.0	**1.5**			
			Ave dia	**1.4**			
				ave MOOR	**2.2**		

PaMS 1138 μ-encapsulated PaMS shells RACI results

5 randomly chosen shells from a larger batch
18 wt% 395k(p) polymer
Fluorobenzene
2 wt% polysciences PVA 88% hydrolyzed 25K Mw
Core water: water +2% NH_4NO_3
Propellar @ 120 rpm / 3h + 150 rpm / 20h
1 wt% NH_4NO_3 salt added to flask during solvent extraction
Bath temp @ 45°C for 23h Hot plate
Rate Oil 0.8 mL/m Rate W1 1.6 mL/m

							<wall>=	42.3
Three views								
	Ellipse fit results Diameter (μm)							Wall Thickness
Sample	Major Axis	Minor Axis	Angle	dia	MOOR	Mass (mg)		(μm)
#1	2154.7	2138.2	8.0	**16.5**	18.8	0.6045		40.5
	2152.6	2135.9	15.0	**16.7**				
	2138.5	2136.4	0.0	**2.1**				
#2	2151.5	2148.1	1.0	**3.4**	22.1	0.7131		47.6
	2162.3	2146.1	51.0	**16.2**				
	2166.9	2144.8	-78.0	**22.1**				
#3	2169.0	2149.4	-19.0	**19.6**	32.9	0.7284		48.3
	2180.6	2147.7	-1.0	**32.9**				
	2162.7	2150.6	55.0	**12.1**				
#4	2090.3	2082.2	80.0	**8.1**	8.1	0.5565		39.3
	2087.3	2083.3	-62.0	**4.0**				
	2087.7	2082.3	78.0	**5.4**				
#5	2152.1	2138.3	-25.0	**13.8**	13.8	0.5367		35.7
	2142.7	2139.6	-28.0	**3.1**				
	2149.8	2139.6	-1.0	**10.2**				
ave diameter	**2137.0**		Ave dia	**12.4**				
				ave MOOR	**19.1**			

PaMS 1140 µ-encapsulated PaMS shells RACI results

5 randomly chosen shells from a larger batch
18 wt% 395k(p) polymer
Fluorobenzene
2 wt% polysciences PVA 88% hydrolyzed 25K Mw
Core water: water +2% NH4NO3
Propellar @ 120 rpm / 3h + 150 rpm / 20h
1 wt% NH4NO3 salt added to flask during solvent extraction
Bath temp @ 45°C for 23h Hot plate
Rate Oil 0.7 mL/m Rate W1 1.6 mL/m

<wall>= 51.5

Three views

	Ellipse fit results Diameter (µm)						Wall Thickness
Sample	Major Axis	Minor Axis	Angle	dia	MOOR	Mass (mg)	(µm)
#1	2214.8	2212.9	0.0	**1.9**	2.6	0.7773	49.1
	2215.0	2213.0	0.0	**2.0**			
	2214.8	2212.4	-31.0	**2.4**			
#2	2182.2	2181.0	0.0	**1.2**	2.5	0.7803	50.9
	2183.1	2180.6	-77.0	**2.5**			
	2182.3	2181.7	0.0	**0.6**			
#3	2380.9	2376.1	-42.0	**4.8**	19.5	0.7846	42.5
	2387.8	2374.8	-63.0	**13.0**			
	2393.7	2374.2	-45.0	**19.5**			
#4	2194.1	2192.1	0.0	**2.0**	2.0	0.8566	55.5
	2193.8	2192.7	0.0	**1.1**			
	2193.6	2192.9	0.0	**0.7**			
#5	2172.8	2170.0	-39.0	**2.8**	4.0	0.8967	59.5
	2173.8	2169.8	-27.0	**4.0**			
	2171.4	2170.0	0.0	**1.4**			
			Ave dia	**4.0**			
				ave MOOR	6.1		

PaMS 1141 μ-encapsulated PaMS shells RACI results

5 randomly chosen shells from a larger batch
18 wt% 395k(p) polymer
Fluorobenzene
4 wt% polysciences PVA 88% hydrolyzed 25K Mw
Core water: water +2% NH4NO3
Propellar @ 120 rpm / 3h + 150 rpm / 20h
No salt added to bath
Bath temp @ 45°C for 23h Hot plate
Rate Oil 0.6-0.7 ml/m Rate W1 1.6 mL/m

<wall>= 38.2

Three views

Sample	Ellipse fit results Diameter (μm) Major Axis	Minor Axis	Angle	dia	MOOR	Mass (mg)	Wall Thickness (μm)
#1	2262.0	2255.3	-72.0	**6.7**	28.7	0.6697	40.1
	2278.0	2253.8	10.0	**24.2**			
	2280.8	2252.1	-69.0	**28.7**			
#2	2250.5	2204.8	88.0	**45.7**	45.7	0.5495	33.9
	2250.5	2205.0	11.0	**45.5**			
	2215.6	2211.2	7.0	**4.4**			
#3	2257.1	2253.7	-44.0	**3.4**	6.3	0.6131	36.8
	2257.7	2256.2	0.0	**1.5**			
	2259.5	2253.2	70.0	**6.3**			
#4	2261.0	2255.5	85.0	**5.5**	11.4	0.6816	41.0
	2260.9	2257.4	64.0	**3.5**			
	2266.9	2255.9	41.0	**11.0**			
#5	2251.7	2236.5	-62.0	**15.2**	15.2	0.6414	39.1
	2240.8	2238.0	2.0	**2.8**			
	2246.0	2237.0	-50.0	**9.0**			
			Ave dia	**14.2**			
				Ave MOOR	**21.5**		

Appendix B - Solution Density Measurements

Table B-I. Quadratic fits of density data, $\rho = c_0 + c_1 T + c_2 T^2$.

Substance	c_0	c_1	c_2	Figure
H_2O	1.0015	-8.6235×10^{-5}	-3.6358×10^{-6}	B-1
60:40 D_2O:H_2O	1.0665	-1.6210×10^{-4}	-3.3206×10^{-6}	B-1
68:32 D_2O:H_2O	1.0739	-1.9207×10^{-4}	-2.9487×10^{-6}	B-1, B-2
70:30 D_2O:H_2O	1.0753	-3.4722×10^{-5}	-5.4765×10^{-6}	B-1, B-2
75:25 D_2O:H_2O	1.0789	-5.1527×10^{-5}	-4.0476×10^{-6}	B-1
D_2O	1.1092	-1.9528×10^{-4}	-5.0001×10^{-6}	B-1
2% PVA	1.0067	-9.8061×10^{-4}	-3.5646×10^{-6}	B-3
1% NH_4Cl/2% PVA	1.0108	-1.1213×10^{-4}	-3.4053×10^{-6}	B-3
17% NH_4Cl/2% PVA	1.0551	-2.3775×10^{-4}	-2.0909×10^{-6}	B-3
18% NH_4Cl/2% PVA	1.0577	-2.5464×10^{-4}	-1.8647×10^{-6}	B-3
19% NH_4Cl/2% PVA	1.0603	-2.7686×10^{-4}	-1.5553×10^{-6}	B-3
25% NH_4Cl/0.5% PVA	1.0725	-2.9351×10^{-4}	-1.3172×10^{-6}	B-3
18.5% NH_4NO_3/2% PVA	1.0829	-3.5704×10^{-4}	-1.8485×10^{-6}	B-3
20% NH_4NO_3/2% PVA	1.0904	-3.7562×10^{-4}	-1.7449×10^{-6}	B-3
Benzene (B)	0.9000	-1.0495×10^{-3}	-3.8000×10^{-7}	B-4
1,2-Dichloroethane (DCE)	1.2789	-1.4212×10^{-3}	-7.3559×10^{-7}	B-4
50:50 B:DCE	1.0856	-1.2119×10^{-3}	-6.5847×10^{-7}	B-4
Fluorobenzene (FB)	1.0485	-1.1667×10^{-3}	-6.5414×10^{-7}	B-4
13%PaMS in qq:qq B:DCE	1.0958	-1.1381×10^{-3}	-4.3342×10^{-7}	B-5
13%PaMS in 43:57 B:DCE	1.1163	-1.1617×10^{-3}	-3.8788×10^{-7}	B-5
13% PaMS in FB	1.0588	-1.0910×10^{-3}	-5.6482×10^{-7}	B-5
18% PaMS in FB	1.0644	-1.0688×10^{-3}	-4.7496×10^{-7}	B-5
32.7% PaMS in FB	1.0742	-1.0020×10^{-3}	-3.0303×10^{-7}	B-6
34.6% PaMS in FB	1.0765	-0.9816×10^{-3}	-3.1818×10^{-7}	B-6
38.3% PaMS in FB	1.0784	-0.9762×10^{-3}	-2.2727×10^{-7}	B-6
39.5% PaMS in FB	1.0791	-0.9708×10^{-3}	-2.1212×10^{-7}	B-6
40.6% PaMS in FB	1.0791	-0.9616×10^{-3}	-3.1818×10^{-7}	B-6

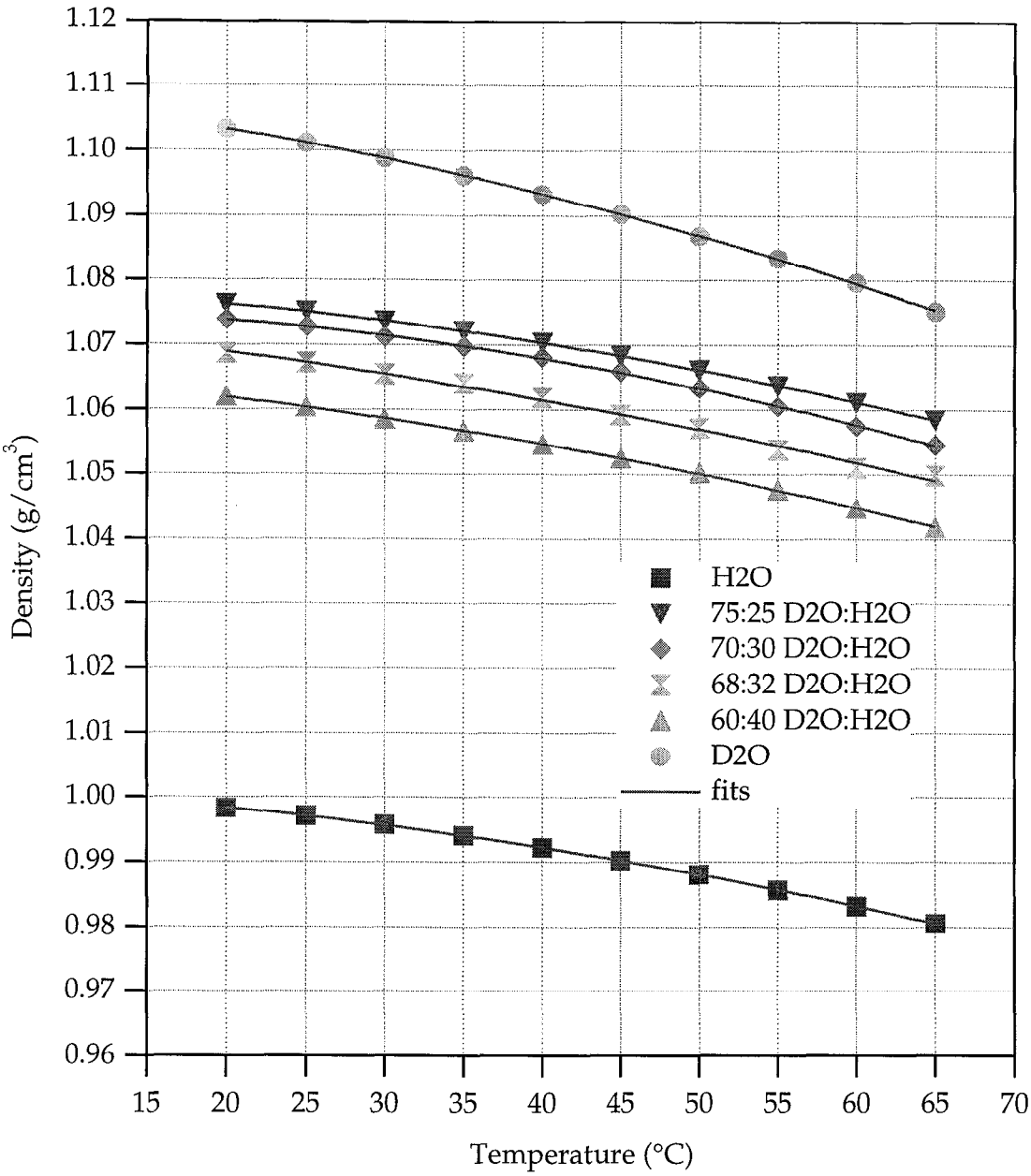

Figure B-1. Density data for H_2O, D_2O , and mixtures thereof.

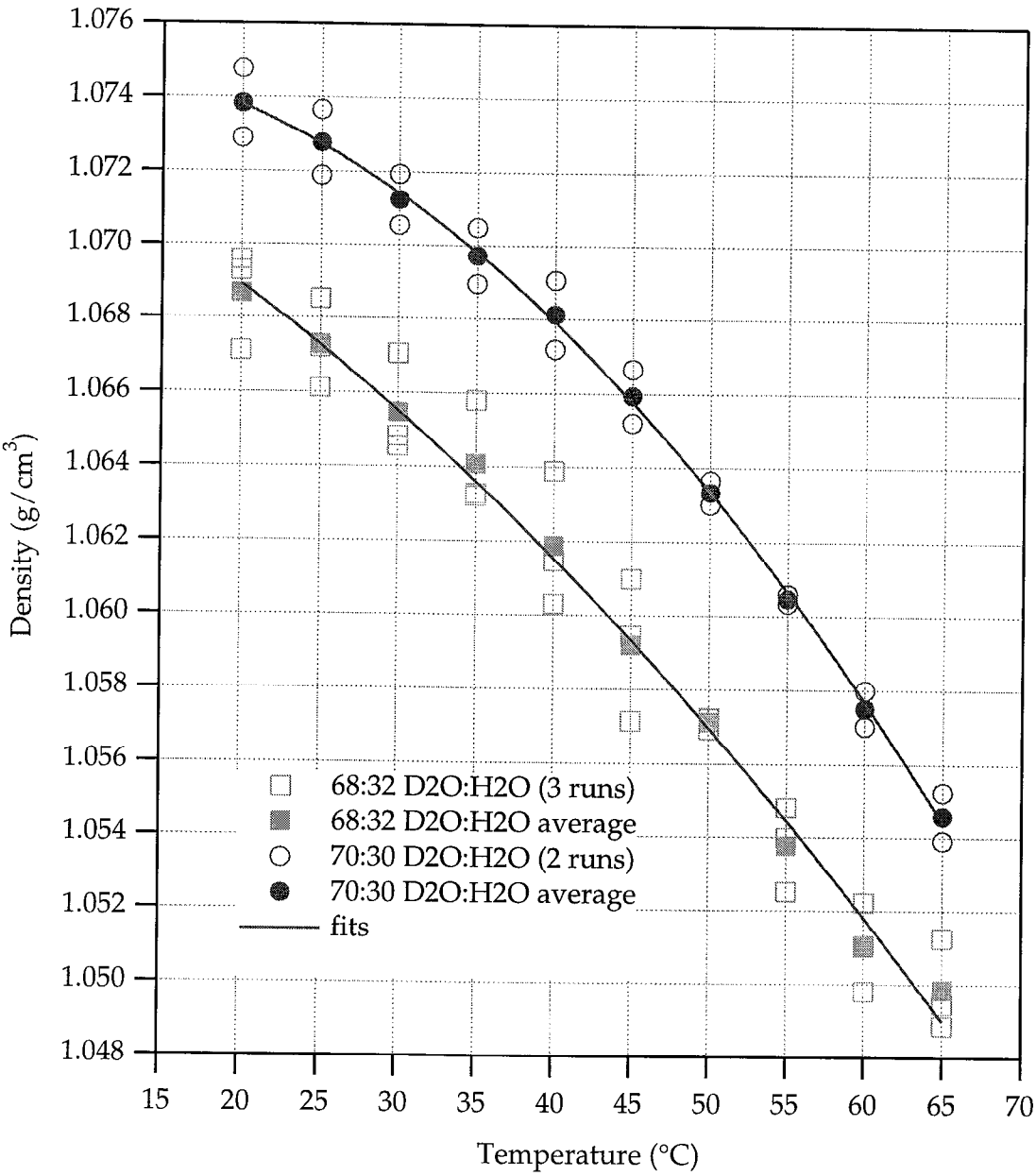

Figure B-2. Repeat density runs for two D_2O:H_2O mixtures.

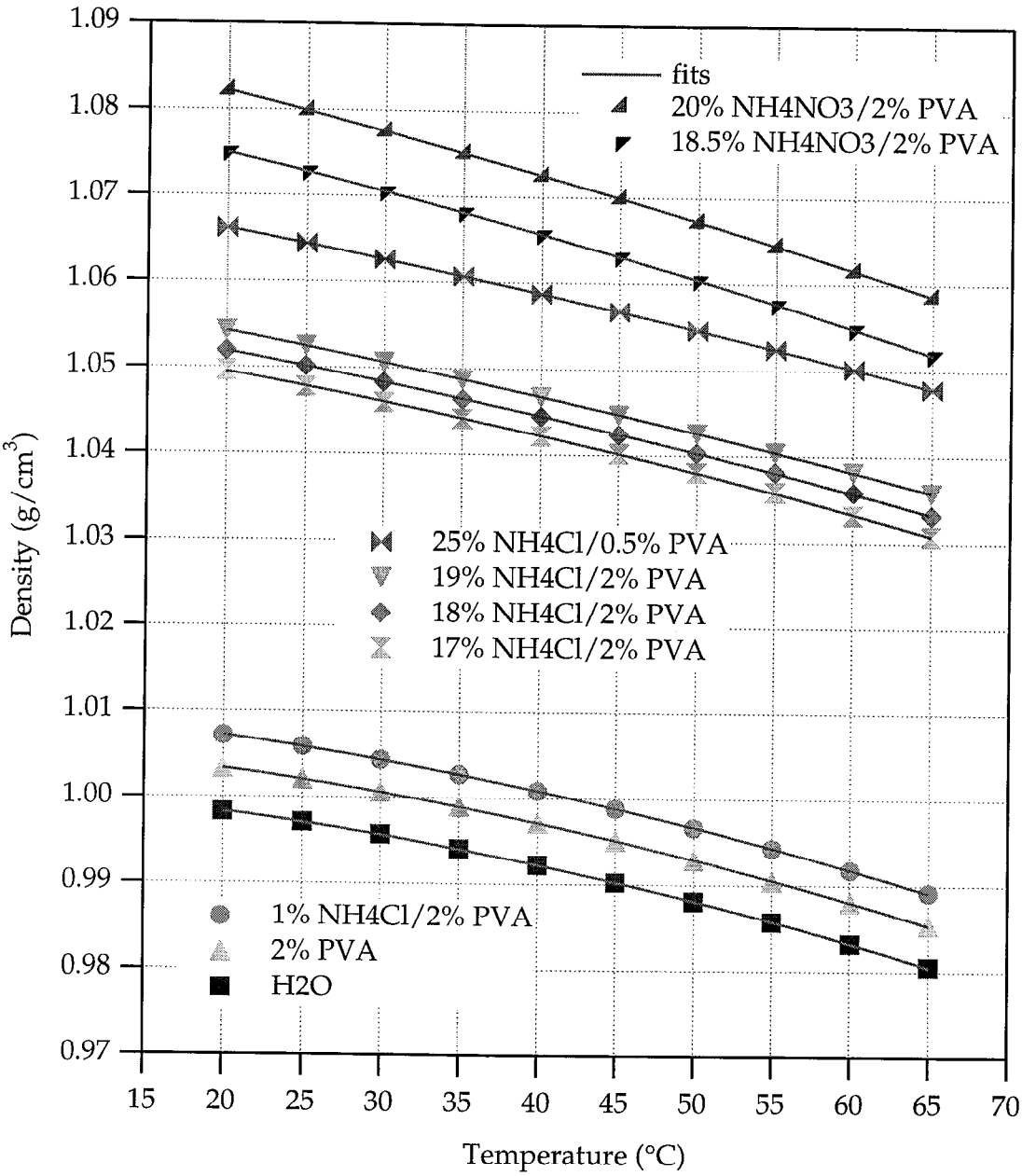

Figure B-3. Density Plots for aqueous PVA/Salt solutions.

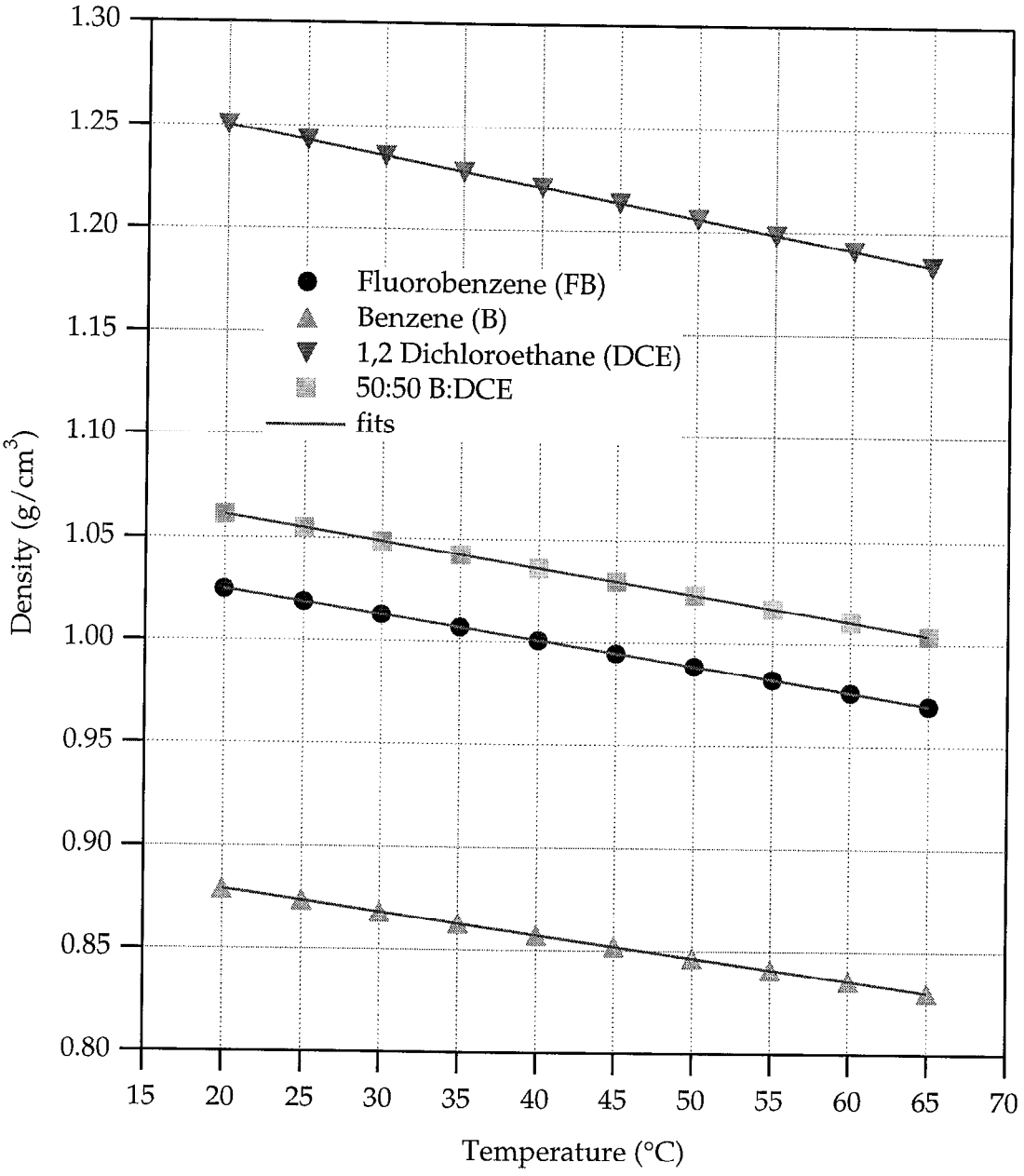

Figure B-4. Density plots for organic solvents.

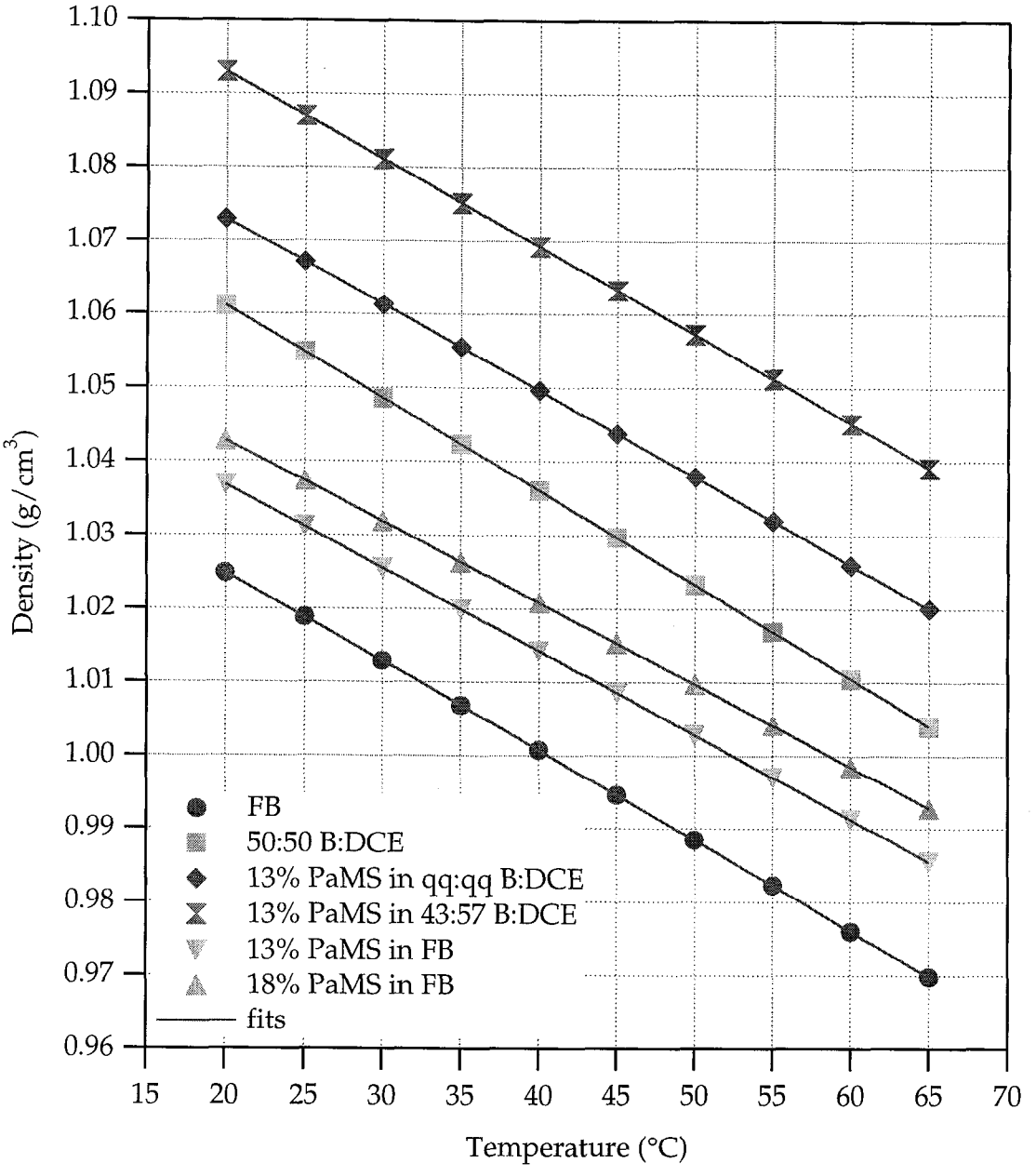

Figure B-5. Density plots for PaMS solutions.

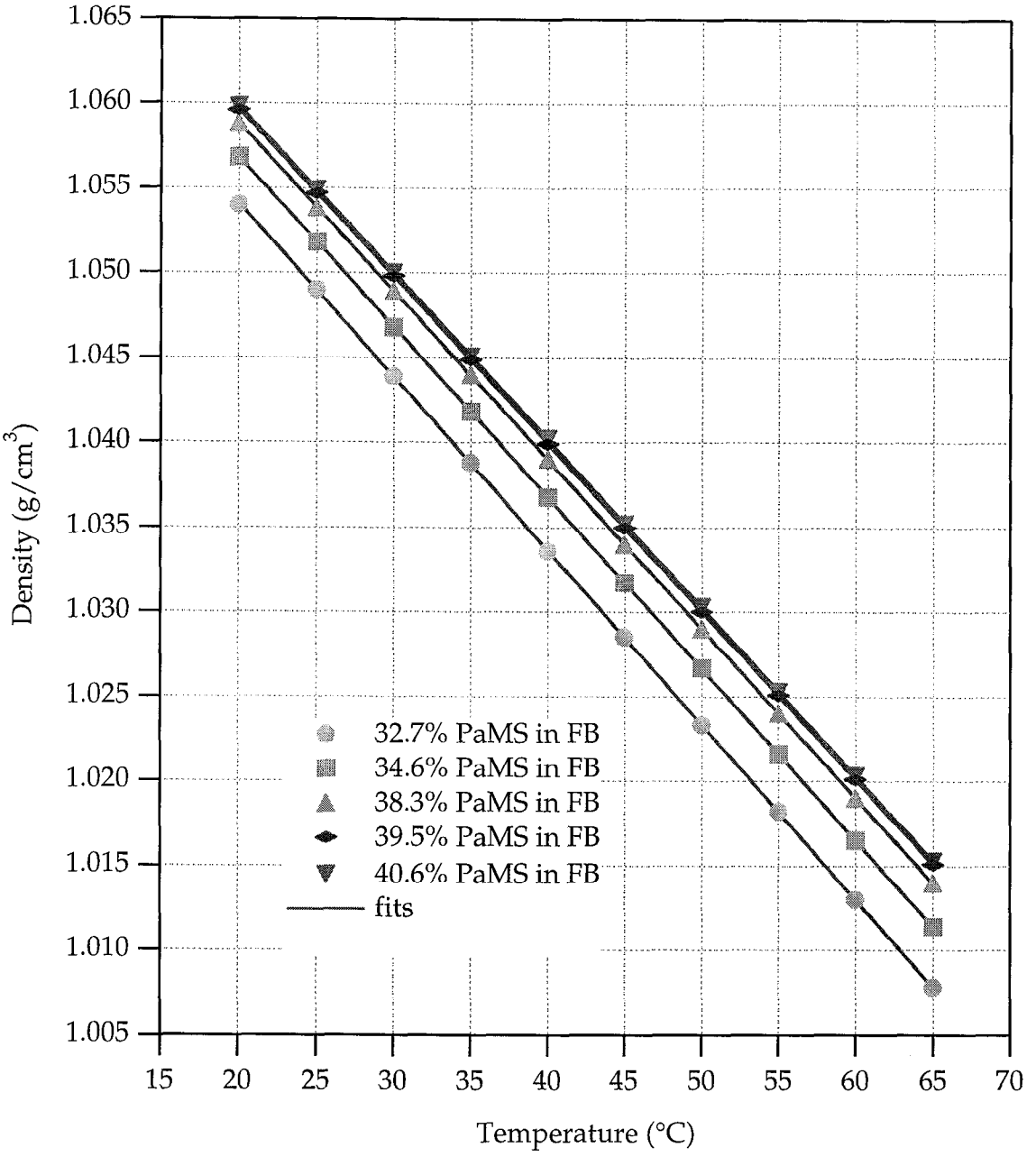

Figure B-6. Density plots for PαMS solutions.

Appendix C. **Full sets of traces for shell 1113#5.**

Before CH coating:

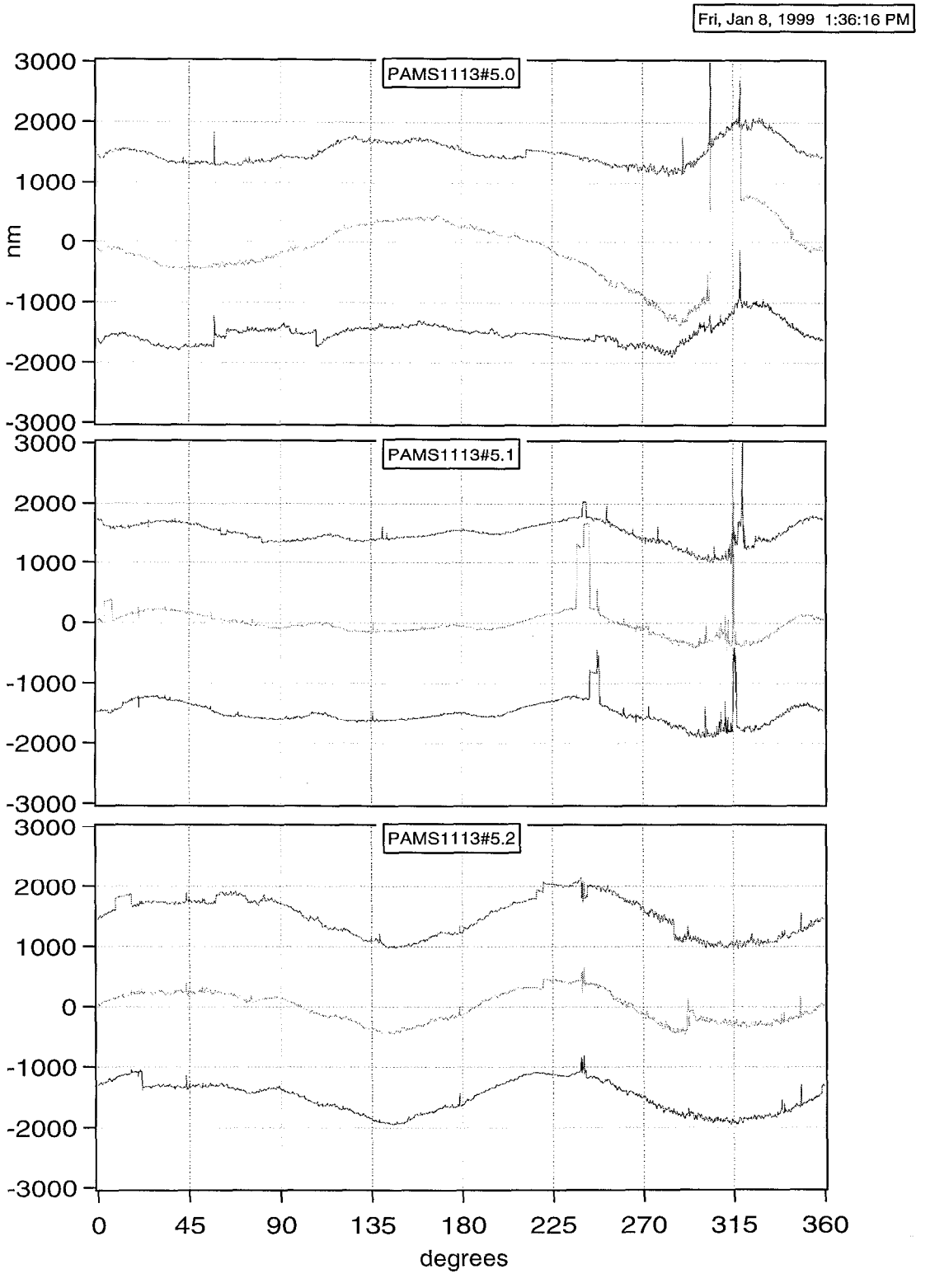

After CH Coating. The circled spikes were mathematically removed in the power spectrum in Figure 6 labled "Cleaned".